Atomic Layer Processing and Surface Properties of Gallium Nitride and Gallium Oxide

by

Kevin Andrew Hatch

A Dissertation Presented in Partial Fulfillment
of the Requirements for the Degree
Doctor of Philosophy

Approved November 2021 by the
Graduate Supervisory Committee:

Robert J. Nemanich, Chair
Fernando A. Ponce
David J. Smith
Yuji Zhao

ARIZONA STATE UNIVERSITY

December 2021

ABSTRACT

In this dissertation, atomic layer processing and surface characterization techniques were used to investigate surface conditions of wide band gap materials, gallium nitride (GaN) and gallium oxide (Ga_2O_3). These studies largely focused on mitigation and removal of defect formation induced by ions used in conventional plasma-based dry etching techniques.

Band bending measured by x-ray photoelectron spectroscopy (XPS) was used to characterize charge compensation at the surface of GaN (0001) and determine densities of charged surface states produced by dry etching. Mitigation and removal of these dry-etch induced defects was investigated by varying inductively coupled plasma (ICP) etching conditions, performing thermal and plasma-based treatments, and development of a novel low-damage, self-limiting atomic layer etching (ALE) process to remove damaged material.

Atomic layer deposition (ALD) and ALE techniques were developed for Ga_2O_3 using trimethylgallium (TMG). Ga_2O_3 was deposited by ALD on Si using TMG and O_2 plasma with a growth rate of 1.0 ± 0.1 Å/cycle. Ga_2O_3 films were then etched using HF and TMG using a fully thermal ALE process with an etch rate of 0.9 ± Å/cycle.

O_2 plasma oxidation of GaN for surface conversion to Ga_2O_3 was investigated as a pathway for ALE of GaN using HF and TMG. This process was characterized using XPS, in situ multi-wavelength ellipsometry, and transmission electron microscopy. This study indicated that the etch rate was lower than anticipated, which was attributed to crystallinity of the converted surface oxide on GaN (0001).

DEDICATION

For my friends and family who helped me along the way

ACKNOWLEDGEMENTS

I would like to express my sincerest gratitude to my advisor and committee chair, Dr. Robert Nemanich, for his continuous mentoring and support. I entered his lab at a moment of extreme uncertainty in my life and Dr. Nemanich's advising helped me find my way. Dr. Nemanich, the comfort and confidence I felt when joining you in your work and your research group made all the difference in completing this degree. The patience, guidance, and support you've given me throughout this journey is extremely appreciated.

I would also like to thank the members of my committee, Dr. Yuji Zhao, Dr. David Smith, and Dr. Fernando Ponce, along with Dr. Stephen Goodnick and all those involved in ASU's ARPA-e PNDiodes collaboration for their valued discussions. Our weekly meetings taught me so much about electronic devices, materials science, and ultimately, how to conduct myself as a researcher.

To my colleagues in the Nanoscience Lab, Dr. Jesse Brown and Dr. Daniel Messina, you have both been there throughout my entire time in this lab and I have thoroughly enjoyed learning and failing alongside you. To the senior members of the lab during my time, Franz Koeck, Dr. Manpuneet Benipal, Dr. Mei Hao, Dr. Xingye Wang, and Dr. Yu Yang, although our interactions were limited, I appreciate the help and guidance you provided me and the confidence you gave me when I first started. To the rest of my colleagues, Robert Mecham, Avani Patel, Dr. Zhiyu Huang, Kari Slotten, Ali Yekta, Holly Johnson, Yichen Yao, Madeleine Jacobs, and Alexandria Semien, I have enjoyed my time working and interacting with each of you and wish you the best of luck in your continued studies and other endeavors.

A special thanks is owed to Dr. Anna Zaniewski and the Sundial Project at ASU. The comfort and community that Sundial provided was a bright spot in my time here. Anna, you are such a wonderful example as a scientist and mentor.

To Dr. Chunqiang Li, I would like to thank you for persuading me to continue my education by pursuing a Master's degree in your biophotonics lab at UTEP and ultimately leading me to the completion of this degree. I'd also like to thank other influential professors from my time at UTEP including Dr. Eric Hagedorn, Dr. Vivian Incera (I likely never would have pursued a Ph.D. if you hadn't demanded it once a week), Dr. Felicia Manciu, Dr. Tunna Baruah, Dr. Osvaldo Mendez, and Dr. Leslie Foged.

I have many friends to thank, but I'd especially like to thank Aaron Hansen, Jorge Martinez, Tucker Manton, Ilian Valev, Sanjana Mukherjee, David Rosas, Tushar Modi, Adway Gupta, Mainak Mukhopadhyay, Nivedita Mahesh, Shanthan Alugubelli, Nicholas C. D. Ward, Joshua Ho-Lopez, Maximillian Archer, and C.J. Huff. I wish I could write a personal note to each of you, but as you can see, I've been doing a ton of writing and I'm tired.

Lastly, I would like to thank my family for their continued love, support, and encouragement. Their continued interest and enthusiasm for my education throughout my lifetime has pushed me to this achievement and I'm grateful for it. From the time I was five years old, copying my older brother's math problems and trying to solve them on my own, to the times I never thought I'd complete this degree, you've stood by me and I've never lost sight of that. I love you all.

This work was financially supported by ARPA-e through the PN-Diodes program under grant No. DE-AR0001691. I would like to acknowledge the use of facilities within the John. M. Cowley Center for High Resolution Electron Microscopy and the NanoFab, at Arizona State University, supported in part by the NSF program NNCI-ECCS-1542160.

TABLE OF CONTENTS

LIST OF TABLES

LIST OF FIGURES

Figure Page

CHAPTER I

INTRODUCTION

1.1 Objectives and Overview

Etching and epitaxial growth are essential aspects in the formation of structures for applied electronic devices. Structural defects at the growth interface may propagate throughout the deposited material. Substrate surface preparation may affect nucleation, growth mechanisms, and overall material quality. Defects resulting from conventional dry etching processes producing poor surface and interface conditions have been shown to negatively affect electronic performance, with significant impact on current leakage and device breakdown. [1–4] It is therefore crucial to understand the nature and cause of surface and interface defects, and develop methods to remove them or mitigate their formation. In this dissertation, I will discuss processing techniques, material properties, and defect characterization at the surfaces and interfaces of two wide-bandgap semiconductors which are currently of great interest; gallium nitride (GaN) and gallium oxide (Ga_2O_3).

1.2 Gallium Nitride and Gallium Oxide

Silicon has primarily been used as the semiconductor switching material in power electronic devices for decades due to low cost, high abundance, high stability, and an expansive foundation of research. However, due to physical limitations, including operating temperature, switching speeds, on-resistance, and high voltage operation, several wide bandgap semiconductors have emerged as potential candidates to replace silicon for the next generation of devices. [5] Among the most promising of these wide bandgap

materials are GaN and Ga_2O_3, which boast higher operating temperatures, higher breakdown fields, lower on-resistance, and higher operating voltages. [5–8] Some of the advantageous material properties of GaN and Ga_2O_3 are highlighted in Table 1.1 and Fig. 1.1.

Starting in the early 1970's, development in GaN was driven primarily for optoelectronic applications. GaN and its III-N alloys, InGaN and AlGaN, possess band gaps with energies that span the visible spectrum, making them ideally suitable for optoelectronic applications. The first blue light emitting diode (LED) was made in 1972 by Herb Maruska and Wally Rhines using Mg-doped GaN. [9] Work on light emission from GaN continued to develop but was limited by material defects and challenges in p-type doping, which made GaN-based light devices highly inefficient. A major improvement was made by Isamu Akasaki and Hiroshi Amano who developed a more efficient growth method and device structure using metal organic vapor phase epitaxy (MOVPE) in 1986. [10] Then, in 1993, Shuji Nakamura finally achieved efficient p-type doping through a thermal annealing technique for Mg-doped GaN. This thermal anneal removed Mg-H complexes responsible for neutralizing p-type conductivity. [11] These developments led to the first highly-efficient blue LED presented in 1994. This work was later recognized by the Nobel prize in physics awarded to Nakamura, Amano, and Akasaki in 2014. [12]

Due to this history in optoelectronic applications, development in GaN processing and device fabrication methods is relatively mature when compared to some competing wide bandgap materials such as diamond and cubic boron nitride (c-BN). GaN-based diodes and transistors have been rapidly developing with high-performance observed in power electronics such as Schottky barrier diodes, p-n diodes, high electron mobility

transistors (HEMTs) and field effect transistors (FETs). GaN-based power electronics have already shown major improvements in critical electric field and specific on-resistance compared to existing Si and 4H-SiC devices. [1,5–7] Expansion of GaN-based devices is currently hindered by limited electrical reliability, demonstrating need for further development of GaN processing. [1]

Table 1.1 – Material properties of Si, 4H-SiC, GaAs, GaN, β-Ga_2O_3, and diamond where E_g is the band gap energy, μ_e is the electron drift mobility, E_{crit} is the critical electric field at $N_D=10^{16}$ cm^{-3}, k is the thermal conductivity, and BFOM is the Baliga figure of merit for unipolar high-power devices, BFOM = ¼ $\epsilon\mu E_{crit}^3$. Table is adapted with permission from J. Tsao, et al. [5] Copyright © 2017, John Wiley and Sons.

	E_g (eV)	μ_e ($cm^2/V{\cdot}s$)	E_{crit} (MV/cm)	k (W/m·K)	BFOM (10^6 $V^2/\Omega cm^2$)
Si	1.1	1240	0.3	145	8.8
4H-SiC	3.3	980	3.1	370	6270
GaN	3.4	1000	4.9	253	27900
β-Ga_2O_3	4.9	150	10.3	27	36300
diamond	5.5	2000	13.0	2290	554000

Ultrawide band gap (UWBG) semiconductors are typically defined as those with band gaps larger than that of SiC (3.3 eV) or GaN (3.4 eV). Ga_2O_3 is among these UWBG materials with a band gap that varies between 4.5 and 4.9 eV depending on crystal phase. The most stable crystalline structure is the monoclinic β-Ga_2O_3 which has a band gap of 4.8 eV and is also an intriguing material for application in power electronics due to favorable material properties, including those shown in Table 1.1 and Fig. 1.1.

Ga_2O_3 has largely been used as a passive component in devices, often as a gate oxide or dielectric layer. [13–15] However, recent development has expanded Ga_2O_3 to applications as the active region in devices such as gas sensors, [16,17] field-effect-transistors (FETs), [18–20] solar cells, [21,22] and deep-UV photon detectors. [23–25]

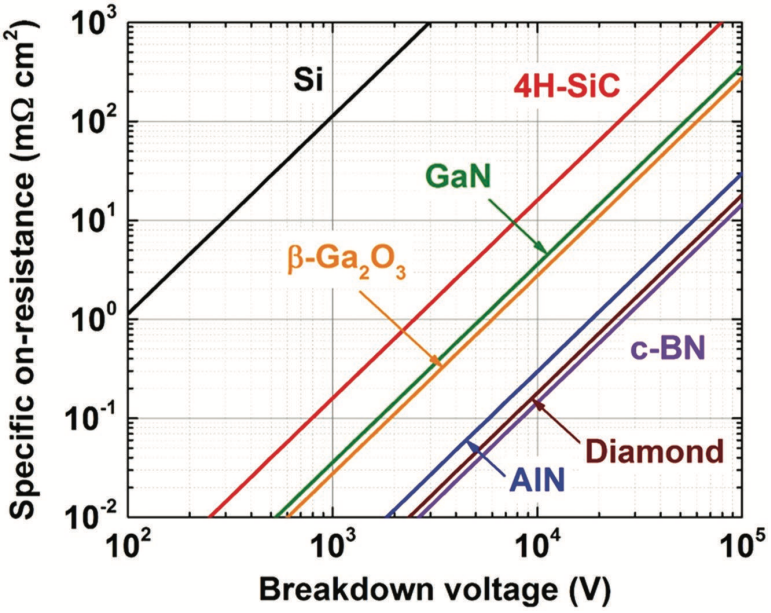

Figure 1.1 – Contours of constant Baliga figure-of-merit (BFOM) for various conventional, WBG and UWBG semiconductors, drawn on a log-log specific on-resistance versus breakdown voltage plot. This is the figure-of- merit of interest for low-frequency unipolar vertical power switches; the lower right region represents higher BFOM, hence higher performance. Reprinted with permission from J. Tsao, et al. [5] Copyright © 2017, John Wiley and Sons.

Controlling conductivity through doping is an essential aspect for device applications of any semiconducting material. Doping of GaN has been achieved for both n-type and p-type conductivity. Doping with Si to produce n-type GaN has been shown to be highly favorable with carrier concentration up to 10^{20} cm^{-3}. [26] Comparatively, p-type

conductivity in GaN has proven to be more challenging with various techniques developed to produce Mg-doping. Challenges in Mg-doping in GaN are related to an unusually high ionization energy of ~250 meV compared to typical shallow acceptor energies in conventional semiconductors. [27] For example, Si can be doped with ionization energies of 45 meV for B-doping and 57 meV for Al-doping. [28] Additionally, as mentioned earlier, doping with Mg also forms Mg-H complexes which inhibit conductivity.

N-type doping in Ga_2O_3 may be achieved with controllable carrier concentrations from 10^{16} to 10^{19} cm^{-3} through Sn or Ge doping in molecular beam epitaxy (MBE) growth and Si or Sn doping in metal organic chemical vapor deposition (MOCVD). [8] Consistent p-type doping of Ga_2O_3 remains elusive. Mg-doping has been shown to produce deep acceptor states and increase the resistivity of Ga_2O_3, inhibiting p-type conductivity. [29,30] A density functional theory (DFT) investigation of potential p-type dopants, including Li, Na, K, Be, Mg, Ca, Zn, Cu, and Au, found each of these produce deep acceptor levels with ionization energies >1 eV. [31] This suggests p-type doping of Ga_2O_3 using conventional doping techniques will continue to elude actualization until an alternative method is developed. A recent report of first-principles calculations suggests co-doping with Al-N or In-N may successfully produce p-type Ga_2O_3, but this has yet to be proven experimentally. [32]

1.3 Dry Etching

Fabrication of electronic devices typically requires dry etching for surface patterning to form device structures. The use of plasmas in dry etching enables anisotropic etching with a distinct advantage compared to wet etching processes in producing high

aspect ratio structures. The studies within this dissertation focus on the development of self-limiting, low-damage etching processes as well as characterization of surface defects formed from the etching processes.

The primary mechanisms of dry etching are physical sputtering and chemical etching. Material removal via physical sputtering occurs through ion bombardment providing momentum transfer to the surface atoms causing them to be ejected from the surface. Chemical etching involves the use of typically high density, low energy plasmas to form atomic neutrals which chemically react with the surface atoms, forming volatile products which desorb from the surface. Most commonly used dry etching methods involve a combination of these mechanisms known as ion assisted plasma etching.

The formation of mesa structures dominated the early focus in dry etching development, where high etch rates, anisotropic profiles, and smooth sidewalls were the most desirable features in the progress of dry etching techniques. Now, demand for high power and high temperature devices requires etching with smoother surface morphology, lower plasma induced damage, and selective etching. Device fabrication and dry etching methods must continue to improve and develop to address these challenges.

Dry etch techniques may vary in the gas chemistries employed and plasma formation techniques. Among the most commonly used dry etching techniques are reactive ion etching (RIE) and inductively coupled plasma (ICP) etching. The RIE process uses a combination of chemical and physical mechanisms to achieve highly anisotropic etch profiles and fast etch rates. To generate the plasma, radio frequency (rf) power of 13.56 MHz is applied between two parallel electrodes within a reactive gas. Ion energies

produced by this method are typically a few hundred eV as they traverse the plasma sheath. Low pressures between 1 – 200 mTorr are typically used in RIE to produce higher inelastic mean free paths and reduce collisions in the plasma resulting in highly anisotropic etching of the device surface. High ion energies produce the best RIE results for GaN. However, the plasma damage caused by these ion energies may severely hinder electronic device performance. Lowering the ion component of the RIE process results in less anisotropic etch profiles and slower etch rates.

ICP etching is a high-density plasma etch technique with plasma densities which are 2 to 4 orders of magnitude higher than RIE. Other high-density plasma etch techniques include electron cyclotron resonance (ECR) and magnetron RIE (MRIE). Inductively coupled plasmas are typically produced using rf of either 2.0 or 13.56 MHz. An rf bias is applied to the surface to accelerate ions and control ion energy while ion flux may be controlled by varying the ICP power. This allows for ion energy and ion density to be more effectively decoupled, allowing for better control of damage produced by the ion component. ICP etch rates for GaN and other III-N materials, including AlN and InN, increase with increasing ion energy or ion flux, but this is known to produce more ion-related damage. [33]

Table 1.2 – Summary of selected dry etching processes for GaN and Ga_2O_3.

Material	Etch Technique	Gas Composition	Reference
GaN	ICP	Cl_2/BCl_3	Zhou, *et al.* [34]
GaN	ICP	Cl_2/Ar	Han, *et al*. [35]
GaN	ICP	Cl_2/N_2	Han, *et al*. [35]
GaN	RIE	SF_6/Ar	Sreenidhi, *et al*. [36]
GaN	RIE	SF_6/N_2	Sreenidhi, *et al*. [36]
GaN	RIE	BCl_3	Lin, *et al*. [37]
GaN	ECR	$Cl_2/H_2/Ar$	Shul, *et al*. [38]
GaN	ECR	$Cl_2/SF_6/Ar$	Shul, *et al*. [38]
Ga_2O_3	ICP	SF_6/Ar	Liang, *et al*. [39]
Ga_2O_3	ICP	BCl_3/Ar	Yang, *et al*. [40]
Ga_2O_3	ICP	Cl_2/Ar	Yang, et al. [40]
Ga_2O_3	RIE	Cl_2/BCl_3	Hogan, *et al*. [41]
Ga_2O_3	RIE	SF_6	Kwon, *et al.* [42]

Various gas chemistries and etch techniques have been investigated for GaN and Ga_2O_3. A collection of dry etching processes for these materials is shown in Table 1.2. Halogen based gas chemistries, particularly F and Cl, are commonly used for both GaN and Ga_2O_3. Ar is also commonly used, as it is chemically inert and highly suitable for material removal through physical bombardment of the surface.

1.3.1 Damage Induced by Dry Etching

Due to the physical bombardment at the surface, damage to the substrate may occur. Etching parameters are typically chosen to optimize etch rates and dimensional control

while minimizing ion-induced damage. However, ion-related damage still occurs, producing high defect concentration in the surface and near surface regions while defects may propagate much deeper into the structure. A previous study has found damage in GaN more than 50 nm from the surface, [43] while etching of Si has found hydrogen ions more than 30 nm from the surface and deuterium more than 200 nm from the surface after just 1 min of plasma exposure. [44] Lee, *et al*. showed ICP plasma etching of GaN increased RMS roughness, sheet resistance, and current leakage, especially at higher rf power. [45]

Mitigation of defect formation from etching processes has been observed through refinement of etching parameters, with improvement observed when limiting ion energies and etching at lower pressure. [33,46–48] Recovery of etch-induced damage through development of post etching treatments has also been shown to improve device performance in both GaN and Ga_2O_3. Post-etch surface treatments have been observed to improve optic and electric properties in GaN through N_2 plasma passivation and thermal annealing. [45,49–53] Improvement in electronic performance of etched Ga_2O_3 has been observed after annealing at 450 °C while surface roughness has been showed to improve using *ex situ* wet chemical treatments. [4,54]

Plasma passivation using N_2 plasma has been found to significantly improve surface and electronic properties of plasma etched GaN in multiple studies. [45,49–53] Wang, *et al*. showed Hall mobility in ICP etched GaN decreased from ~600 $cm^2V^{-1}s^{-1}$ to ~50 $cm^2V^{-1}s^{-1}$ with increasing Ar component, but N_2 plasma exposure at 705 °C improved the Hall mobility of etched GaN to ~550 $cm^2V^{-1}s^{-1}$. [55] Mouffak, *et al*. showed N_2 plasma treatment after RIE recovered voltage breakdown from 13% of the non-etched to 70%. [49] A combination of high temperature annealing and N_2 plasma treatment proved to be most

effective in recovering etch damage. [51,53,55] These results are largely attributed to nitrogen radicals improving surface stoichiometry by satisfying dangling bonds and filling N vacancies.

ICP etching has been shown to degrade Ga_2O_3 Schottky diodes using current-voltage measurements. However, annealing at 450 °C was shown to recover Schottky barrier height, reverse breakdown voltage, and ideality factor. [4] Additionally, wet chemical treatments including tetramethyl ammonium hydroxide (TMAH) or a mixture of sulfuric acid and hydrogen peroxide were effective in recovering surface roughness of ICP-RIE Ga_2O_3.[55] The TMAH treatment proved to be more effective as the sulfuric acid and hydrogen peroxide mixture weren't able to remove pinholes that were formed during etching.

1.3.2 Atomic Layer Etching

The etching methods discussed above are typically referred to as 'conventional dry etching'. Atomic layer etching (ALE) is a more recent dry etching technique in which the etching occurs through the use of sequential discrete exposures of reactants to perform self-limiting, atomic scale etching of material. Compared to 'conventional' dry etching methods discussed above, ALE exhibits high selectivity, low damage, and has been suggested as a method to remove damaged material produced by conventional dry etching techniques. ALE processing and reaction mechanisms are discussed further in section 2.3.

Although conventional dry etching techniques have proven to be effective methods for designing device architectures, these techniques have also been shown to produce damage that ultimately hinders device performance. The focus of this dissertation is the

mitigation or removal of dry etching-induced defects in GaN and Ga_2O_3 using atomic layer etching, high temperature annealing, and plasma treatments. Background of atomic layer processing is given in Chapter 2, leading to the development of thermal ALE. A background and description of the processing and characterization techniques used in these studies are presented in Chapter 3. The development of a thermal ALE method for Ga_2O_3 is presented in Chapter 4 using HF and trimethylgallium for self-limiting, low damage etching. In Chapter 5, this thermal ALE technique is investigated as a pathway for GaN ALE using an O_2 plasma conversion. A surface characterization technique using x-ray photoelectron spectroscopy to determine external surface charge concentration of GaN is introduced in Chapter 6. This technique is applied to determine surface state concentrations in ICP etched GaN and investigate methods for reduction of these charged surface states. Methods for expansion and continuation of this work are proposed in Chapter 7.

REFERENCES

[1] J. A. del Alamo and J. Joh, *GaN HEMT Reliability*, Microelectronics Reliability **49**, 1200 (2009).

[2] G. Meneghesso, G. Verzellesi, F. Danesin, F. Rampazzo, F. Zanon, A. Tazzoli, M. Meneghini, and E. Zanoni, *Reliability of GaN High-Electron-Mobility Transistors: State of the Art and Perspectives*, IEEE Transactions on Device and Materials Reliability **8**, 332 (2008).

[3] J. Yang, S. Ahn, F. Ren, S. Pearton, R. Khanna, K. Bevlin, D. Geerpuram, and A. Kuramata, *Inductively Coupled Plasma Etching of Bulk, Single-Crystal Ga_2O_3*, Journal of Vacuum Science & Technology B, Nanotechnology and Microelectronics: Materials, Processing, Measurement, and Phenomena **35**, 031205 (2017).

[4] J. Yang, F. Ren, R. Khanna, K. Bevlin, D. Geerpuram, L.-C. Tung, J. Lin, H. Jiang, J. Lee, E. Flitsiyan, L. Chernyak, S. J. Pearton, and A. Kuramata, *Annealing of Dry Etch Damage in Metallized and Bare (-201) Ga_2O_3*, Journal of Vacuum Science & Technology B **35**, 051201 (2017).

[5] J. Y. Tsao, S. Chowdhury, M. A. Hollis, D. Jena, N. M. Johnson, K. A. Jones, R. J. Kaplar, S. Rajan, C. G. Van de Walle, E. Bellotti, C. L. Chua, R. Collazo, M. E. Coltrin, J. A. Cooper, K. R. Evans, S. Graham, T. A. Grotjohn, E. R. Heller, M. Higashiwaki, M. S. Islam, P. W. Juodawlkis, M. A. Khan, A. D. Koehler, J. H. Leach, U. K. Mishra, R. J. Nemanich, R. C. N. Pilawa-Podgurski, J. B. Shealy, Z. Sitar, M. J. Tadjer, A. F. Witulski, M. Wraback, and J. A. Simmons, *Ultrawide-*

Bandgap Semiconductors: Research Opportunities and Challenges, Advanced Electronic Materials **4**, (2018).

[6] B. J. Baliga, *Gallium Nitride Devices for Power Electronic Applications*, Semiconductor Science and Technology **28**, (2013).

[7] U. K. Mishra, L. Shen, T. E. Kazior, and Y. F. Wu, *GaN-Based RF Power Devices and Amplifiers*, Proceedings of the IEEE **96**, 287 (2008).

[8] S. J. Pearton, J. Yang, P. H. Cary, F. Ren, J. Kim, M. J. Tadjer, and M. A. Mastro, *A Review of Ga_2O_3 Materials, Processing, and Devices*, Applied Physics Reviews **5**, (2018).

[9] H. P. Maruska, W. C. Rhines, and D. A. Stevenson, *Preparation of Mg-Doped GaN Diodes Exhibiting Violet Electroluminescence*, Materials Research Bulletin **7**, 777 (1972).

[10] H. Amano, N. Sawaki, I. Akasaki, and Y. Toyoda, *Metalorganic Vapor Phase Epitaxial Growth of a High Quality GaN Film Using an AlN Buffer Layer*, Applied Physics Letters **48**, 353 (1986).

[11] S. Nakamura, M. Senoh, and T. Mukai, *P-GaN / N-InGaN / N-GaN Double-Heterostructure Blue-Light-Emitting Diodes*, Japanese Journal of Applied Physics **32**, 8 (1993).

[12] S. Nakamura, *Background Story of the Invention of Efficient Blue InGaN Light Emitting Diodes (Nobel Lecture)*, Reviews of Modern Physics **87**, 1139 (2015).

[13] F. Ren, M. Hong, J. P. Mannaerts, J. R. Lothian, and A. Y. Cho, *Wet Chemical and*

Plasma Etching of $Ga_2O_3(Gd_2O_3)$, Journal of the Electrochemical Society **144**, 239 (1997).

[14] F. Ren, M. Hong, W. S. Hobson, J. M. Kuo, J. R. Lothian, J. P. Mannaerts, J. Kwo, S. N. G. Chu, Y. K. Chen, and A. Y. Cho, *Demonstration of Enhancement-Mode p- and n-Channel GaAs MOSFETs with $Ga_2O_3(Gd_2O_3)$ as Gate Oxide*, Solid-State Electronics **41**, 1751 (1997).

[15] Y. C. Wang, M. Hong, J. M. Kuo, J. P. Mannaerts, J. Kwo, H. S. Tsai, J. J. Krajewski, J. S. Weiner, Y. K. Chen, and A. Y. Cho, *Advances in GaAs MOSFETs Using $Ga_2O_3(Gd_2O_3)$ as Gate Oxide*, Materials Research Society Symposium - Proceedings **573**, 219 (1999).

[16] L. Mazeina, F. K. Perkins, V. M. Bermudez, S. P. Arnold, and S. M. Prokes, *Functionalized Ga_2O_3 Nanowires as Active Material in Room Temperature Capacitance-Based Gas Sensors*, Langmuir **26**, 13722 (2010).

[17] A. V. Almaev, E. V. Chernikov, V. V. Novikov, B. O. Kushnarev, N. N. Yakovlev, E. V. Chuprakova, V. L. Oleinik, A. D. Lozinskaya, and D. S. Gogova, *Impact of Cr_2O_3 Additives on the Gas-Sensitive Properties of β-Ga_2O_3 Thin Films to Oxygen, Hydrogen, Carbon Monoxide, and Toluene Vapors*, Journal of Vacuum Science & Technology A **39**, 023405 (2021).

[18] H. Zhou, K. Maize, G. Qiu, A. Shakouri, and P. D. Ye, *β-Ga_2O_3 on Insulator Field-Effect Transistors with Drain Currents Exceeding 1.5 A/Mm and Their Self-Heating Effect*, Applied Physics Letters **111**, (2017).

[19] M. Higashiwaki, K. Sasaki, A. Kuramata, T. Masui, and S. Yamakoshi, *Gallium*

Oxide (Ga_2O_3) Metal-Semiconductor Field-Effect Transistors on Single-Crystal β-Ga_2O_3 (010) Substrates, Applied Physics Letters **100**, 1 (2012).

[20] M. Higashiwaki, K. Sasaki, T. Kamimura, M. Hoi Wong, D. Krishnamurthy, A. Kuramata, T. Masui, and S. Yamakoshi, *Depletion-Mode Ga_2O_3 Metal-Oxide-Semiconductor Field-Effect Transistors on β-Ga_2O_3 (010) Substrates and Temperature Dependence of Their Device Characteristics*, Applied Physics Letters **103**, 1 (2013).

[21] T. Minami, Y. Nishi, T. Miyata, and J. I. Nomoto, *High-Efficiency Oxide Solar Cells with ZnO/Cu_2O Heterojunction Fabricated on Thermally Oxidized Cu_2O Sheets*, Applied Physics Express **4**, 2 (2011).

[22] A. K. Chandiran, N. Tetreault, R. Humphry-Baker, F. Kessler, E. Baranoff, C. Yi, M. K. Nazeeruddin, and M. Grätzel, *Subnanometer Ga_2O_3 Tunnelling Layer by Atomic Layer Deposition to Achieve 1.1 v Open-Circuit Potential in Dye-Sensitized Solar Cells*, Nano Letters **12**, 3941 (2012).

[23] H. Feng, W. Hao, C. Zhao, X. Xin, J. Cheng, Y. Cui, Y. Chen, and W. Wang, *Fabrication and UV-Sensing Properties of One-Dimensional β-Ga_2O_3 Nanomaterials*, Physica Status Solidi (A) Applications and Materials Science **210**, 1861 (2013).

[24] T. Oshima, T. Okuno, and S. Fujita, *Ga_2O_3 Thin Film Growth on c-Plane Sapphire Substrates by Molecular Beam Epitaxy for Deep-Ultraviolet Photodetectors*, Japanese Journal of Applied Physics, Part 1: Regular Papers and Short Notes and Review Papers **46**, 7217 (2007).

[25] T. Oshima, T. Okuno, N. Arai, N. Suzuki, S. Ohira, and S. Fujita, *Vertical Solar-Blind Deep-Ultraviolet Schottky Photodetectors Based on β-Ga_2O_3 Substrates*, Applied Physics Express **1**, (2008).

[26] J. K. Sheu and G. C. Chi, *The Doping Process and Dopant Characteristics of GaN*, Journal of Physics Condensed Matter **14**, (2002).

[27] C. G. Van De Walle, *Defects and Doping in GaN*, Brazilian Journal of Physics **27**, 74 (1997).

[28] H. J. Hrostowski and R. H. Kaiser, *Infrared Spectra of Group III Acceptors in Silicon*, Journal of Physics and Chemistry of Solids **4**, 148 (1958).

[29] Y. P. Qian, D. Y. Guo, X. L. Chu, H. Z. Shi, W. K. Zhu, K. Wang, X. K. Huang, H. Wang, S. L. Wang, P. G. Li, X. H. Zhang, and W. H. Tang, *Mg-Doped p-Type β-Ga_2O_3 Thin Film for Solar-Blind Ultraviolet Photodetector*, Materials Letters **209**, 558 (2017).

[30] E. Chikoidze, C. Sartel, H. Mohamed, I. Madaci, T. Tchelidze, M. Modreanu, P. Vales-Castro, C. Rubio, C. Arnold, V. Sallet, Y. Dumont, and A. Perez-Tomas, *Enhancing the Intrinsic P-Type Conductivity of the Ultra-Wide Bandgap Ga_2O_3 Semiconductor*, Journal of Materials Chemistry C **7**, 10231 (2019).

[31] A. Kyrtsos, M. Matsubara, and E. Bellotti, *On the Feasibility of P-Type Ga_2O_3*, Applied Physics Letters **112**, (2018).

[32] J. Ma, J. Lin, J. Liu, F. Li, Y. Liu, and G. Yang, *Achieving High Conductivity P-Type Ga_2O_3 through Al-N and In-N Co-Doping*, Chemical Physics Letters **746**,

137308 (2020).

[33] S. J. Pearton, R. J. Shul, and F. Ren, *A Review of Dry Etching of GaN and Related Materials*, MRS Internet Journal of Nitride Semiconductor Research **5**, 1 (2000).

[34] S. Zhou, B. Cao, and S. Liu, *Dry Etching Characteristics of GaN Using Cl_2/BCl_3 Inductively Coupled Plasmas*, Applied Surface Science **257**, 905 (2010).

[35] Y. J. Han, S. Xue, W. P. Guo, C. Z. Sun, Z. B. Hao, and Y. Luo, *Characteristics of N-GaN after Cl_2/Ar and Cl_2/N_2 Inductively Coupled Plasma Etching*, Japanese Journal of Applied Physics, Part 1: Regular Papers and Short Notes and Review Papers **42**, 6409 (2003).

[36] T. Sreenidhi, K. Baskar, A. Dasgupta, and N. Dasgupta, *Reactive Ion Etching of GaN in SF_6 + Ar and SF_6 + N_2 Plasma*, Semiconductor Science and Technology **23**, (2008).

[37] M. E. Lin, Z. F. Fan, Z. Ma, L. H. Allen, and H. Morkoç, *Reactive Ion Etching of GaN Using BCl_3*, Applied Physics Letters **64**, 887 (1994).

[38] R. J. Shul, C. I. . Ashby, D. J. Rieger, A. J. Howard, S. J. Pearton, C. R. Abernathy, C. B. Vartuli, P. A. Barnes, and P. Davis, *Plasma Chemsitry Dependent ECR Etching of GaN*, Materials Research Society Symposium - Proceedings **395**, 751 (1996).

[39] H. Liang, Y. Chen, X. Xia, C. Zhang, R. Shen, Y. Liu, Y. Luo, and G. Du, *A Preliminary Study of SF_6 Based Inductively Coupled Plasma Etching Techniques for Beta Gallium Trioxide Thin Film*, Materials Science in Semiconductor

Processing **39**, 582 (2015).

[40] J. Yang, S. Ahn, F. Ren, R. Khanna, K. Bevlin, D. Geerpuram, S. J. Pearton, and A. Kuramata, *Inductively Coupled Plasma Etch Damage in (-201) Ga_2O_3 Schottky Diodes*, Applied Physics Letters **110**, 1 (2017).

[41] J. E. Hogan, S. W. Kaun, E. Ahmadi, Y. Oshima, and J. S. Speck, *Chlorine-Based Dry Etching of β-Ga_2O_3*, Semiconductor Science and Technology **31**, 065006 (2016).

[42] Y. Kwon, G. Lee, S. Oh, J. Kim, S. J. Pearton, and F. Ren, *Tuning the Thickness of Exfoliated Quasi-Two-Dimensional β-Ga_2O_3 Flakes by Plasma Etching*, Applied Physics Letters **110**, (2017).

[43] X. A. Cao, H. Cho, S. J. Pearton, G. T. Dang, A. P. Zhang, F. Ren, R. J. Shul, L. Zhang, R. Hickman, and J. M. Van Hove, *Depth and Thermal Stability of Dry Etch Damage in GaN Schottky Diodes*, Applied Physics Letters **75**, 232 (1999).

[44] G. S. Oehrlein, *Dry Etching Damage of Silicon: A Review*, Materials Science and Engineering B **4**, 441 (1989).

[45] J. M. Lee, K. M. Chang, S. W. Kim, C. Huh, I. H. Lee, and S. J. Park, *Dry Etch Damage in N-Type GaN and Its Recovery by Treatment with an N_2 Plasma*, Journal of Applied Physics **87**, 7667 (2000).

[46] F. Ren, J. R. Lothian, S. J. Pearton, C. R. Abernathy, C. B. Vartuli, J. D. Mackenzie, R. G. Wilson, and R. F. Karlicek, *Effect of Dry Etching on Surface Properties of III-Nitrides*, Journal of Electronic Materials **26**, 1287 (1997).

[47] R. Khanna, K. Bevlin, D. Geerpuram, J. Yang, F. Ren, and S. J. Pearton, *Dry Etching of Ga_2O_3*, Gallium Oxide 263 (2019).

[48] S. J. Pearton and R. J. Shul, *Etching of III Nitrides*, **50**, 103 (1997).

[49] Z. Mouffak, A. Bensaoula, and L. Trombetta, *The Effects of Nitrogen Plasma on Reactive-Ion Etching Induced Damage in GaN*, Journal of Applied Physics **95**, 727 (2004).

[50] Z. Mouffak, A. Bensaoula, and L. Trombetta, *A Photoluminescence Study of Plasma Reactive Ion Etching-Induced Damage in GaN*, Journal of Semiconductors **35**, 3 (2014).

[51] L. Ji-Myon, H. Chul, K. Dong-Joon, and P. Seong-Ju, *Dry-Etch Damage and Its Recovery in InGaN/GaN Multi-Quantum-Well Light-Emitting Diodes*, Semiconductor Science and Technology **18**, 530 (2003).

[52] D. G. Kent, K. P. Lee, A. P. Zhang, B. Luo, M. E. Overberg, C. R. Abernathy, F. Ren, K. D. Mackenzie, S. J. Pearton, and Y. Nakagawa, *Effect of N_2 Plasma Treatments on Dry Etch Damage in n- and p-Type GaN*, Materials Research Society Symposium - Proceedings **45**, 467 (2001).

[53] D. G. Kent, K. P. Lee, A. P. Zhang, B. Luo, M. E. Overberg, C. R. Abernathy, F. Ren, K. D. Mackenzie, S. J. Pearton, and Y. Nakagawa, *Electrical Effects of N_2 Plasma Exposure on Dry-Etch Damage in p- and n-GaN Schottky Diodes*, Solid-State Electronics **45**, 1837 (2001).

[54] H. K. Lee, H. J. Yun, K. H. Shim, H. G. Park, T. H. Jang, S. N. Lee, and C. J.

Choi, *Improvement of Dry Etch-Induced Surface Roughness of Single Crystalline β-Ga_2O_3 Using Post-Wet Chemical Treatments*, Applied Surface Science **506**, 144673 (2020).

[55] X. Wang, G. Yu, B. Lei, X. Wang, C. Lin, Y. Sui, S. Meng, M. Qi, and A. Li, *Recovery of Dry Etching-Induced Damage in n-GaN by Nitrogen Plasma Treatment at Growth Temperature*, Journal of Electronic Materials **36**, 697 (2007).

CHAPTER II

ATOMIC LAYER PROCESSING

Atomic level control in material fabrication and processing has become increasingly vital for many applications, particularly in the semiconductor electronics industry. [1–7] These needs have facilitated the development of atomic layer processes involving sequential, self-limiting surface reactions for the deposition or etching of material. The self-limiting behavior of atomic layer processing enables the growth of ultra-thin, uniform, conformal films with minimal or no effect to the underlying material. [1–9] These qualities make atomic layer processing ideally suitable for producing high aspect structures.

Atomic layer deposition has become an established technique in material processing, used for the deposition of dielectrics, including gate oxides on MOSFETs, [10–12] nanolaminates, [13,14] and nonvolatile memory devices (NVM). [15,16] Comparatively, atomic layer etching is less widely used with plasma-based ALE methods moving towards practical use in manufacturing and increasing production of commercially available plasma-based ALE reactors. [4,5,17,18] Meanwhile, thermal ALE remains a relatively new field in materials research. [3,4,6,8,17,19]

2.1 Atomic Layer Deposition

Atomic layer deposition (ALD) is a chemical vapor deposition (CVD) technique using metal precursors held at a temperature sufficient for vapor withdrawal into the growth chamber. In typical CVD, the chamber is flooded with reactant gas as the vapor-phase metal precursor is introduced to the chamber, allowing continuous reaction between the

reactants and substrate surface. Alternatively, ALD employs sequential discrete exposures of vapor phase reactants for self-limiting half-reactions at the substrate surface to produce material growth. An individual ALD cycle may deposit 0.1-2.0Å of material and consists of precursor delivery, chamber purge/abatement, reactant gas delivery, and then another chamber purge. Although the deposition rates are much lower than typical CVD processes, repeated cycles of ALD may produce ultra-thin, conformal, and uniform films with atomic scale precision. [1,7,20,21]

An ALD cycle begins with precursor adsorption to the growth surface, primarily through chemisorption. This reaction is limited by the finite available reaction sites at the surface and produces a layer of one monolayer or less. [1] The chamber is then purged with inert gas to remove reaction byproducts and excess unreacted precursor molecules. The second reactant then interacts with the surface groups to deposit material and remove unwanted surface species. Another chamber purge is necessary to remove reaction byproducts and excess reactants before the ALD cycle repeats. The reactions are determined to be self-limiting by the saturation of growth rates with increasing exposure times of the individual half-reactions.

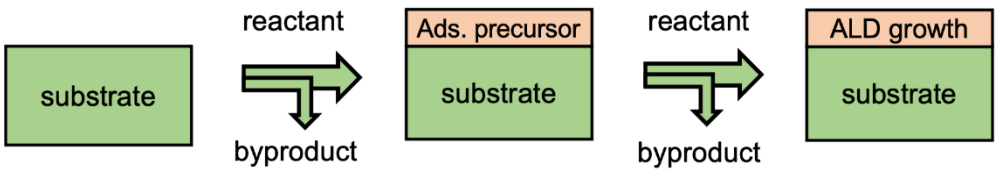

Figure 2.1 – Schematic of a typical ALD process including precursor adsorption and a second exposure to produce ALD growth. The intermediate chamber purge is not pictured.

Precursors must be volatile, but thermally stable, and be able to chemisorb to the surface, react with surface species, and saturate reactions in a relatively short time to be effective for ALD. Adsorption may occur through either physisorption or chemisorption. Physisorption occurs through weak interactions and does not affect the structure of the molecule, and allows for stacking of multilayers of physisorbed molecules. Alternatively, chemisorption involves changing of chemical bonds, which will be limited by chemically active sites at the surface. The requirement for ALD to be self-limiting and able to saturate individual reactions therefore limits precursor choice to those capable of chemisorption with surface species.

When there are no plasma or energy enhanced methods used, the surface reactions are driven by thermal energy and the process is described as thermal ALD. The substrate temperature is therefore critical to ALD as it can affect the deposition in several ways. The deposition rate is limited by the finite number of reactive surface sites where the precursor molecules are able to adsorb. The concentration of reactive sites and reaction rates may decrease with decreasing temperature, resulting in less adsorption and lower deposition rates. [22–24] The temperature may also affect reaction mechanisms, typically enabling more reactions at higher temperatures and producing higher growth rates. High temperatures may also cause decomposition of precursors which may result in the adsorption of ligands to the surface, inhibiting reactions and incorporating impurities into the film. The deposition rate may also be unaffected by changes in temperature if the growth is self-saturating. This may occur if the deposition is limited by steric hindrance, which is the effect of the space occupied by the precursor molecules at the surface, as ligands block reactive surface sites from accepting other precursor molecules. Considering

that each of these mechanisms may affect the deposition rate within the same ALD process, the temperature range in which no change of growth per cycle (GPC) is observed is considered ideal ALD behavior and is known as the "ALD window", as shown in Fig. 1.1.

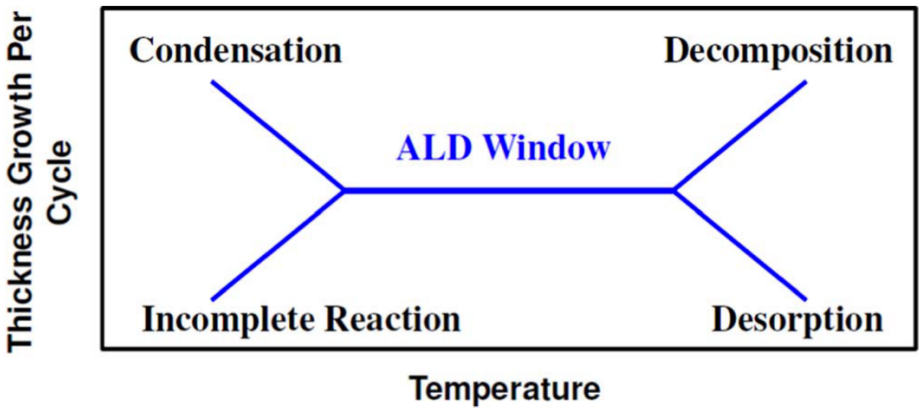

Figure 2.2 – Schematic of the "ALD Window" temperature range for ideal ALD behavior. Reprinted from Oehrlein, et al. [5]

2.2 Plasma Enhanced Atomic Layer Deposition

The use of plasma or energy enhanced species in the ALD process enables thin film deposition at significantly lower substrate temperatures compared to thermal ALD. Rather than thermal energy, the energy to drive reactions is provided by the reactivity of plasma species, primarily highly reactive radicals. Plasma enhanced ALD (PEALD) enables greater choice in precursors, increased growth rates, better control of film stoichiometry, and greater processing versatility. The use of plasma species expands available precursors as the reaction mechanisms are simplified compared to thermal reactants.

While thermal ALD typically requires substrate temperatures of approximately 150 - 500° C, PEALD processes enable deposition at significantly lower temperatures due to

the reactivity of the plasma species. PEALD of Ga_2O_3 has been performed at temperatures as low as 60°C. [25–27] Room temperature PEALD at temperatures as low as 25-35°C has been demonstrated for various materials, including Al_2O_3, ZnO, and Pt. [28–30]

Deposition of single-element materials such as Si, Ge, and Ti is possible through PEALD while thermal ALD of these materials remains elusive. [1,31] Surface reactions for these processes is greatly simplified by the use of plasma species to induce reactions which are not possible via thermal energy. The plasma species may effectively remove adsorbed precursor ligands to result in single-element deposition.

2.3 Atomic Layer Etching

Atomic layer etching (ALE) occurs in a process similar to ALD, involving sequential discrete exposures of vapor-phase reactants, which results in the removal of material from the substrate surface. ALE reactions are chosen to be highly selective and self-limiting, producing minimal to no damage to underlying material. A typical ALE process consists of two reactions: surface modification and selective removal, as shown in Fig. 1.2. The use of two discrete reactions for etching enables processes to minimize subsurface damage by limiting the reactive region to surface species.

2.3.1 Plasma-Based Atomic Layer Etching

The first proposed method of atomic layer etching appeared in a patent in 1988 detailing an etching system that used a plasma-enhanced process to etch diamond via sequential exposures of NO_2 and an energized mixture of H_2 and noble gases. [32] Plasma based ALE processes have since expanded to commercially available systems. Plasmas are commonly used due to the high reactivity of radicals produced as well as the momentum

of ions to eject material from the surface. Plasma based processes therefore rely on a combination of physical and chemical interactions to etch material through momentum transfer of incident ions and/or volatile product formation.

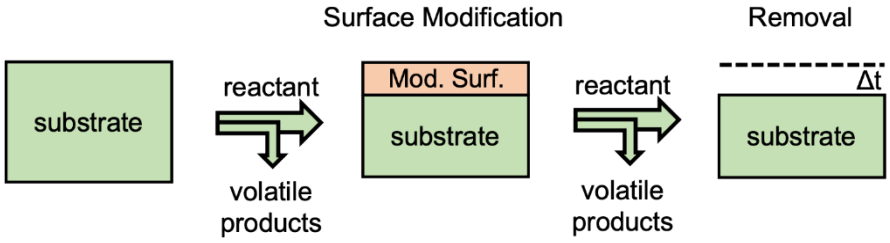

Figure 2.3 – Reaction schematic for a typical ALE process involving surface modification followed my material removal, resulting in a change of thickness Δt. The reactants may be either plasmas for plasma ALE or metal precursors in thermal ALE.

Halogen chemistries, specifically F- and Cl-based species, are commonly used for plasma ALE surface modification including F_2, Cl_2, SF_6, NF_3, CHF_3, BCl_3, and Cl_2. The highly reactive F and Cl interact with the surface to produce metal halides, some of which may be volatile and thermally desorb from the surface. They may also produce surface species with relatively low binding energy allowing for easier removal through a second reaction. [4,17] Etching using these halogen species has been demonstrated for many materials, including Si, Ge, C, W, Ta, Ru, SiO_2, AlN, and GaN. [5,8,17,33–36]

In plasma based ALE processes, the ideal operating conditions are known as the "ALE window", and are defined by the synergy,

$$ALE\ synergy\ (\%) = \frac{EPC - (\alpha + \beta)}{EPC} \times 100\%,$$

which represents the dependence of etching on the interaction of the two reactions, where EPC is the etch per cycle, and α and β are the etch rates of the individual half-reactions. The ALE synergy depends on the ion energy during the removal step, and the relation between etch rate and ion energy can be seen in Fig. 2.4. Ion energies below the ALE window result in incomplete removal of the modified surface and are therefore insufficient for etching. Within the ALE window, the etch rate does not increase with the ion energy. At ion energies above the ALE window, the process is dominated by physical sputtering.

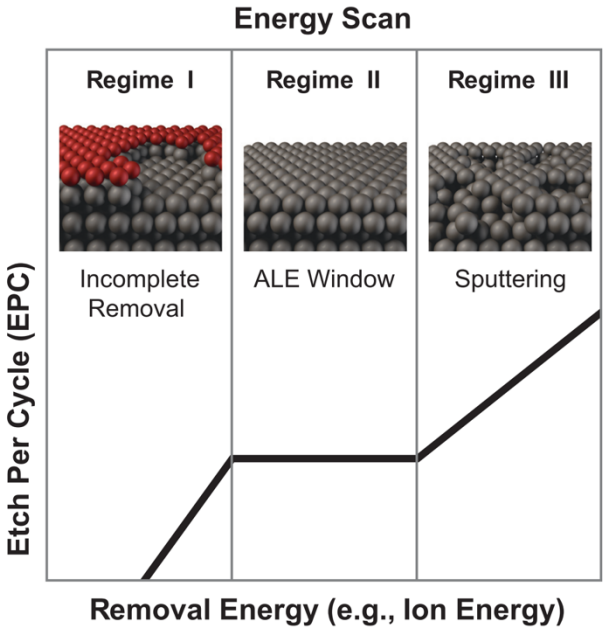

Figure 2.4 - Illustration of an energy scan for the ALE removal step. The ALE window in Regime II indicates the desirable operating range. Reprinted with permission from K.J. Kanarik, et al. [4] Copyright © 2015, American Vacuum Society

2.3.2 Thermal Atomic Layer Etching

ALE is also possible using thermochemical reactions via sequential exposures of gas or vapor phase reactants to remove material. Thermal ALE has been referred to as a reverse ALD process as the operation and reaction mechanisms are similar. Like plasma based or energy enhanced methods of ALE, thermal ALE is a multistep process involving surface modification followed by selective removal. The common mechanism for material removal is a ligand-exchange between the modified surface and a vapor-phase precursor which results in stable but volatile complexes that desorb from the surface. These reactions must be thermodynamically favorable and produce stable reactants that desorb from the surface at sufficient temperature. Similar to ALD, the self-limiting behavior of thermal ALE is determined by the saturation of etch rates from increasing the reactant exposure times.

The development of thermal ALE methods is a recent advancement which has gained significant interest in the materials community. In 2015, the Intel Etch team proposed ligand-exchange as a mechanism to form volatile products to desorb from substrate surfaces in a thermal ALE process. [8,35] The first reported method for thermal ALE appeared a year later, from Steven George's group at Colorado University-Boulder, and involved the use of HF and tin acetylacetonate [$Sn(acac)_2$] to etch Al_2O_3. [19] Trimethylaluminum [TMA, $Al(CH_3)_3$] was also found to be an effective precursor for the ligand-exchange reaction in etching Al_2O_3 at substrate temperatures above 250°C. [37,38] This is significant as TMA is commonly used as an Al precursor for Al_2O_3 ALD with H_2O, O_3, or O_2 plasma as the oxygen source. [22,39–41] These reactions using TMA therefore

permit the use of a single reaction chamber for both the ALD and ALE of Al_2O_3 using only TMA, HF and an oxygen source.

Fluorination and ligand-exchange has proven to be an effective mechanism for etching many materials, including Al_2O_3, Ga_2O_3, HfO_2, and ZnO_2. However, these reactions aren't favorable for all materials, which has led to development of various other mechanisms for ALE. For some materials, ALE is still possible using two-step processes such as oxidation and ligand-exchange or halogenation and ligand-exchange. [42,43] For select materials, the mechanisms are more complicated, requiring multiple steps in a conversion process to exploit ALE processes of other materials. A review of reported thermal ALE mechanisms was reported by George, [8] and a collection of ALE mechanisms are shown in Fig. 2.5.

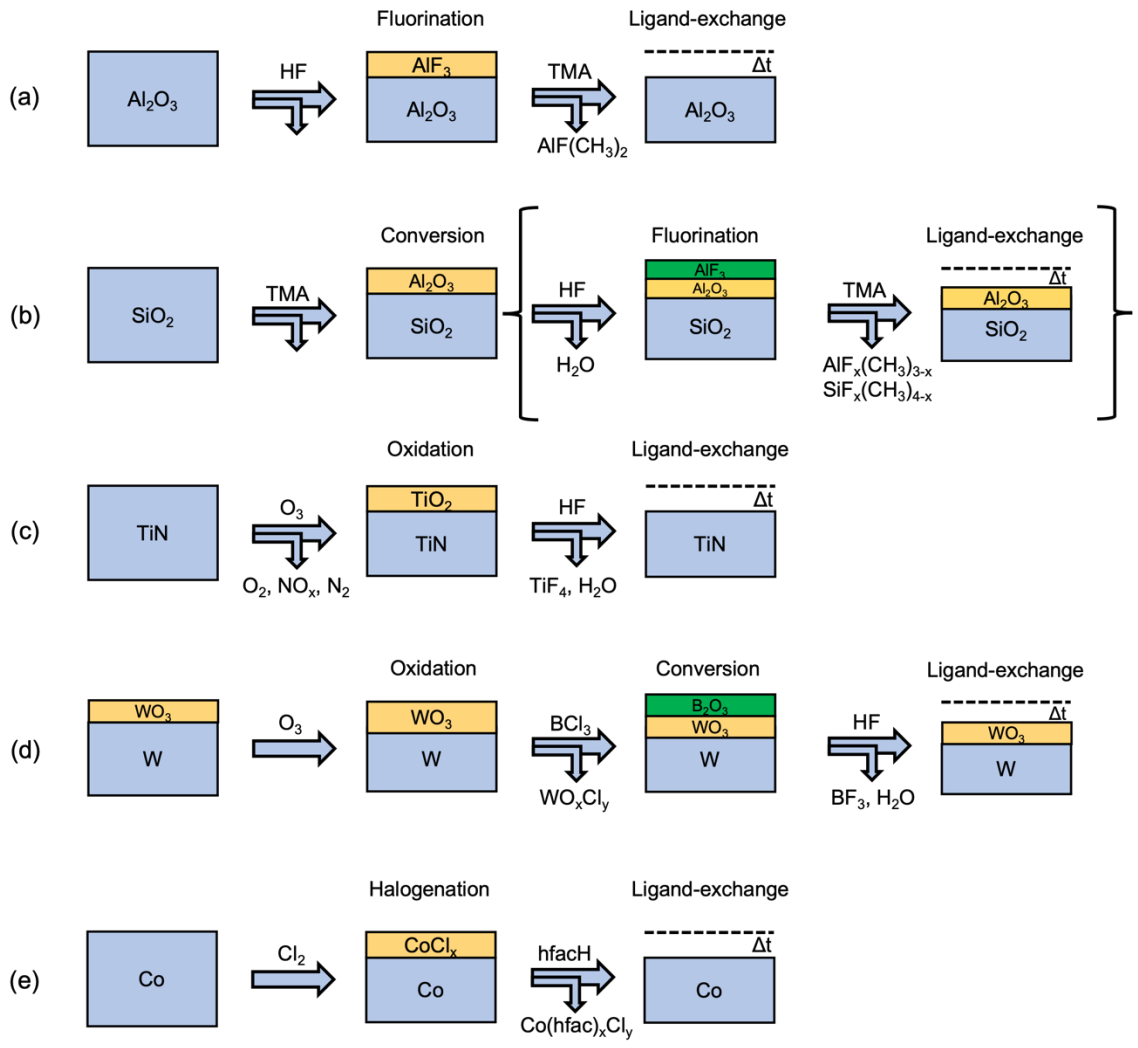

Figure 2.5 - Reaction schematics for ALE using various mechanisms, including; (a) fluorination and ligand-exchange to etch Al_2O_3 using HF and TMA; [37] (b) conversion etch of SiO_2 using TMA and HF; [44] (c) oxidation and ligand-exchange to etch TiN using O_3 and HF; [42] (d) oxidation, conversion, and ligand-exchange to etch W using O_3 BCl_3, and HF; [45] and (e) halogenation and ligand-exchange to etch Co using Cl_2 and hexafluoroacetylacetone (hfacH). [43]

Conversion etch mechanisms are typically used when etching by fluorination and ligand-exchange is not viable, or when fluorination leads to spontaneous etching. For SiO_2,

fluorination and ligand-exchange did not produce volatile etch products. [46] To circumvent this, the SiO_2 surface is converted to Al_2O_3, which may then be etched using HF and TMA. This process is shown in Fig. 2.5(b). An oxidation, conversion, and fluorination mechanism is used for ALE of tungsten. [47] First, oxidation by O_3 exposure increases the thickness of the native oxide WO_3. Then, the oxide surface is partially converted to B_2O_3. Fluorination by HF produces a volatile boron trifluoride (BF_3) which desorbs from the surface. This process is shown in Fig. 2.5(d).

Substrate temperature is critical to the etching behavior of these thermal processes due to the thermal volatility of the ligand-exchange products. Cyclic exposures of TMA and HF may be used to deposit AlF_3 by ALD at temperatures below 250°C, and etch AlF_3 or Al_2O_3 at temperatures above 250°C. [38] At low temperatures, desorption of reaction byproducts is incomplete or insufficient, resulting in accumulation at the surface. Higher temperatures may enable more reactions and produce greater desorption of reaction products typically resulting in higher etch rates. However, sufficiently high temperatures may result in decomposition and dissociation of the precursor molecules, thereby incorporating carbon and other impurities into the film, which inhibit surface reactions.

ALE using temperature modulation for desorption has also been demonstrated for Si_3N_4, Si, and MoS_2. [48–50] In these processes, the surfaces are first modified using a plasma exposure. Then, the modified surface is removed through thermal desorption at elevated temperatures. For both Si_3N_4 and Si, surface modification is used to form an ammonium salt layer of $(NH_4)_2SiF_6$, which is thermally desorbed by increasing the substrate temperature to 150 °C. Modification for Si_3N_4 occurs through exposure of a hydrofluorocarbon-based plasma mixture containing CF_4 at 20 °C. [48] For Si, the

modification occurs in two steps through an O_2 plasma to oxidize the surface followed by an NH_3/NF_3 plasma exposure to produce $(NH_4)_2SiF_6$. [49] For MoS_2, an O_2 plasma exposure at 200 °C is used to form an amorphous MoO_3 surface, which is then desorbed by increasing the temperature to 500 °C. [50]

While most studies in thermal ALE have been performed on amorphous ALD films, thermal ALE of crystalline metal nitrides has been reported, including AlN and GaN. [34,51] Murdzek, et al. investigated the effect of crystallinity on thermal ALE and have shown that amorphous and polycrystalline films of HfO_2 and ZrO_2 can be etched using HF and either dimethyl aluminum chloride (DMAC) or titanium tetrachloride ($TiCl_4$), although the etch rates were considerably smaller for the crystalline films. [52,53]

Using a combination of ALD and ALE processes may enable more controlled and selective processing through growth and etch back methods. For some materials, ultrathin films grown by ALD produce films with inconsistent thickness due to nucleation. ALE would enable ultrathin films by growing a thicker layer through ALD with lower roughness, then ALE could be employed to reduce thickness and smooth the surface. Additionally, selective-area ALD sometimes produces islands of growth in unwanted regions. ALE could be used to remove this unwanted material to improve selective-area depositions.

A discussion of ALD and ALE processing equipment may be found in Sect. 3.4.1, including a description of the processing systems used in the studies discussed in this dissertation.

REFERENCES

[1] S. M. George, *Atomic Layer Deposition: An Overview*, Chemical Reviews **110**, 111 (2010).

[2] H. Kim and I. K. Oh, *Review of Plasma-Enhanced Atomic Layer Deposition: Technical Enabler of Nanoscale Device Fabrication*, Japanese Journal of Applied Physics **53**, 0 (2014).

[3] K. Nojiri, K. J. Kanarik, S. Tan, E. A. Hudson, and R. A. Gottscho, *Atomic Layer Etching-Breaking Through the Limitation of Etch*, 1 (2018).

[4] K. J. Kanarik, T. Lill, E. A. Hudson, S. Sriraman, S. Tan, J. Marks, V. Vahedi, and R. A. Gottscho, *Overview of Atomic Layer Etching in the Semiconductor Industry*, Journal of Vacuum Science & Technology A: Vacuum, Surfaces, and Films **33**, 020802 (2015).

[5] G. S. Oehrlein, D. Metzler, and C. Li, *Atomic Layer Etching at the Tipping Point: An Overview*, ECS Journal of Solid State Science and Technology **4**, N5041 (2015).

[6] S. M. George and Y. Lee, *Prospects for Thermal Atomic Layer Etching Using Sequential, Self-Limiting Fluorination and Ligand-Exchange Reactions*, ACS Nano **10**, 4889 (2016).

[7] M. Kariniemi, J. Niinistö, M. Vehkamäki, M. Kemell, M. Ritala, M. Leskelä, and M. Putkonen, *Conformality of Remote Plasma-Enhanced Atomic Layer Deposition Processes: An Experimental Study*, Journal of Vacuum Science & Technology A:

Vacuum, Surfaces, and Films **30**, 01A115 (2012).

[8] S. M. George, *Mechanisms of Thermal Atomic Layer Etching*, Accounts of Chemical Research **53**, 1151 (2020).

[9] S. E. Potts, L. Schmalz, M. Fenker, B. Díaz, J. Światowska, V. Maurice, A. Seyeux, P. Marcus, G. Radnóczi, L. Tóth, and W. M. M. Kessels, *Ultra-Thin Aluminium Oxide Films Deposited by Plasma-Enhanced Atomic Layer Deposition for Corrosion Protection*, Journal of The Electrochemical Society **158**, C132 (2011).

[10] T. Lee, J. Ahn, J. Oh, Y. Kim, Y. B. Kim, D. K. Choi, and J. Jung, *Characterization of Ultra-Thin HfO_2 Gate Oxide Prepared by Using Atomic Layer Deposition*, Journal of the Korean Physical Society **42**, 272 (2003).

[11] P. D. Ye, G. D. Wilk, J. Kwo, B. Yang, H. J. L. Gossmann, M. Frei, S. N. G. Chu, J. P. Mannaerts, M. Sergent, M. Hong, K. K. Ng, and J. Bude, *GaAs MOSFET with Oxide Gate Dielectric Grown by Atomic Layer Deposition*, IEEE Electron Device Letters **24**, 209 (2003).

[12] Z. Ren, G. Yuan, J. Zhang, L. Xu, J. Zhang, W. Chen, and Y. Hao, *Hydrogen-Terminated Polycrystalline Diamond MOSFETs with Al_2O_3 Passivation Layers Grown by Atomic Layer Deposition at Different Temperatures*, AIP Advances **8**, 1 (2018).

[13] J. W. Elam, Z. A. Sechrist, and S. M. George, *ZnO/Al_2O_3 Nanolaminates Fabricated by Atomic Layer Deposition: Growth and Surface Roughness Measurements*, Thin Solid Films **414**, 43 (2002).

[14] H. Zhang and R. Solanki, *Atomic Layer Deposition of High Dielectric Constant Nanolaminates*, Journal of The Electrochemical Society **148**, F63 (2001).

[15] R. Zazpe, M. Ungureanu, F. Golmar, P. Stoliar, R. Llopis, F. Casanova, D. F. Pickup, C. Rogero, and L. E. Hueso, *Resistive Switching Dependence on Atomic Layer Deposition Parameters in HfO_2-Based Memory Devices*, Journal of Materials Chemistry C **2**, 3204 (2014).

[16] D. J. Lee, S. S. Yim, K. S. Kim, S. H. Kim, and K. B. Kim, *Nonvolatile Memory Characteristics of Atomic Layer Deposited Ru Nanocrystals with a SiO_2/Al_2O_3 Bilayered Tunnel Barrier*, Journal of Applied Physics **107**, (2010).

[17] K. J. Kanarik, S. Tan, and R. A. Gottscho, *Atomic Layer Etching: Rethinking the Art of Etch*, Journal of Physical Chemistry Letters **9**, 4814 (2018).

[18] K. J. Kanarik, S. Tan, J. Holland, A. Eppler, V. Vahedi, J. Marks, and R. A. Gottscho, *Moving Atomic Layer Etch from Lab to Fab*, Solid State Technology **56**, 14 (2013).

[19] Y. Lee, J. W. Dumont, and S. M. George, *Atomic Layer Etching of Al_2O_3 Using Sequential, Self-Limiting Thermal Reactions with $Sn(Acac)_2$ and Hydrogen Fluoride*, Journal of Physical Chemistry C **119**, 25385 (2015).

[20] H. B. Profijt, S. E. Potts, M. C. M. van de Sanden, and W. M. M. Kessels, *Plasma-Assisted Atomic Layer Deposition: Basics, Opportunities, and Challenges*, Journal of Vacuum Science & Technology A: Vacuum, Surfaces, and Films **29**, 050801 (2011).

[21] H. Kim, *Characteristics and Applications of Plasma Enhanced-Atomic Layer Deposition*, Thin Solid Films **519**, 6639 (2011).

[22] R. L. Puurunen, *Surface Chemistry of Atomic Layer Deposition: A Case Study for the Trimethylaluminum/Water Process*, Journal of Applied Physics **97**, (2005).

[23] R. L. Puurunen, T. A. Zeelie, and A. O. I. Krause, *Cobalt(III) Acetylacetonate Chemisorbed on Aluminum-Nitride-Modified Silica: Characteristics and Hydroformylation Activity*, Catalysis Letters **83**, 27 (2002).

[24] R. L. Puurunen, M. Lindblad, A. Rootc, and A. O. I. Krausea, *Successive Reactions of Gaseous Trimethylaluminium and Ammonia on Porous Alumina*, Physical Chemistry Chemical Physics **3**, 1093 (2001).

[25] I. Donmez, C. Ozgit-Akgun, and N. Biyikli, *Low Temperature Deposition of Ga_2O_3 Thin Films Using Trimethylgallium and Oxygen Plasma*, Journal of Vacuum Science & Technology A: Vacuum, Surfaces, and Films **31**, 01A110 (2013).

[26] R. O'Donoghue, J. Rechmann, M. Aghaee, D. Rogalla, H. W. Becker, M. Creatore, A. D. Wieck, and A. Devi, *Low Temperature Growth of Gallium Oxide Thin Films via Plasma Enhanced Atomic Layer Deposition*, Dalton Transactions **46**, 16551 (2017).

[27] A. Mahmoodinezhad, C. Janowitz, F. Naumann, P. Plate, H. Gargouri, K. Henkel, D. Schmeißer, and J. I. Flege, *Low-Temperature Growth of Gallium Oxide Thin Films by Plasma-Enhanced Atomic Layer Deposition*, Journal of Vacuum Science & Technology A **38**, 022404 (2020).

[28] A. Singh, A. Mathur, D. Pal, A. Sengupta, R. Singh, and S. Chattopadhyay, *Near Room Temperature Atomic Layer Deposition of ZnO Thin Films on Poly (Methyl Methacrylate) (PMMA) Templates: A Study of Structure, Morphology and Photoluminescence of ZnO as an Effect of Template Confinement*, Vacuum **161**, 398 (2019).

[29] M. Kot, C. Das, Z. Wang, K. Henkel, Z. Rouissi, K. Wojciechowski, H. J. Snaith, and D. Schmeisser, *Room-Temperature Atomic Layer Deposition of Al_2O_3: Impact on Efficiency, Stability and Surface Properties in Perovskite Solar Cells*, ChemSusChem **9**, 3401 (2016).

[30] A. J. M. MacKus, D. Garcia-Alonso, H. C. M. Knoops, A. A. Bol, and W. M. M. Kessels, *Room-Temperature Atomic Layer Deposition of Platinum*, Chemistry of Materials **25**, 1769 (2013).

[31] H. Kim, *Atomic Layer Deposition of Metal and Nitride Thin Films: Current Research Efforts and Applications for Semiconductor Device Processing*, Journal of Vacuum Science & Technology B: Microelectronics and Nanometer Structures **21**, 2231 (2003).

[32] M. N. Yoder, *Atomic Layer Etching*, U.S. Patent No. 4756794 (1988).

[33] T. Ohba, W. Yang, S. Tan, K. J. Kanarik, and K. Nojiri, *Atomic Layer Etching of GaN and AlGaN Using Directional Plasma-Enhanced Approach*, Japanese Journal of Applied Physics **56**, (2017).

[34] N. R. Johnson, J. K. Hite, M. A. Mastro, C. R. Eddy, and S. M. George, *Thermal Atomic Layer Etching of Crystalline GaN Using Sequential Exposures of XeF_2 and*

BCl_3, Applied Physics Letters **114**, (2019).

[35] C. T. Carver, J. J. Plombon, P. E. Romero, S. Suri, T. A. Tronic, and R. B. Turkot, *Atomic Layer Etching: An Industry Perspective*, ECS Journal of Solid State Science and Technology **4**, N5005 (2015).

[36] R. Rahman, E. C. Mattson, J. P. Klesko, A. Dangerfield, S. Rivillon-Amy, D. C. Smith, D. Hausmann, and Y. J. Chabal, *Thermal Atomic Layer Etching of Silica and Alumina Thin Films Using Trimethylaluminum with Hydrogen Fluoride or Fluoroform*, ACS Applied Materials and Interfaces **10**, 31784 (2018).

[37] Y. Lee, J. W. Dumont, and S. M. George, *Trimethylaluminum as the Metal Precursor for the Atomic Layer Etching of Al_2O_3 Using Sequential, Self-Limiting Thermal Reactions*, Chemistry of Materials **28**, 2994 (2016).

[38] J. W. DuMont and S. M. George, *Competition between Al_2O_3 Atomic Layer Etching and AlF_3 Atomic Layer Deposition Using Sequential Exposures of Trimethylaluminum and Hydrogen Fluoride*, Journal of Chemical Physics **146**, (2017).

[39] S. B. S. Heil, J. L. Van Hemmen, M. C. M. Van De Sanden, and W. M. M. Kessels, *Reaction Mechanisms during Plasma-Assisted Atomic Layer Deposition of Metal Oxides: A Case Study for Al_2O_3*, Journal of Applied Physics **103**, (2008).

[40] S. B. S. Heil, P. Kudlacek, E. Langereis, R. Engeln, M. C. M. Van De Sanden, and W. M. M. Kessels, *In Situ Reaction Mechanism Studies of Plasma-Assisted Atomic Layer Deposition of Al_2O_3*, Applied Physics Letters **89**, 1 (2006).

[41] D. N. Goldstein, J. A. McCormick, and S. M. George, *Al_2O_3 Atomic Layer Deposition with Trimethylaluminum and Ozone Studied by in Situ Transmission FTIR Spectroscopy and Quadrupole Mass Spectrometry*, Journal of Physical Chemistry C **112**, 19530 (2008).

[42] Y. Lee and S. M. George, *Thermal Atomic Layer Etching of Titanium Nitride Using Sequential, Self-Limiting Reactions: Oxidation to TiO_2 and Fluorination to Volatile TiF_4*, Chemistry of Materials **29**, 8202 (2017).

[43] M. Konh, C. He, X. Lin, X. Guo, V. Pallem, R. L. Opila, A. V. Teplyakov, Z. Wang, and B. Yuan, *Molecular Mechanisms of Atomic Layer Etching of Cobalt with Sequential Exposure to Molecular Chlorine and Diketones*, Journal of Vacuum Science & Technology A **37**, 021004 (2019).

[44] A. I. Abdulagatov and S. M. George, *Thermal Atomic Layer Etching of Silicon Using O_2, HF, and $Al(CH_3)_3$ as the Reactants*, Chemistry of Materials **30**, 8465 (2018).

[45] U. Kilic, A. Mock, D. Sekora, S. Gilbert, S. Valloppilly, N. Ianno, M. Langell, E. Schubert, and M. Schubert, *Precursor-Surface Interactions Revealed during Plasma-Enhanced Atomic Layer Deposition of Metal Oxide Thin Films by in-Situ Spectroscopic Ellipsometry*, Scientific Reports **10**, 1 (2020).

[46] J. W. DuMont, A. E. Marquardt, A. M. Cano, and S. M. George, *Thermal Atomic Layer Etching of SiO_2 by a "Conversion-Etch" Mechanism Using Sequential Reactions of Trimethylaluminum and Hydrogen Fluoride*, ACS Applied Materials and Interfaces **9**, 10296 (2017).

[47] N. R. Johnson and S. M. George, *WO_3 and W Thermal Atomic Layer Etching Using "Conversion-Fluorination" and "Oxidation-Conversion-Fluorination" Mechanisms*, ACS Applied Materials and Interfaces **9**, 34435 (2017).

[48] N. Miyoshi, H. Kobayashi, K. Shinoda, M. Kurihara, T. Watanabe, Y. Kouzuma, K. Yokogawa, S. Sakai, and M. Izawa, *Atomic Layer Etching of Silicon Nitride Using Infrared Annealing for Short Desorption Time of Ammonium Fluorosilicate*, Japanese Journal of Applied Physics **56**, (2017).

[49] E. J. Song, J. H. Kim, J. D. Kwon, S. H. Kwon, and J. H. Ahn, *Silicon Atomic Layer Etching by Two-Step Plasma Process Consisting of Oxidation and Modification to Form $(NH_4)_2SiF_6$, and Its Sublimation*, Japanese Journal of Applied Physics **57**, (2018).

[50] H. Zhu, X. Qin, L. Cheng, A. Azcatl, J. Kim, and R. M. Wallace, *Remote Plasma Oxidation and Atomic Layer Etching of MoS_2*, ACS Applied Materials and Interfaces **8**, 19119 (2016).

[51] N. R. Johnson, H. Sun, K. Sharma, and S. M. George, *Thermal Atomic Layer Etching of Crystalline Aluminum Nitride Using Sequential, Self-Limiting Hydrogen Fluoride and $Sn(Acac)_2$ Reactions and Enhancement by H_2 and Ar Plasmas*, Journal of Vacuum Science & Technology A: Vacuum, Surfaces, and Films **34**, 050603 (2016).

[52] J. A. Murdzek and S. M. George, *Thermal Atomic Layer Etching of Amorphous and Crystalline Hafnium Oxide, Zirconium Oxide, and Hafnium Zirconium Oxide*, 2019 International Symposium on VLSI Technology, Systems and Application

(VLSI-TSA) **38**, 1 (2019).

[53] J. A. Murdzek and S. M. George, *Effect of Crystallinity on Thermal Atomic Layer Etching of Hafnium Oxide, Zirconium Oxide, and Hafnium Zirconium Oxide*, Journal of Vacuum Science & Technology A **38**, 022608 (2020).

CHAPTER III

EXPERIMENTAL METHODS

3.1 Introduction

In this chapter, I will detail the methods used in the following studies as well as unsuccessful efforts in the development of atomic layer etching and surface passivation methods for GaN. These studies utilized a variety of techniques for characterization, including XPS and ellipsometry, as well as thin film processing, including atomic layer deposition, atomic layer etching, molecular beam epitaxy, and electron cyclotron resonance plasma processing.

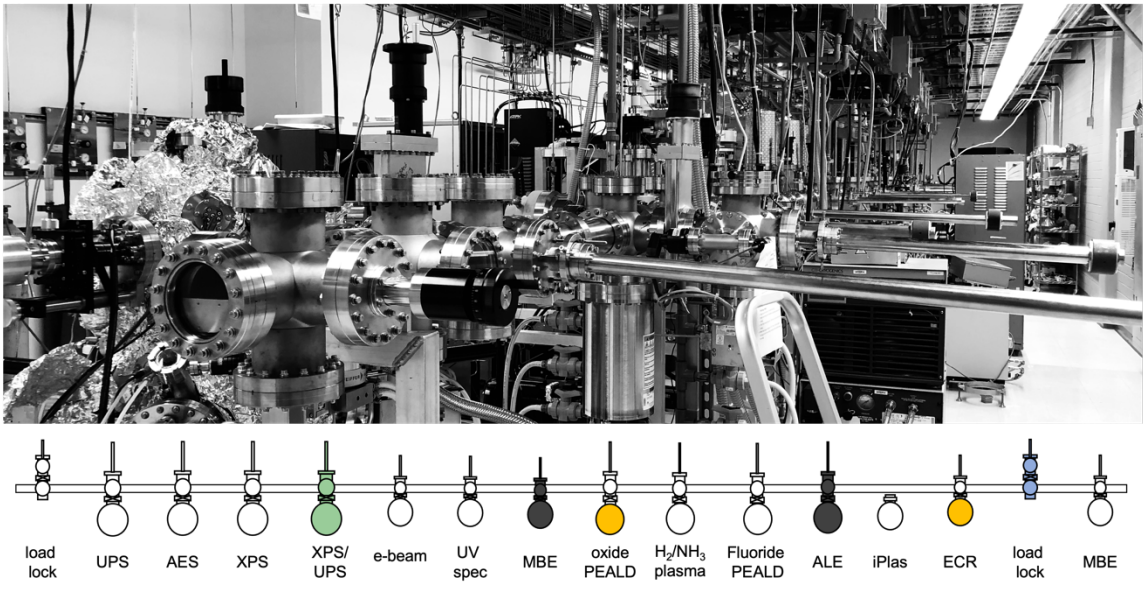

Figure 3.1 – (a) image and (b) schematic of the UHV processing and characterization systems in the Nanoscience Lab at ASU (color available online).

The primary facility used in this study is shown in Fig. 3.1, with processing and characterization performed using a stainless steel multi-chamber system referred to as the

"transfer line". The systems used in these studies are highlighted by color. All systems, including the transfer line, are maintained at ultra-high vacuum (UHV) pressures to minimize contamination by atmospheric exposure between processing and characterization procedures. The system shaded in blue, labeled "load lock", was used for transferring samples from atmosphere to the UHV transfer line. The samples are then transported using a cart and pulley system. Samples may be transferred between the cart and each processing and characterization system using rods with a magnetic arm that extend into each system. Manually controlled gate valves are placed between each system and the transfer line. The green system labeled "XPS/UPS" was used for characterization throughout all studies and is described in section 3.2. The systems shaded black, labeled "MBE" and "ALE", were the primary processing chambers used in the studies reported in chapter 4 through chapter 6 of this document, and are described in sections 2.4 and 3.4.1. The systems shaded yellow and labeled, "oxide PEALD" and "ECR", were used for N_2 plasma processing as well as an independent study of plasma-based atomic layer etching of GaN described in sections 2.4, 3.4.1, and 3.5.2.

3.2 Photoelectron Spectroscopy

3.2.1 Principles of Photoelectron Spectroscopy

Photoelectron spectroscopy or photoemission spectroscopy (PES) is an application of the photoelectric effect. The photoelectric effect was first observed by Heinrich Hertz as electrons emitted from a metal surface when irradiated by ultraviolet light. [1] Albert Einstein later developed (1905) a more formal description, using the Planck postulate, [2] in which Einstein postulated the existence of light quanta, which could be absorbed by an

electron, transferring energy to the electron and causing it to be emitted from the surface of a material. [3] The understanding of this phenomenon was improved further by H.Y. Fan, *et al*. in 1945 when they showed that momentum could be conserved in a bulk optical transition by scattering the photoelectron off the periodic potential of the lattice. [4] Then, in 1958, a full description of the photoemission process was developed and published by William Spicer. [5] This model suggested photoemission could be described in a three step process. First, the photon is absorbed by an electron. Then, the electron transport through the solid with energy losses due to scattering processes. Lastly, the electron escapes the surface barrier.

PES was realized in the 1960's due in part to major developments in vacuum technology and monochromatic light sources. Berglund and Spicer were instrumental in the development of the technique and understanding of PES, and showed d bands of Cu and Ag measured by PES for the first time.[4],[5] Much of the early work had been done using ultraviolet (UV) sources as they're sufficient for photoemission of shallow electrons near the valence band. This technique is known today as ultraviolet photoelectron spectroscopy (UPS). Kai Siegbahn and colleagues reported results in which x-ray sources ($h\nu \approx 1500$ eV) were used to study core level electrons. [8] Siegbahn named this technique electron spectroscopy for chemical analysis (ESCA), but today it is known as x-ray photoelectron spectroscopy (XPS).

Due to conservation of energy, the kinetic energy of the emitted electron is given by Einstein's relation, [3]

$$E_k = h\nu - E_b - \phi,$$

where ν is the photon frequency, E_b is the binding energy of the emitted electron, and ϕ is the work function and is defined as the minimum energy required to liberate an electron from the material. It then follows that the binding energy of the photoelectron from the material may be determined from the measured kinetic energy. A diagram of these energy transitions is shown in Fig. 3.2.

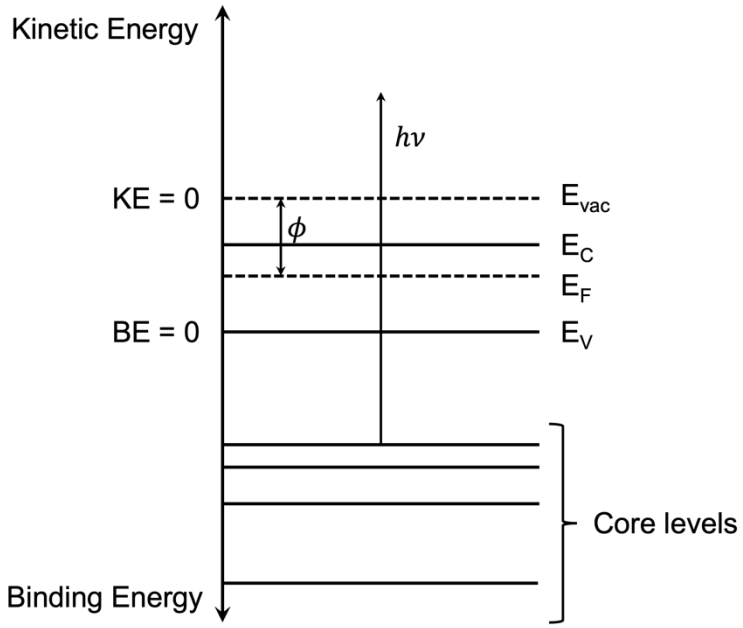

Figure 3.2 - Energy diagram of a photoelectron emitted from a semiconductor with energy hν. The binding energy of emitted electrons may be deduced using the measured kinetic energy and conservation of energy from Einstein's relation.

The depth of emitted electrons is limited not by the x-ray penetration depth but the ability of the electrons to exit the surface. This is limited by energy loss from scattering processes within the material and the probability of emission goes as $e^{-x/L(E)}$, where x is the depth of the excited electron and L(E) is the scattering length dependent on the electron energy E.

After high-energy light, or electron bombardment, raises a system to an ionized state, relaxation may result in a doubly ionized state by the Auger effect in which an additional electron is emitted to compensate for energy loss between orbital transitions. This occurs due to an unstable state after emission of the initial core electron. An electron from an outer shell may relax into the vacancy created, losing energy equal to the difference of energies between the two orbitals. This transition energy may sometimes be coupled to another outer shell electron ,which may then be emitted if the energy is sufficient. An example of an Auger transition is shown in Fig. 3.3. Although better known for her work in nuclear fission, Lise Meitner was the first to measure electrons emitted by this effect and reported on this in 1922.[8],[9] Pierre Auger then also measured and reported this phenomenon in 1923 and is more commonly credited for the discovery. [11]

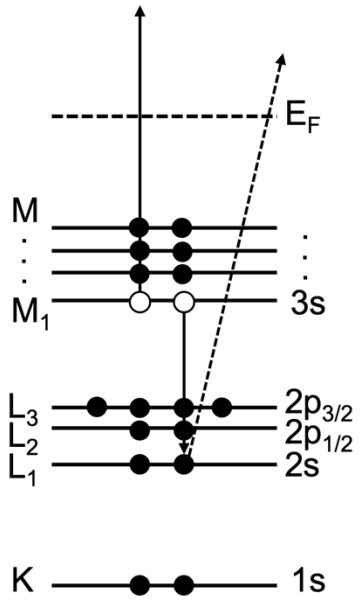

Figure 3.3 - Energy diagram of an LMM Auger transition. After an electron has been excited from the L_1 (2s), the system relaxes by the decay of an M1 (3s) electron to fill the vacancy in L_1 (2s). The transition energy is coupled to another electron, which is then emitted from M_1 (3s).

Auger electrons are identified by the electron orbitals involved in the Auger transition. An example of an LMM Auger transition is shown in Fig. 3.3 in which an L_1 (2s) electron is emitted. The system relaxes through an electron transition from the M_1 (3s) band transitioning to the L_1 (2s) band vacated by the emitted electron. The transition energy is then coupled to another outer shell electron, which is emitted if the energy is sufficient. Auger electron energies are independent of x-ray source or photon energy as the phenomenon is dependent only on the core level energies.

Spin-orbit coupling arises from the interaction between an electron's spin and its orbital momentum about the nucleus. This electromagnetic interaction causes shifts in the

electron energy levels, resulting in a discrete splitting of the electron orbital. The splitting of these core energy levels is observed in the binding energies measured of emitted electrons. Identification of core levels in XPS uses the convention nl_j, where n is the principal quantum number, l is the angular momentum quantum number, and $j = l + s$, where $s = \pm\frac{1}{2}$ is the spin angular momentum. An XPS scan of Si 2p is shown in Fig. 3.4. Within the spectrum, two peaks corresponding to elemental silicon are observed with binding energies centered at 99.7 eV and 100.3 eV. The presence of these two peaks is due to spin-orbit splitting of the 2p orbital with $j = \frac{1}{2}, \frac{3}{2}$.

Measured binding energies are not solely determined by atomic levels but also dependent on chemical environment. Atomic bonds shift the binding energy of core level electrons, which may be considered surprising because core level electrons are not involved in the bonding process. These chemical shifts are related to the oxidation state or effective charge of the atom. It has been observed that increasing positive charge of the atom increases the binding energy of the atom.[8],[12]

There are three peaks observed in the Si 2p spectrum of a Si wafer shown in Fig. 3.4. The peaks centered at binding energies of 99.7 eV and 100.3 eV are resultant of spin-orbit splitting of the Si 2p core level. A third peak is observed centered at binding energy of 103.6 eV. This core level is known to be from the Si-O bond in the native oxide layer. This core level is also from the Si 2p spectra, however, the difference in binding energy from the elemental Si is due to a chemical shift resulting from the effective charge of the Si. For elemental Si the oxidation state is 0 (or Si^0), whereas Si bonded to oxygen has an

oxidation state of 4 (or Si^{4+}). The larger positive effective charge on the Si atom produces higher binding energy of the Si 2p electron.

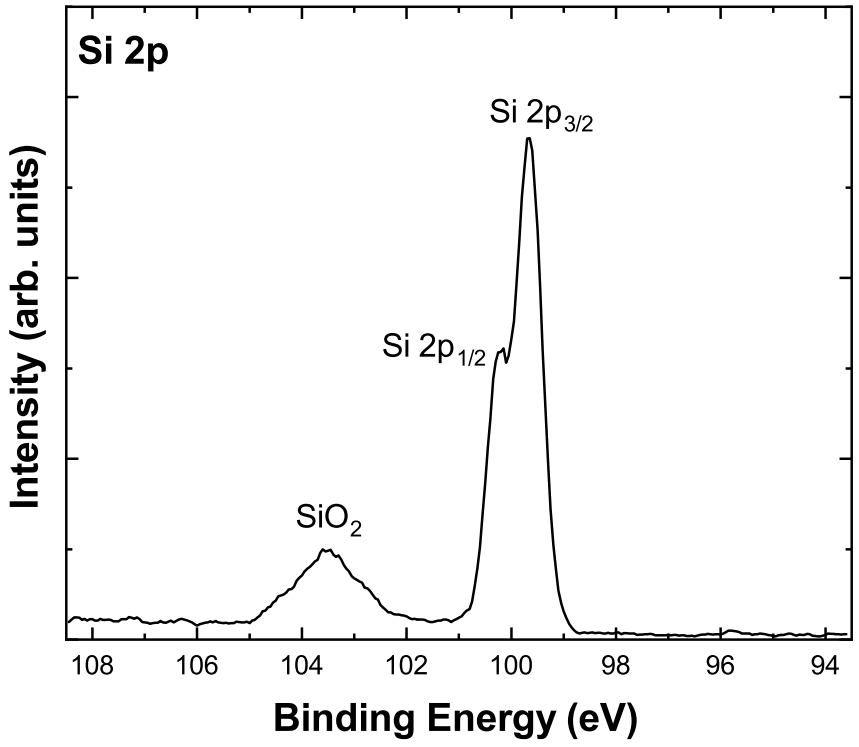

Figure 3.4 - Si 2p XPS scan of a Si wafer with native surface oxide. Three peaks are observed due to spin-orbit splitting and chemical bonding. These peaks correspond to Si $2p_{1/2}$, Si $2p_{3/2}$, and Si-O 2p.

Because PES is a surface characterization technique, it is critical to consider the effect of the surface on energy level positions. Bulk electron energy bands arise due to periodic translational symmetry throughout the crystal lattice. The surface is effectively a termination of the lattice and therefore a break in this symmetry. This produces several effects through the presence of dangling bonds, surface states, and surface adsorbates.

These conditions produce band bending at the surfaces of semiconductors through the formation of a depletion region due to poor screening of the surface charge-induced electric field. Poor screening is a result of the low free electron density in semiconductors, typically ~10^{17} cm^{-3}, depending on doping levels, requiring screening lengths on the order of ~10 nm. Conversely, the free electron density in metals is ~10^{22} cm^{-3}, producing short screening of a few atomic lengths. [13] Surface states may be present within the band gap and can affect band banding and cause Fermi level pinning. Surface adsorbates may also screen or compensate field-effects, further affecting band bending.

Band bending affects XPS core level positions and thus can be determined by XPS measurements using a method determined by Waldrop, Grant [14] and Kraut, et al. [15] by the relation,

$$\phi_{BB} = (E_{CL} - E_V)_{bulk} + E_g - E_C - E_{CL,XPS}$$

where E_g is the semiconductor bandgap, E_C is the conduction band position relative to the fermi level, $(E_{CL} - E_V)_{bulk}$ is the energy spacing of the valence band from a core level in the bulk material, and $E_{CL,XPS}$ is the position of that core level as measured by XPS. Band bending measurements from XPS are further discussed in chapter 6, "External Charge Compensation in Etched Gallium Nitride Measured by X-ray Photoelectron Spectroscopy.

Alternatively, band bending may also be deduced from UPS measurements, with the relation

$$\phi_{BB} = E_g - E_C - VBM$$

where the VBM is determined from the binding energy cutoff as measured by UPS.

Accurate spacing of the bulk Fermi level E_F and conduction band E_C is necessary for determination of band bending from PES measurements. E_F position may be determined from the doping concentration N_D of a nondegenerate semiconductor from the relation, [16]

$$(E_C - E_F) = kT \ln (\mathrm{N_C}/\mathrm{N_D}),$$

where k is the Boltzmann constant and N_C is the effective density of states at the conduction band.

Estimation of surface atomic percentage (at. %) from XPS peaks is an essential application of XPS. From theory, [17] the spectral peak area of a given surface element measured by XPS is

$$I = nf\sigma\phi yAT\lambda,$$

where n is the number of atoms of a given element per cm^3 of the surface, f is the x-ray flux, σ is the photoelectric cross-section, ϕ is an angular correction factor, y is a photoelectric ground state efficiency factor, A is the area from which photoelectrons are detected, and T is the efficiency of detection of emitted photoelectrons of the energy by the analyzer. The density of a given surface element measured by XPS can thus be given by

$$n = \frac{I}{f\sigma\phi yAT\lambda'},$$

where the denominator is typically represented by an "atomic sensitivity factor",

$$S = f\sigma\phi yAT\lambda.$$

Atomic sensitivity factors have been calculated from first principles calculations and empirically derived from experiment. This study used empirically derived sensitivity factors from Wagner, *et al*. [18]

Atomic concentration of each surface element present can then be found as a fraction of total surface composition, calculated by considering contribution of each surface species,

$$\sigma_a = \frac{I_a/S_a}{\frac{I_1}{S_1} + \frac{I_2}{S_2} + \frac{I_3}{S_3} + \cdots} = \frac{I_a/S_a}{\sum_i \frac{I_i}{S_i}}.$$

Native oxides on GaN are often present which affect signal intensity of the basis elements. Oxygen coverage is defined as the number of adsorbed oxygen atoms at the (0001) surface, where one monolayer (ml) corresponds to one oxygen atom per surface lattice site. The oxygen coverage on GaN was calculated from XPS intensities using the following relation, [19]

$$\Theta_O = \frac{I_O S_{Ga}}{S_0 I_{Ga}} \sum_{n=0}^{\infty} \exp\left[-\frac{n d_{GaN}}{\lambda_{Ga}\, cos[\phi]}\right],$$

where I_O and I_{Ga} are the integrated intensity of the O 1s and Ga 3d core level peaks, S_O and S_{Ga} are the atomic sensitivity factors for O 1s and Ga 3d electrons (0.66 and 0.31), [17] d_{GaN} is the distance between two GaN planes (2.6 Å), λ_{Ga} is the inelastic mean free path (IMFP = 2.4 nm) of Ga 3d electrons with kinetic energies ~1450 eV, and $\phi = 0$ is the angle to the detector.

3.2.2 XPS Equipment

X-rays are produced by electron bombardment of a metal anode, typically composed of aluminum (Al) or magnesium (Mg). For either source, the electron transition relevant to x-ray formation is the transition from 2p to 1s, referred to as the Kα transition. This produces photons of energy 1486.6 eV for Al Kα and 1253.6 eV for Mg Kα. A monochromator may be used to improve resolution of the incident x-rays through diffraction with a series of quartz crystals.

A hemispherical analyzer collects emitted electrons through an entrance slit and directs them through a series of magnetic lenses to focus the incoming electron beam. Electrostatic forces are used to retard the kinetic energy of the electrons to limit only electrons of a desired "pass energy" to be collected. The analyzer slit size and pass energy contribute to the resolution of the measured spectra.

The XPS (VG-Scienta, R3000) in this study was performed using an Al Kα x-ray source which produced an x-ray spot size of approximately 1 mm x 7mm at the sample surface and monochromatic photon energy of 1486.6 ± 0.2 eV. An analyzer pass energy of 100 eV and slit size of 0.4 mm were used for these studies, enabling energy resolution of ± 0.15 eV. However, spectral fitting can resolve the binding energy positions to ± 0.1 eV. The signal was collected using the manufacturer supplied software (VG-Scienta, SES) and a step size of 0.05 eV was used. Pressure was maintained below $7x10^{-10}$ Torr during measurements.

3.3 Multi-Wavelength Ellipsometry

3.3.1 Principles of Ellipsometry

Ellipsometry is an optical technique using changes in the polarization of light to determine thickness and optical properties of epitaxial films. This technique uses linearly polarized light incident on a film where it may interact with the material structure through reflection, absorption, transmission, or scattering. A polarization state detector (PSD) is used to measure the polarization of the collected light. The polarization state of a plane wave may be fully described by its four-dimensional Stokes vector,

$$\boldsymbol{S} = \begin{pmatrix} S_0 \\ S_1 \\ S_2 \\ S_3 \end{pmatrix} = \begin{pmatrix} I_{0^\circ} + I_{90^\circ} \\ I_{0^\circ} - I_{90^\circ} \\ I_{45^\circ} - I_{45^\circ} \\ I_R - I_L \end{pmatrix},$$

where I_{0°, I_{90°, I_{45°, and I_{-45° are measured intensities of a plane wave after passing through linear polarizers with azimuthal angles, 0°, 90°, 45°, and -45°. I_R and I_L are the intensities of a plane wave after passing through right and left circular polarizers.[20],[21]

Although the Stokes parameters are defined here using six measured intensities, they may be determined using only four measured intensities. The division of amplitudes polarimeter (DOAP) method uses a beam splitter to simultaneously acquire four intensities of light with photodetectors. The measurement of these four intensities allows simultaneous determination of all four Stokes parameters using the relation,

$$\boldsymbol{S} = \begin{pmatrix} S_0 \\ S_1 \\ S_2 \\ S_3 \end{pmatrix} = \boldsymbol{A}^{-1} \begin{pmatrix} I_1 \\ I_2 \\ I_3 \\ I_4 \end{pmatrix},$$

where

$$\boldsymbol{A} = \frac{1}{2}\begin{pmatrix} R & -R\cos 2\Psi_r & R\cos\Delta_r \sin 2\Psi_r & R\sin\Delta_r \sin 2\Psi_r \\ R & -R\cos 2\Psi_r & -R\cos\Delta_r \sin 2\Psi_r & -R\sin\Delta_r \sin 2\Psi_r \\ T & -T\cos 2\Psi_t & -T\cos\Delta_t \sin 2\Psi_t & T\sin\Delta_t \sin 2\Psi_t \\ T & -T\cos 2\Psi_t & -T\cos\Delta_t \sin 2\Psi_t & -T\sin\Delta_t \sin 2\Psi_t \end{pmatrix}.$$

Here, R and T are the reflectance and transmittance, respectively. Δ_r and Ψ_r are defined as,

$$tan(\Psi_r)\, exp(i\Delta_r) = \frac{r_p}{r_s},$$

where r_p and r_s are the reflection coefficients for p-polarized (parallel to the plane of incidence) and s-polarized (perpendicular to the plane of incidence) light, respectively. [20],[21] It has been determined that Δ_r the ellipsometric angle, is more sensitive to changes in surface conditions. [22]

3.3.2 Multi-Wavelength Ellipsometry Equipment

The studies described in this dissertation used an *in situ* multi-wavelength ellipsometer (MWE) (Film Sense, FS-1) mounted onto the chamber viewports at a 45° angle to the sample surface for dynamic measurements of film thickness throughout deposition and etching. The MWE has four light emitting diodes (LED) that produce light at four wavelengths centered at 465nm, 525nm, 580nm, and 635nm. The polarization state of the reflected beams was determined using the division of amplitude polarimeter (DOAP) method for simultaneous measurement of all four Stokes parameters. Data was collected using manufacturer supplied software, Film Sense desktop version 1.15 with measurements taken at 1 s intervals. The thickness of GaN films >500 nm can not be resolved using this MWE. Ellipsometry measurements for these samples are then given in terms of the optical

parameter Δ for the blue LED wavelength since Δ is the parameter most sensitive to surface conditions.

3.4 Processing Methods

3.4.1 Atomic Layer Deposition and Etching Equipment

Atomic layer deposition and etching in these studies was performed using a custom-built stainless steel hot-wall reactor. A detailed description of the chamber construction can be found in Daniel Messina's dissertation. A schematic of the system is shown in Fig. 3.5. Chamber walls and precursor tubing were maintained at 100 °C to prevent precursor condensation. A turbomolecular pump (Pfeiffer, HiPace 80) backed by a dry roots pump (Pfeiffer, ACP 15) was used to reach a base pressure of $2x10^{-8}$ Torr for UHV sample transfer. During processing, a two-stage dry roots pump (Ebara, A70W) was used to achieve a base pressure of $4x10^{-5}$ Torr. A N_2 (99.998% purity) dilution flow with a flow rate of 14.2 slm was used to ensure longevity of the process pump. Reactor pressure was dynamically controlled using an exhaust throttling valve (MKS, 253B), a capacitance manometer (MKS, 627F), and a PID controller (MKS, 651C).

The system was equipped with precursors, trimethylgallium (TMG, $Ga(CH_3)_3$) (STREM, 97% purity) and hydrogen fluoride-pyridine (HF-P, $C_5H_5N\cdot(HF)_x$) (Alfa-Aesar, 70 % HF by weight). Processing gases used in the system included O_2 (Matheson Tri-gas, 99.9999 % purity), N_2 (Matheson Tri-gas, 99.9999 % purity), and Ar (Matheson Tri-gas, 99.9999 % purity). Precursors were dosed into an Ar carrier gas (5 sccm) and N_2 (30 sccm) was used as the purge gas during ALD and ALE processes. Timing of precursor delivery is essential and enabled by the use of mass flow controllers (MKS, GE50A) and pneumatic

valves controlled through computer control with a real-time machine. Computer control of precursor delivery was enabled using a custom LabVIEW program.

The system is capable of generating remote radio frequency (rf) inductively coupled plasma (ICP) using a 13.56 MHz rf generator (MKS, Elite 300), a 50 Ω impedance matching network (MKS, MWH-05), and a 13-turn copper coil around a 32 mm diameter fused quartz tube. The quartz tube extended into the reactor at a distance of ~25 cm above the sample surfaces. This enables remote generation of an rf plasma with limited ion components at the surface and high concentrations of plasma generated radicals.

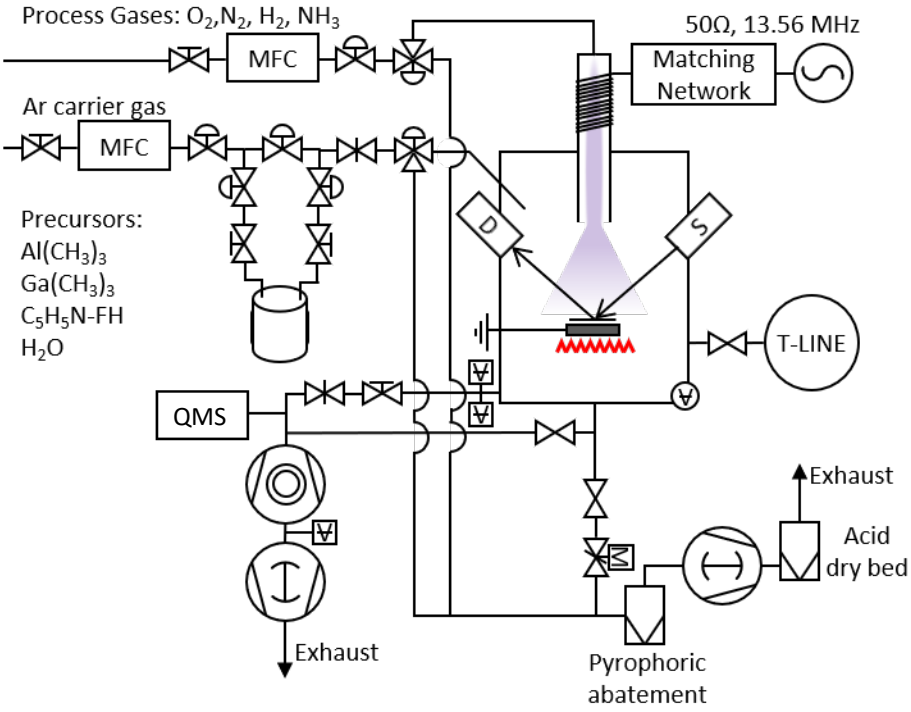

Figure 3.5 - a schematic of the custom-built atomic layer deposition and atomic layer etching chamber in the Nanoscience Lab at Arizona State University. Precursor delivery occurs through the operation of mass flow controllers and pneumatically controlled valves.

3.4.2 Electron Cyclotron Resonance

For these studies, plasma processing was performed on GaN samples using electron cyclotron resonance (ECR) microwave plasma. The ECR excitation process is explained by the Lorentz force. Free electrons in a large magnetic field will move in a circular path called cyclotron motion with an angular frequency,

$$\omega_c = \frac{eB}{m_e}.$$

This is called the electron cyclotron frequency. The electromagnetic force causing this motion is proportional to the excitation frequency of the magnetic field. Microwaves are injected into the chamber at a frequency corresponding with the electron cyclotron frequency, producing electron cyclotron resonance (ECR). This energizes the free electrons within the gas, producing ionization and a plasma discharge.

These studies used an ECR microwave plasma chemical vapor deposition (ECR MPCVD) chamber for ECR microwave plasma formation. The 14 inch diameter chamber uses a 10 inch turbomolecular pump (Balzers-Pfeiffer, TMU 1600) backed by a roughing pump (Leybold, D16B) to reach a base pressure of $3x10^{-9}$ Torr. Gases are delivered through the bottom of the chamber through a series of mass flow controllers and pneumatically controlled valves. The system is equipped with H_2, N_2, Ar, He, and BF_3 (Matheson Tri-gas, 99.999% purity) processing gases. Two ECR magnets are positioned approximately 30 cm apart below the chamber. The magnets produce a magnetic field gradient intended to funnel and reflect ions into the reaction chamber. A microwave (2.45 GHz, 1.5 kW) power generator (ASTeX, S1500-I) produced microwaves which enter the ECR MPCVD chamber through a quartz window. A manually controlled wave guide is used to direct the

microwaves into the chamber while minimizing reflected power. Samples were heated radiatively using a toroidal tungsten filament and temperatures were measured using an optical pyrometer (Mikron M90Q) with uncertainty ± 5 °C.

3.4.3 Molecular Beam Epitaxy

High temperature thermal annealing in these studies was performed in a molecular beam epitaxy (MBE) chamber. MBE is a deposition method using thermally excited atoms from pure metal sources to produce incident atomic or molecular fluxes at crystalline surface for epitaxial growth. A combination of molecular beam and gas phase reactants may be used to produce compound films. [23]

The MBE system used in this study is a custom-built reactor used for the deposition of metal nitride films with sources of Ga, Al, Sc and UHP NH_3 ("ammonia blue", 99.99994% purity). For the purposes of these studies, MBE was used solely for high temperature annealing in NH_3 ambient gas with no use of metal sources. An NH_3 flow rate of 10 sccm was used to maintain a chamber pressure of $5x10^{-5}$ Torr during heating, annealing, and cool down stages. Samples were heated radiatively using a toroidal tungsten filament located behind the sample backside.

3.4.4 Inductively Coupled Plasma Etching

Conventional dry etching was performed using a conventional inductively coupled plasma (ICP) etch chamber (PlasmaTherm, Apex ICP). The system uses a 13.56 MHz rf power to excite a plasma and is equipped with BCl_3, Cl_2, O_2, Ar, and N_2 processing gases. Sample temperatures were maintained at 23 °C using He cooling to prevent heating caused by the plasma exposure. ICP etching of GaN was performed using Cl_2 and BCl_3 at a

pressure of 5 mTorr. The system allowed control of the ICP power and the rf power. ICP power primarily affects ion density while the rf power affects ion energy. The rf power was varied in these studies to change the ion energy, producing rapid and slow etch rates. A discussion of ICP and other conventional dry etching methods may be found in Sect. 1.2.

3.5 Experiments

3.5.1 Plasma-Based Atomic Layer Etching of Gallium Nitride Using O_2 Plasma Oxidation and Removal by N_2/H_2 Plasma

ALE of GaN has previously been performed using conventional reactive ion etching (RIE) systems and RIE plasma species. Kauppinen, *et al*. reported Cl_2 and Ar were effective in plasma-based ALE of GaN with an etch per cycle (EPC) of 2.87 Å. [24] More recently, thermal ALE of GaN has been reported by Johnson, *et al*. using XeF_2 and BCl_3. [25] Prior to the study detailed in Chapter 5, "Atomic Layer Etching of Gallium Nitride Using Plasma Oxidation, Fluorination, and Ligand-Exchange", a plasma-based ALE process for GaN was investigated using O_2 plasma oxidation and removal by a plasma mixture of N_2 and H_2.

N_2 and H_2 plasma exposures on GaN at temperatures between 600 °C and 800 °C have shown surface improvement with smooth surface morphology as indicated with reflection high-energy electron diffraction (RHEED) streak patterns. [26] However, other studies have shown that H_2 plasma can create significant damage to the surface and near surface regions. H_2 ICP treatment of GaN has shown to significantly reduce the breakdown voltage in GaN Schottky diodes, which was attributed to the formation of a conducting n-type surface layer produced during ion bombardment. [27] This study also found plasma-

related damage to extend 60 nm into the material, which was attributed to ion diffusion. An additional study of H_2 ECR plasma effects on GaN observed the formation of hexagonal-shaped etch pits.

A 35 sccm flow of O_2 and a butterfly valve were used to maintain a pressure of 100 mTorr during 1 min O_2 plasma exposure. The O_2 plasma was produced using rf power (100 W, 13.56 MHz) in a custom-built stainless-steel hot wall ALD reactor. The sample was heated to 100 °C by radiative heating from a nichrome heating element located behind the sample backside during 30 s plasma exposure. N_2 and H_2 plasma was produced using a microwave ECR plasma (300 W, 2.45 GHz) using the system described in Sect. 3.4.2. The samples were heated to 700 °C by radiative heating using a tungsten filament located behind the sample backside in N_2 and H_2 ambient gas at $1x10^{-4}$ Torr, and during a 10 min plasma exposure, followed by cooling in ambient gas. A bias was not applied to the grounded substrate during both plasma exposures.

This study was performed on GaN grown by metalorganic chemical vapor deposition (MOCVD). ALE was investigated for as-grown and ICP etched GaN to study the removal of ICP etch-induced defects. The process was characterized using *in situ* XPS to measure changes in the Ga 3d and N 1s peak position. Changes in binding energy are indicative of band bending and surface states, as described further in chapter 6, "External Charge Compensation in Etched Gallium Nitride Using X-ray Photoelectron Spectroscopy". This process required the use of two reaction chambers for sequential plasma reactions. It is noted that the use of O_2 and H_2 in a single chamber may present a safety risk due to the volatility of mixing the two gases. The use of two chambers allowed for safe use of both plasma species for plasma-based ALE.

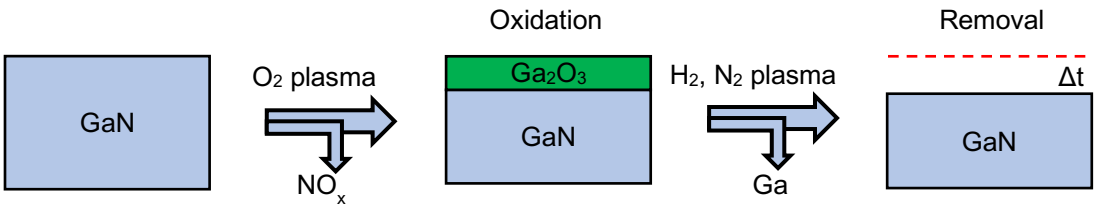

Figure 3.6 – Schematic of plasma-based ALE process for GaN using O_2 plasma exposure followed by N_2/H_2 plasma exposure, producing a change in thickness, Δt.

XPS was used to characterize the surface after each O_2 and N_2/H_2 plasma reaction throughout three cycles of plasma-based ALE. XPS scans of the ICP etched GaN after each plasma-based ALE exposure are shown in Fig. 3.7. A large increase in O 1s intensity and a broadening of the Ga 3d peak was observed after each O_2 plasma exposure, indicating ~2 nm of oxygen coverage at the surface. The oxygen coverage is shown in monolayers after each plasma exposure in Fig. 3.8(a), as well as the N/Ga ratio. Broadening of the Ga 3d peak was attributed to the formation of Ga-O bonds, which have higher binding energy than Ga-N. The combination of these two chemical states produces a broader Ga 3d peak, which was observed as an increase in the full width at half maximum (FWHM). A decrease in the N 1s signal indicated substitution of N and formation of an oxide layer at the surface. This was observed in the change of N/Ga ratio after each O_2 plasma exposure, shown in Fig. 3.8(a). Nearly complete reduction of the O 1s intensity was observed after each N_2/H_2 plasma exposure, accompanied by a corresponding increase in N 1s intensity.

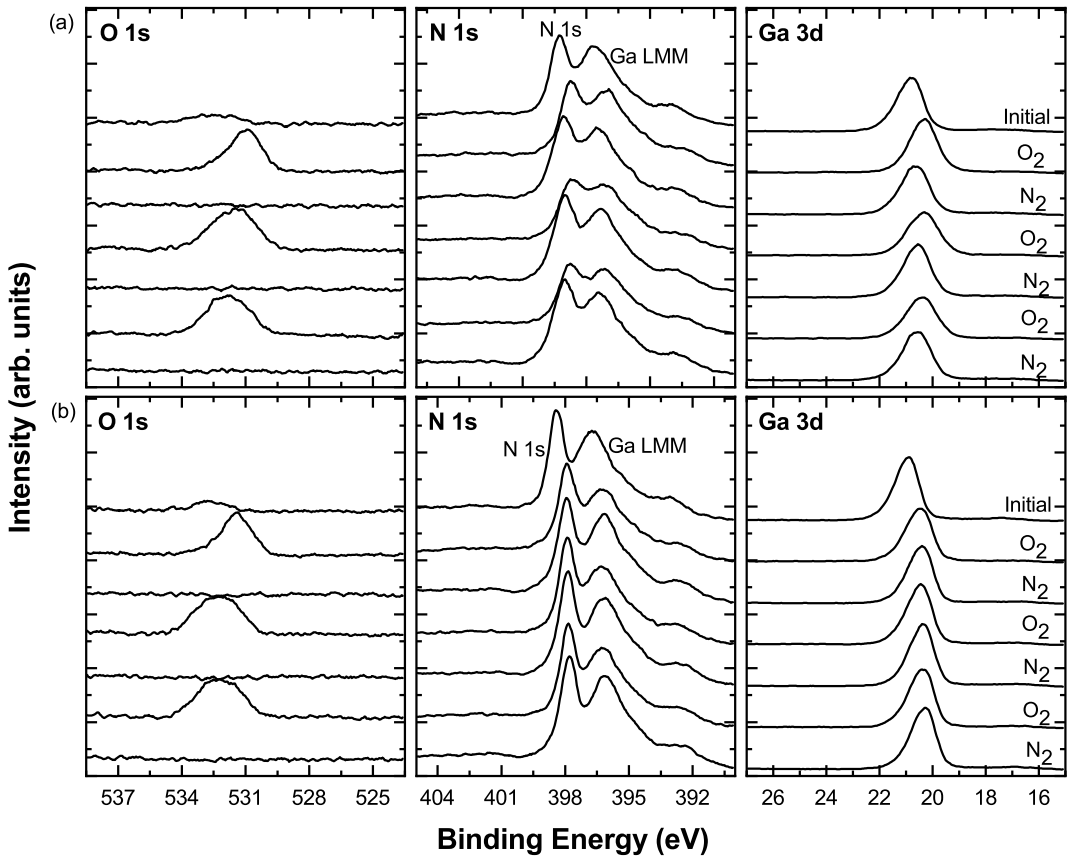

Figure 3.7 - XPS scans of (a) ICP etched GaN, and (b) non-etched GaN through three cycles of sequential O_2 plasma and N_2/H_2 plasma exposures for plasma-based ALE

Core level positions of the Ga 3d and N1s were observed to change after each plasma exposure. A shift in binding energy is indicative of a change in band bending and observed for both the ICP etched and as-grown GaN samples. The change in core level peak positions is shown in Fig. 3.8(b). The core-level peak positions of both Ga 3d and N 1s for the as-grown sample showed little change after each exposure. The initial change in peak position for as-grown GaN was attributed to removal of surface contaminants resulting from air exposure during sample transfer between MOCVD and the plasma

reactors used for this study. After initial removal of contaminants, the surface reaches a steady-state and shows little change in peak position. Conversely, larger changes in peak position are observed for the ICP etched GaN after each ALE reaction approaching the positions of the as-grown sample. This was attributed to continued removal of high-damage density material produced by the ICP etch process.

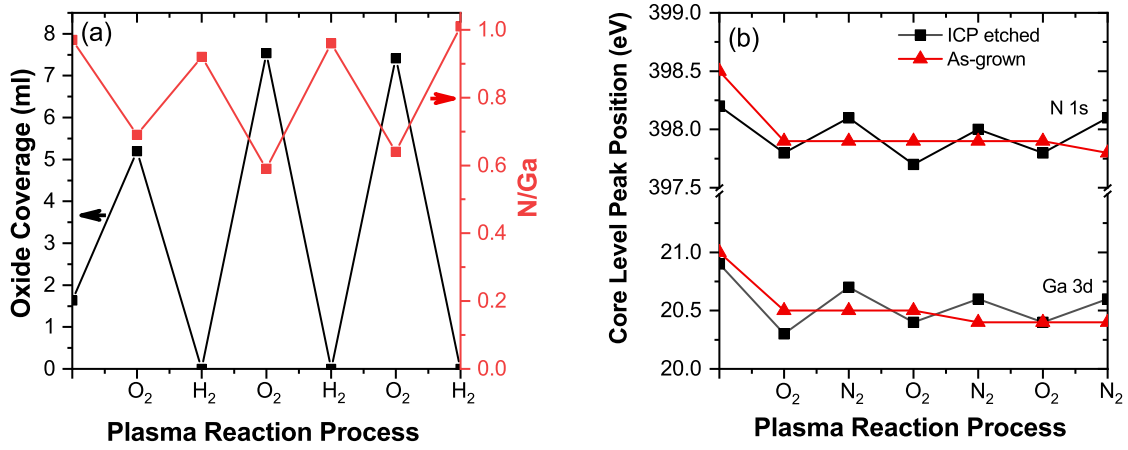

Figure 3.8 – (a) Oxygen coverage, N/Ga atomic ratios, and (b) core level binding energy peak position of GaN after each plasma reaction process of the plasma-based ALE of GaN.

Transmission electron microscopy (TEM) of these structures after 3 cycles of plasma-based ALE using discrete exposures of O_2 plasma and N_2/H_2 ECR plasma are shown in Fig. 3.9. Dark 'pits' are observed approximately 5 – 50 nm below the GaN surface. These pits were attributed to diffusion of atomic H and related defects. Although some studies have found high temperature N_2/H_2 plasmas to improve surface quality of GaN, [26] other studies have found that H_2 plasma treatment on GaN may produce damage through ion bombardment, atomic H diffusion, and the formation of etch pits. [27,28] It is suggested that reduced H_2 flow rate or reduced microwave power used in the N_2/H_2 ECR

plasma process may reduce damage from H_2 ions and diffusion of atomic hydrogen. An alternative plasma formation method for the removal process may also reduce plasma damage. Plasma-based ALE of GaN using O_2 plasma for modification has recently been reported (2021) using BCl_3 as the other reactant for material removal. [29]

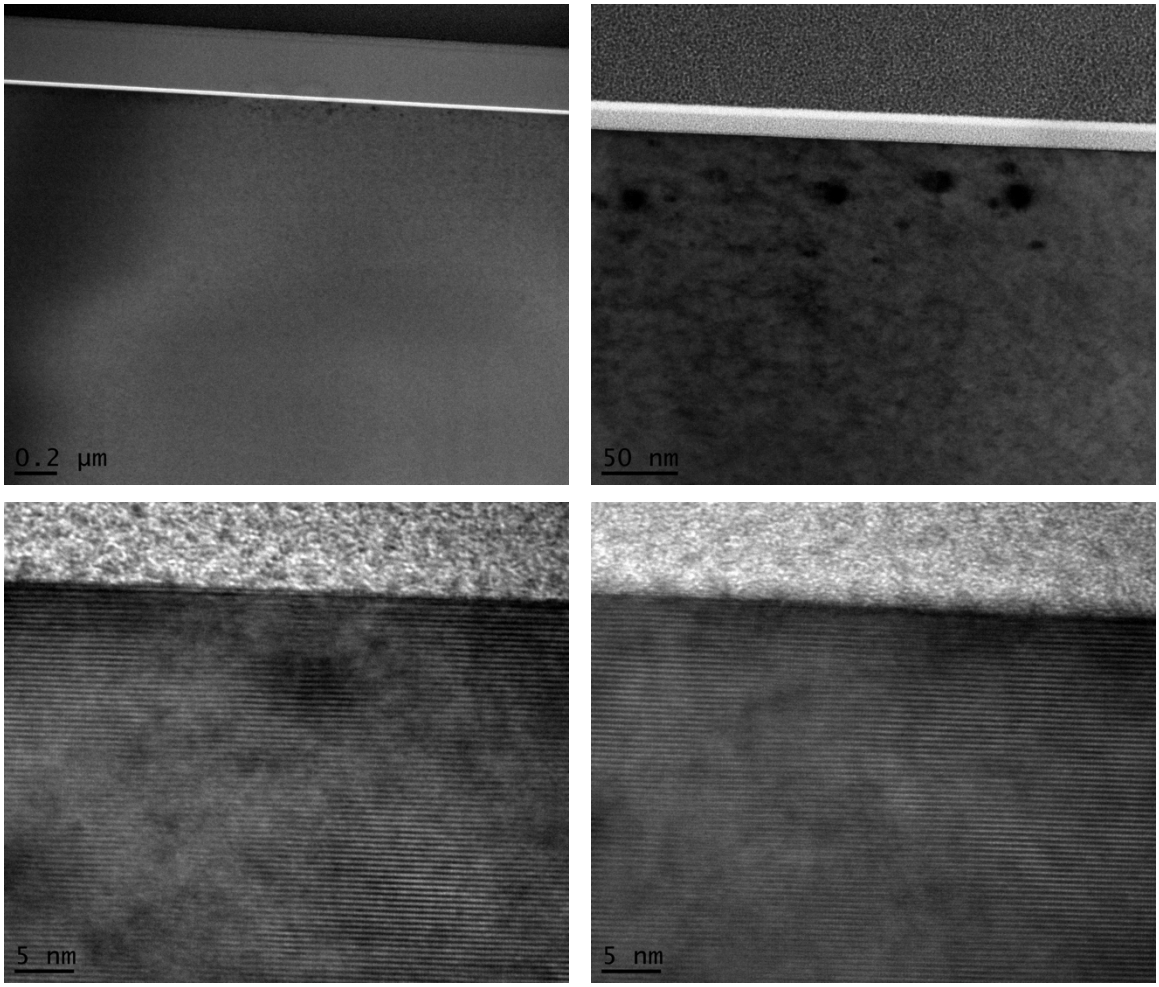

Figure 3.9 - TEM images of GaN after 3 cycles of plasma-based ALE using sequential exposures of O_2 plasma and N_2/H_2 plasma.

3.5.2 Plasma Enhanced Atomic Layer Etching of Gallium Nitride With Molybdenum Sample Mounting

Plasma Enhanced ALE (PEALE) occurred through cycles of one O_2 plasma exposure followed by five alternating exposures of HF and TMG. This process is detailed further in chapter 5 of this document, "Plasma Enhanced Atomic Layer Etching of Gallium Nitride".

GaN samples were mounted to molybdenum (Mo) sample holders and mounting plates for use in etching and characterization chambers. Previous studies have shown that Mo can be etched using plasmas with various O and F chemistries, including CF_4/O_2, [30] SF_6/O_2, [31] and NF_3/O_2. [32] An investigation of etching mechanisms and gas roles in CF_4/O_2 RIE of Mo showed formation of MoF_6, MoO_2F_2, and $MoOF_3$, suggesting etching occurred through O and F chemical reactions. [30]

This study was performed on GaN grown by metalorganic chemical vapor deposition (MOCVD). Ten ALE supercycles were used prior to epitaxial growth of p-type GaN by MOCVD. Samples were then characterized by SEM and TEM.

Visible changes to the GaN substrate and Mo mounting were observed and are shown in Fig. 3.10. Discoloration of the Mo mounting plate and GaN was observed with significant discoloration of the GaN backside around the exposed areas where holes are present in the Mo. Image of the Mo mounting plate without GaN after PEALE, shown in Fig. 3.10 (b), shows significant discoloration compared to the areas that were covered by GaN or tantalum wire during the PEALE process. This level of discoloration was not

observed for all samples, however, it is expected that other samples experienced similar contamination from Mo complexes produced by etching in O_2 plasma and HF.

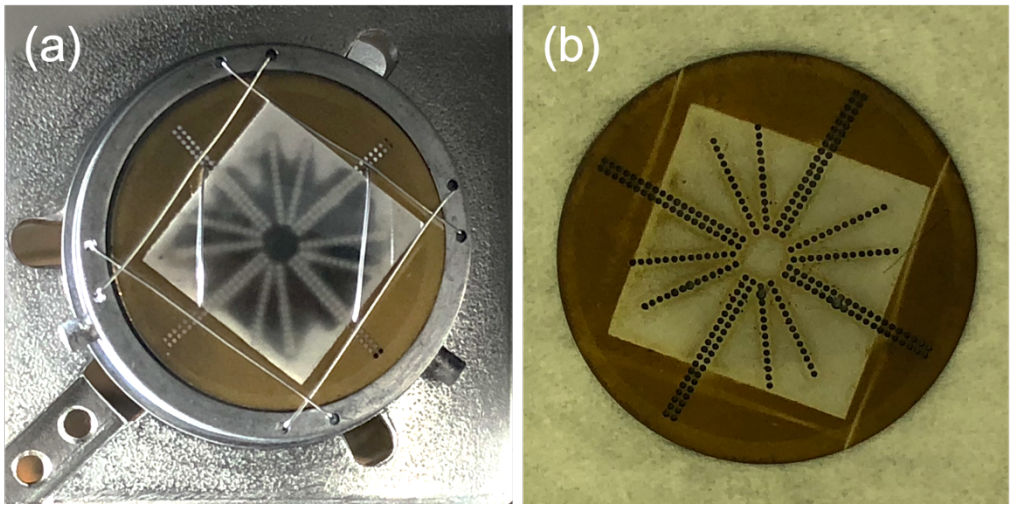

Figure 3.10 – Photos of (a) GaN mounted on Mo mounting plate after PEALE, and (b) Mo mounting plate after PEALE process.

SEM and TEM were used to study epitaxial MOCVD of p-type GaN on ALE etched GaN. These images are shown in Fig. 3.11. Hexagonal island growth of GaN is shown in SEM images with significant surface roughness. Significant structural defects were observed in the epitaxial p-GaN via TEM. This was attributed to structural defects resulting from poor nucleation on a poor GaN surface. Poor surface conditions, including surface impurities, are known to affect nucleation of epitaxial growth and produce structural defects throughout the epitaxial layer. Implanted defects are attributed to incorporation of Mo complexes originating from etching of the sample plate and holder with O_2 plasma and HF.

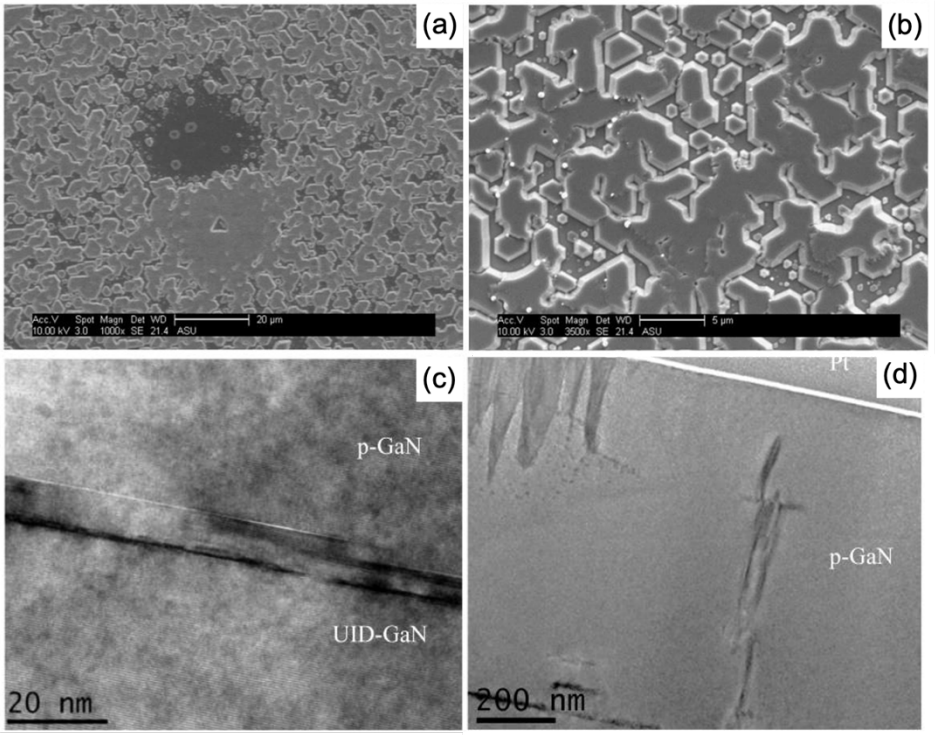

Figure 3.11 - (a,b) SEM and (c,d) TEM images of MOCVD grown p-GaN on UID GaN after PEALE using Mo substrate holder. Reprinted/adapted from Peri, *et al*. [33]

Poor surface conditions and epitaxial growth on PEALE GaN using oxidation, fluorination, and ligand-exchange is attributed to the use of Mo sample holders during etching. Previous studies have shown that etching using O and F plasma chemistries is effective in etching Mo. [30–32] An investigation of the individual roles of specific gases during etching suggested Mo was chemically etched by F and O due to observed formation of MoF_6, MoO_2F_2, and $MoOF_3$. Atomic oxygen was shown to enhance the etch rate.

This PEALE process of GaN uses similar chemistry, including C, O, and F in the forms of O_2 plasma, HF, and TMG. Additionally, the plasma ignition of O_2 can be expected to produce atomic oxygen, which increases the etch rate of Mo. The presence of Mo etch products are suggested to have contaminated the GaN samples, causing the damage

observed by SEM, TEM, and visual inspection. To avoid future issues with sample mounting for studies of GaN ALE using this process, new sample holders and mounting plates were designed and fabricated using alloys composed primarily of nickel and chromium (inconel) and nickel and copper (monel). These materials are expected to be more resistant to etching using C, O, and F.

ACKNOWLEDGEMENTS

This work was supported by the Advanced Research Projects Agency-Energy under the PN-Diodes program through grant No. DE-AR000086. I would like to acknowledge Dr. Houqiang Fu and Dr. Fu for performing MOCVD growth of epitaxial GaN and ICP etching, and Dr. Prudhvi Peri for his contribution in performing transmission electron microscopy (TEM). I would also like to thank Dr. David Smith, Dr. Yuji Zhao, Dr. Fernando Ponce, Dr. Stephen Goodnick, Dr. Xingye Wang, Dr. Mei Hao, Dr. Shanthan Alugubelli, and Dr. Hanxiao Liu for their useful discussions.

REFERENCES

[1] H. Hertz, *Ueber Einen Einfluss Des Ultravioletten Lichtes Auf Die Electrische Entladung*, Annalen Der Physik **267**, 983 (1887).

[2] M. Planck, *On the Theory of the Energy Distribution Law of the Normal Spectrum*, Verh. Dtsch. Phys. Ges. Berlin **237**, 1 (1900).

[3] A. Einstein, *Über Einen Die Erzeuyunq Und Verwandlung Des Lichtes Betreffenden Heuristischen Gesichtspunkt*, Annalen Der Physik **4**, 132 (1905).

[4] H. Y. Fan, *Theory of Photoelectric Emission from Metals*, Physical Review **68**, 43 (1945).

[5] W. E. Spicer, *Photoemissive, Photoconductive, and Optical Absorption Studies of Alkali-Antimony Compounds*, Physical Review **112**, 114 (1958).

[6] C. N. Berglund and W. E. Spicer, *Photoemission Studies of Copper and Silver: Theory*, Physical Review **136**, 1030 (1964).

[7] C. N. Berglund and W. E. Spicer, *Photoemission Studies of Copper and Silver: Experiment*, Physical Review **136**, (1964).

[8] A. Fahlman, C. Nordling, and K. Siegbahn, *ESCA : Atomic, Molecular and Solid State Structure Studied by Means of Electron Spectroscopy* (Uppsala : Almqvist and Wiksell, 1967).

[9] L. Meitner, *Über Die Entstehung Der β-Strahl-Spektren Radioaktiver Substanzen*, Zeitschrift Für Physik **9**, 131 (1922).

[10] L. Meitner, *Über Den Zusammenhang Zwischen β- Und γ-Strahlen*, Zeitschrift Für Physik **9**, 145 (1922).

[11] P. Auger, *Sur Les Rayons β Secondaires Produits Dans Un Gaz Par Des Rayons*

X, Comptes Rendus Des Séances Hebdomadaires de l'Académie Des Sciences **177**, 169 (1923).

[12] L. Pauling, *The Nature of the Chemical Bond*, 3rd ed. (Cornell University Press, Ithaca, NY, 1960).

[13] Z. Zhang and J. T. Yates, *Band Bending in Semiconductors: Chemical and Physical Consequences at Surfaces and Interfaces*, Chemical Reviews **112**, 5520 (2012).

[14] J. R. Waldrop and R. W. Grant, *Measurement of AlN/GaN (0001) Heterojunction Band Offsets by x-Ray Photoemission Spectroscopy*, Applied Physics Letters **68**, 2879 (1995).

[15] E. A. Kraut, R. W. Grant, J. R. Waldrop, and S. P. Kowalczyk, *Heterojunction Band Discontinuities: Physics and Device Applications* (Elsevier, New York, 1987).

[16] O. Ambacher, *Growth and Applications of Group III-Nitrides*, Journal of Physics D: Applied Physics **31**, 2653 (1998).

[17] C. D. Wagner, *Sensitivity Factors for XPS Analysis of Surface Atoms*, Journal of Electron Spectroscopy and Related Phenomena **32**, 99 (1983).

[18] C. D. Wagner, L. E. Davis, M. V. Zeller, J. A. Taylor, R. M. Raymond, and L. H. Gale, *Empirical Atomic Sensitivity Factors for Quantitative Analysis by Electron Spectroscopy for Chemical Analysis*, Surface Interface Analysis **3**, 1981 (1981).

[19] V. M. Bermudez, *Study of Oxygen Chemisorption on the GaN(0001)-(1x1) Surface*, Journal of Applied Physics **80**, 1190 (1996).

[20] C. Negara, Z. Li, T. Längle, and J. Beyerer, *Simplified Stokes Polarimeter Based*

on Division-of-Amplitude, 44 (2019).

[21] E. Compain and B. Drevillon, *Broadband Division-of-Amplitude Polarimeter Based on Uncoated Prisms*, Applied Optics **37**, 5938 (1998).

[22] A. V. Tikhonravov, M. K. Trubetskov, E. Masetti, A. V. Krasilnikova, and I. V. Kochikov, *Sensitivity of the Ellipsometric Angles Psi and Delta to the Surface Inhomogeneity*, Advances in Optical Interference Coatings **3738**, 173 (1999).

[23] A. Y. Cho and J. R. Arthur, *Molecular Beam Epitaxy*, Solid-State Chemistry **10**, 157 (1975).

[24] C. Kauppinen, S. A. Khan, J. Sundqvist, D. B. Suyatin, S. Suihkonen, E. I. Kauppinen, and M. Sopanen, *Atomic Layer Etching of Gallium Nitride (0001)*, Journal of Vacuum Science & Technology A: Vacuum, Surfaces, and Films **35**, 060603 (2017).

[25] N. R. Johnson, J. K. Hite, M. A. Mastro, C. R. Eddy, and S. M. George, *Thermal Atomic Layer Etching of Crystalline GaN Using Sequential Exposures of XeF_2 and BCl_3*, Applied Physics Letters **114**, (2019).

[26] F. W. Amalraj, A. K. Dhasiyan, Y. Lu, N. Shimizu, O. Oda, K. Ishikawa, H. Kondo, M. Sekine, N. Ikarashi, and M. Hori, *Effect of N_2/H_2 Plasma on GaN Substrate Cleaning for Homoepitaxial GaN Growth by Radical-Enhanced Metalorganic Chemical Vapor Deposition (REMOCVD)*, AIP Advances **8**, (2018).

[27] X. A. Cao, A. P. Zhang, G. T. Dang, H. Cho, F. Ren, S. J. Pearton, R. J. Shul, L. Zhang, R. Hickman, and J. M. Van Hove, *Inductively Coupled Plasma Damage in GaN Schottky Diodes*, Journal of Vacuum Science & Technology B **17**, 1540 (1999).

[28] R. N. Tiwari and L. Chang, *Etching of GaN by Microwave Plasma of Hydrogen*, Semiconductor Science and Technology **25**, (2010).

[29] I. H. Hwang, H. Y. Cha, and K. S. Seo, *Low-damage and Self-limiting (Al)Gan Etching Process through Atomic Layer Etching Using O_2 and BCl_3 Plasma*, Coatings **11**, 1 (2021).

[30] S.-J. Park, C. P. Sun, J. T. Yeh, J. K. Cataldo, and N. Metropoulos, *Reactive Ion Etching of Molybdenum In CF4/O2 Plasma*, MRS Proceedings **68**, 65 (1986).

[31] S. Park, C. Sun, and R. J. Purtell, *A Mechanistic Study of SF_6/O_2 Reactive Ion Etching of Molybdenum*, Journal of Vacuum Science & Technology B **5**, 1372 (1987).

[32] T. P. Chow and A. J. Steckl, *Plasma Etching of Sputtered Mo and $MoSi_2$ Thin Films in NF_3 Gas Mixtures*, Journal of Applied Physics **53**, 5531 (1982).

[33] P. R. Peri, K. Hatch, D. Messina, K. Fu, Y. Zhao, R. Nemanich, and D. Smith, *Plasma Enhanced Atomic Layer-Etched and Regrown GaN-on-GaN High Power p-n Diodes*, Microscopy and Microanalysis **26**, 840 (2020).

CHAPTER IV

PLASMA ENHANCED ATOMIC LAYER DEPOSITION AND ATOMIC LAYER ETCHING OF GALLIUM OXIDE USING TRIMETHYLGALLIUM

Research performed in collaboration with Daniel C. Messina and Robert J. Nemanich

ABSTRACT

Atomic layer etching driven by self-limiting thermal reactions has recently been developed as a highly conformal and isotropic technique for low damage atomic scale material removal by sequential exposures of vapor phase reactants. Gallium oxide (Ga_2O_3) is currently among the materials of interest due to a large variety of applications including power electronics, solar cells, gas sensors, and photon detectors. We report a newly developed method for Ga_2O_3 thermal atomic layer etching, in which surface modification is achieved through HF exposure resulting in a gallium fluoride surface layer. The surface fluoride is then removed through volatile product formation via ligand-exchange with trimethylgallium (TMG, $Ga(CH_3)_3$). Saturation of the precursor exposure at substrate temperature of 300 °C resulted in an etch rate of 1.0 ± 0.1 Å/cycle for amorphous Ga_2O_3. Uniformity and conformality of the ALE process was confirmed via atomic force microscopy with a measured surface roughness of 0.55 ± 0.05 nm that remains unchanged after etching.

4.1 Introduction

Gallium oxide (Ga_2O_3) is an ultrawide bandgap material which has recently gained considerable interest due to its large direct bandgap (~4.9 eV), high thermal and chemical

stability, large dielectric constant (>10), and unique transparency in the visible and ultraviolet (UV) spectral regions. [1–5] With multiple crystal poylmorphs, the band gap of Ga_2O_3 may vary between reported values of 4.5-4.9 eV. Among these, the monoclinic β-Ga_2O_3 is the most stable phase with a band gap of 4.9 eV. Ga_2O_3 thin films have been formed using various deposition techniques including metalorganic chemical vapor deposition (MOCVD), [6] molecular beam epitaxy (MBE), [7] metalorganic vapor phase epitaxy (MOVPE), [8] atomic layer deposition (ALD), [3,9–13] pulsed laser deposition (PLD), [2] and electron beam evaporation. [14] Reported applications of Ga_2O_3 include gas sensors, [15,16] field-effect-transistors (FETs), [17,18] solar cells, [19,20] and deep-UV photon detectors. [21–23]

Atomic layer deposition of Ga_2O_3 using trimethylgallium (TMG, $Ga(CH_3)_3$) and O_2 plasma has previously been reported. [3,9,10,13] Other reported Ga_2O_3 ALD precursors include gallium acetylacetonate $Ga(acac)_3$, [12] dimethylgallium isopropoxide, [11] gallium tri-isopropoxide, [24] and tris(dimethylamino)gallium. The films described in these reports were typically amorphous, polycrystalline β-Ga_2O_3 may be produced by annealing at temperatures between 700-1000 °C. Phase selectivity of crystalline α-, β-, and ϵ-Ga_2O_3 was demonstrated using a TMG and O_2 plasma enhanced ALD process and tuning the plasma parameters. TMG with O_2 plasma also demonstrated a large Ga_2O_3 ALD window (RT - 400 °C). [9,10]

Dry etching, required for semiconductor device fabrication, involves the use of plasma and vapor phase reactants rather than wet chemicals for removal of surface material, enabling patterning of small features. “Conventional” dry etching methods employ plasma ions and involve a combination of chemical and physical mechanisms to

remove material. Several dry etching techniques for Ga_2O_3 have previously been investigated using a variety of F- and Cl- based species, including SF_6, NF_3, CHF_3, BCl_3, and Cl_2. [18,25–30] These reactants modify the surface, often producing nonvolatile material, which require removal by physical bombardment from ions, typically Ar. [18,25,26] Due to the strong chemical bonding of Ga_2O_3, the ion energies required for material removal are typically high. [26,29–31] Therefore, these plasma based etching techniques often result in ion-induced damage to the material, including electrically active damage which may affect device performance. [26,29,30] Development of a dry etching method for Ga_2O_3 with low surface damage is therefore necessary for advancement of Ga_2O_3 processing.

Atomic layer etching (ALE) is a dry etching technique using cycles of sequential reactions for controlled material removal for atomic scale processing. [32–36] One cycle of ALE typically consists of a surface modification process followed by removal of the modified surface by either volatile release or assisted desorption. These reactions may occur through either thermochemical mechanisms or energy-assisted processes through the use of ions and plasmas.

Plasma-based ALE has been in development for decades, beginning with ALE of Si being reported in 1996. [37] These processes have been further expanded through implementation in fabrication processing as well as commercial availability of ALE systems. [32,33,35,38] In plasma-based ALE, the modification step serves to lower the ion energy threshold to remove material from the surface relative to the unmodified material. Ions are then required to remove the modified surface through momentum transfer of the ions to surface atoms. [32,33,35,38] Typical plasma ALE processes require Ar ion energies

of 30-70 eV. [38] Plasma ALE is highly anisotropic, enabling directional etching for high aspect ratio nanoscale patterning. Due to the use of energy-assisted reactions in plasma-based ALE, ion-induced damage to the material may occur. Ion-free ALE processes could have the advantage of preventing ion-induced damage and to produce conformal etching.

ALE via thermally driven reactions is a more recent development as a highly conformal and ion-free technique for low damage atomic scale material removal using sequential exposures of vapor phase reactants. [39–41] Thermal ALE requires self-limiting behavior of the reactant exposures, requiring the use of one reactant to modify or passivate the surface and another reactant to remove only the modified surface layer, enabling etching without ion induced damage to the underlying material. Choice of precursor is therefore critical to utilize thermally favorable reactions while avoiding spontaneous etching.

Thermal ALE occurs through surface modification followed by the formation of stable and volatile complexes. Surface modification of previously reported thermal ALE processes typically occurs through fluorination via exposure to HF, SF_4, or XeF_2. [42] The reported mechanism for volatile product formation is a ligand exchange between the modified surface species with metal organic precursors, typically involving chlorine, methyl, or ethyl groups. A report of thermal ALE of Al_2O_3 involved the use of HF and tin acetylacetonate ($Sn(acac)_2$, $Sn(CH_3COCHCOCH_3)_2$). [39]

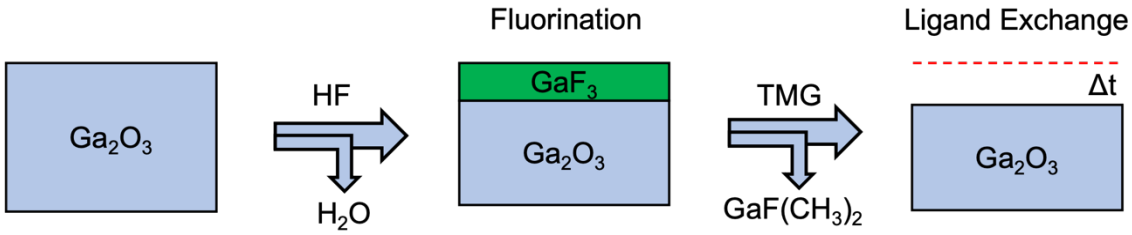

Figure 4.1 – Schematic of surface reactions during Ga_2O_3 ALE process using sequential exposures of HF and TMG, producing a change in thickness Δt.

HF and trimethylaluminum (TMA, $Al(CH_3)_3$) have previously been reported as effective reactants for thermal ALE of Al_2O_3 and HfO_2. [40,43] Aqueous HF has also been used for wet chemical etching of Ga_2O_3 at room temperature. [44] Thermal ALE of Ga_2O_3 was recently reported by Lee, et al. using HF with BCl_3, $AlCl(CH_3)_2$, $Al(CH_3)_3$, $TiCl_4$, and $Ga(N(CH_3)_2)_3$ as ligand exchange precursors. In this study, we report that HF and trimethylgallium (TMG, $Ga(CH_3)_3$), used in discrete, subsequent exposures are effective reactants for Ga_2O_3 ALE. Fig. 4.1 shows the reaction steps during the ALE process. Firstly, exposure of the Ga_2O_3 film to HF fluorinates the surface. Secondly, the proposed mechanism during the TMG exposure is a ligand exchange process between fluorine and methyl groups, resulting in volatile $GaF_x(CH_3)_y$ species which desorb from the surface.

$$Ga_2O_{3(s)} + 2HF_{(g)} \rightarrow 2GaF_{3(ads)} + H_2O_{(g)}$$

$$GaF_{3(ads)} + 2\ Ga(CH_3)_{3(g)} \rightarrow 3\ GaF(CH_3)_{2(g)}$$

where "s" denotes the substrate surface, "ads" indicates adsorbed surface species, and "g" indicates gas or vapor phase species.

4.2 Experimental Methods

Ga_2O_3 thin films were deposited by PEALD using TMG and O_2 plasma onto 25.4 mm diameter boron-doped Si (100) wafers supplied by Virginia Semiconductor, and then etched by ALE using TMG and HF. The PEALD and ALE reactions were both performed in a custom stainless-steel hot wall ALD reactor with a multi-wavelength ellipsometer (Film Sense, FS-1) mounted at ~45° to wafer surface. A two-stage dry processing pump (Ebara, A70W) with a N_2 (99.999%, 14.2 SLM) dilution flow was used to reach a base pressure of 4 x 10^{-5} Torr during processing. Remote plasma generation occurred in a fused quartz tube using an inductively coupled 13.56 MHz RF generator (MKS, Elite 300) which was located approximately 25 cm above the wafer surface. This distance between the plasma formation and the sample surface enables a sufficient flux of oxygen radicals while limiting the density of ions at the surface. Due to the operating pressure (100 mTorr) the O radicals are expected to be completely thermalized. A bias was not applied to the grounded substrate during the deposition.

HF vapor was derived from HF-pyridine $(C_5H_5N)\cdot(HF)_x$ (70% HF by weight, Alfa-Aesar). The HF-pyridine was transferred into the precursor bubbler in a dry Ar filled PTFE glove bag. The HF-pyridine and TMG (99.998 wt%+, STREM Chemicals, Inc.) precursors were held at 30 ºC. Precursor vapor delivery occurred using ultra-high purity Ar (99.999%) carrier gas with flow rates of 5.0 standard cubic centimeters per minute (sccm) for TMG and 15.0 sccm for HF. Precursor exposure times of 30 seconds were used resulting in pressure transients of 600 – 800 mTorr and 200 – 400 mTorr for HF and TMG, respectively.

A 30.0 sccm flow of N_2 was used between reactant exposures to purge the system of unreacted precursor and byproducts. Precursor pulse times were varied to achieve saturation of reactions.

This study was performed on Ga_2O_3 deposited on Si (100) substrates by plasma enhanced atomic layer deposition (PEALD) using TMG and O_2 plasma and a substrate temperature of 250 ºC. Prior to deposition, Si wafers were cleaned using a 10 min UV O_3 exposure at atmospheric pressure. The PEALD process was monitored by *in situ* ellipsometry and characterized by x-ray photoelectron spectroscopy (XPS).

Ellipsometry measurements were made *in situ* during the processing using a multi-wavelength ellipsometer (Film Sense, FS-1) mounted at ~45° to the wafer surface. The ellipsometer used four light emitting diodes (LED) to produce light of wavelengths centered at 465 nm, 525 nm, 580 nm, and 635 nm. Optical parameters of the Ga_2O_3 films were determined by *ex situ* spectroscopic ellipsometry (M2000, J.A. Woollam) from a 20 nm PEALD Ga_2O_3 film grown at 250 °C. Thickness measurements from this device were confirmed using XPS of 5 nm and 10 nm of Ga_2O_3 grown by PEALD on Si (100).

For *in situ* measurements samples were transferred in ultra-high vacuum (UHV) for XPS (VG-Scienta, R3000). Measurements were made using an Al K_α x-ray source producing monochromatic light at 1486.7 eV and a system base pressure of $\sim 4\times10^{-10}$ Torr. Using an analyzer pass energy of 100 eV and slit size of 0.4 mm, the system may resolve binding energies to ± 0.15 eV. XPS scans were fit using Gaussian-Lorentzian line shapes after a standard Shirley background was subtracted. Empirically derived atomic sensitivity

factors were used to determine surface stoichiometry. [45] The Ga 3d, O 1s, C 1s, and F 1s XPS core level spectra were used for chemical state analysis at the wafer surface.

Ex situ atomic force microscopy (AFM) (Asylum Research, MFP-3D) measurements were used to determine the surface roughness of the Ga_2O_3 films and were performed using scan sizes of 25.0 μm^2 and 400 μm^2.

4.3 Results

TMG and O_2 plasma were used to deposit Ga_2O_3 films by PEALD. Alternating exposures of HF and TMG were then used to etch Ga_2O_3 films by thermal ALE. Deposition and etching processes were monitored *in situ* using a multi-wavelength ellipsometer. *In situ* x-ray photoelectron spectroscopy (XPS) was employed to identify chemical states and determine surface composition.

Thickness measurements were recorded via ellipsometry throughout depositions. The change in thickness throughout 15 cycles of a typical deposition is shown in Fig. 4.2(a). An average linear increase in thickness of 0.9 ± 0.1 Å was noted for the 15-cycle deposition. The ellipsometric response for a three ALD cycles is shown in Fig. 4.2(b) with the individual TMG and O_2 plasma half-cycles of one ALD cycle identified. We note that the ellipsometric thickness change could be due to adsorbed species or to changes of the surface optical properties. A large thickness increase is observed as TMG is adsorbed onto the surface. Then, a slight decrease in thickness after the O_2 plasma exposure, which is interpreted as the combustion of methyl groups and oxidation of the surface.

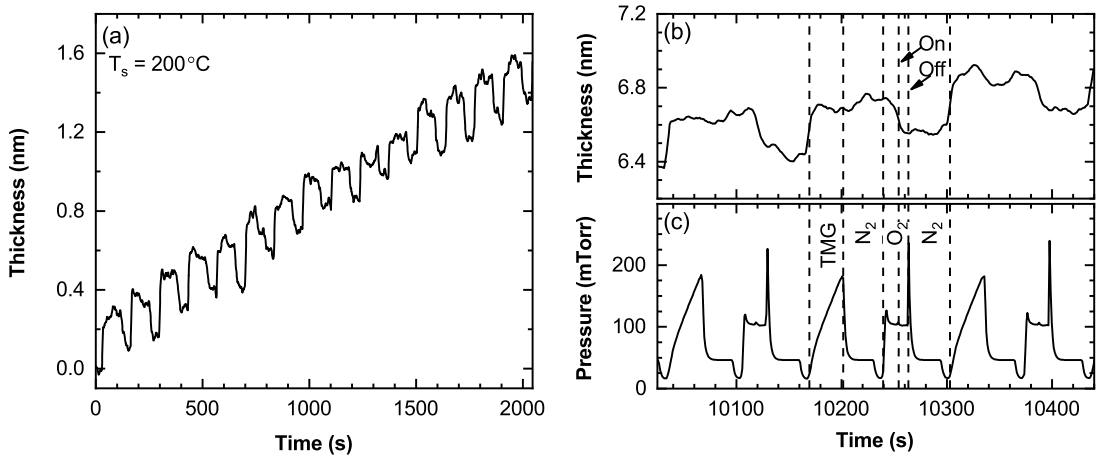

Figure 4.2 – Ga_2O_3 thickness change observed by *in situ* ellipsometry throughout (a) 15 cycles and (b) 3 cycles of PEALD using TMG and O_2 plasma. (c) Chamber pressure throughout three cycles of TMG, O_2 plasma exposure, and N_2 purge, with dashed lines and labels indicating individual exposures of reactants during one ALD cycle.

XPS was used to examine the surface composition after deposition and etching, as well as to calculate film thickness to verify deposition and etch rates. Fig. 4.3(a) shows the XPS spectrum of the Ga 3d core level of a 20 nm Ga_2O_3 film after PEALD. A spectral deconvolution is indicated by dashed lines. An O 1s core level at 23.0 ± 0.2 eV is also visible within this spectrum. Based on the ratio of the integrated Ga 3d and O 1s areas and photoionization cross-sections, an O:Ga ratio of 3:2 was obtained. The oxygen centration was measured to be 59 ± 10%. [45] Spectral deconvolution of Ga 3d indicated two peaks with energies 18.9 ± 0.1 and 20.2 ± 0.1 eV, which are consistent with Ga-OH and Ga-O, respectively. [10] Presence of the Ga-OH peak is attributed to a surface termination species. Additionally, carbon impurities were below the XPS detection limit for the PEALD Ga_2O_3 films.

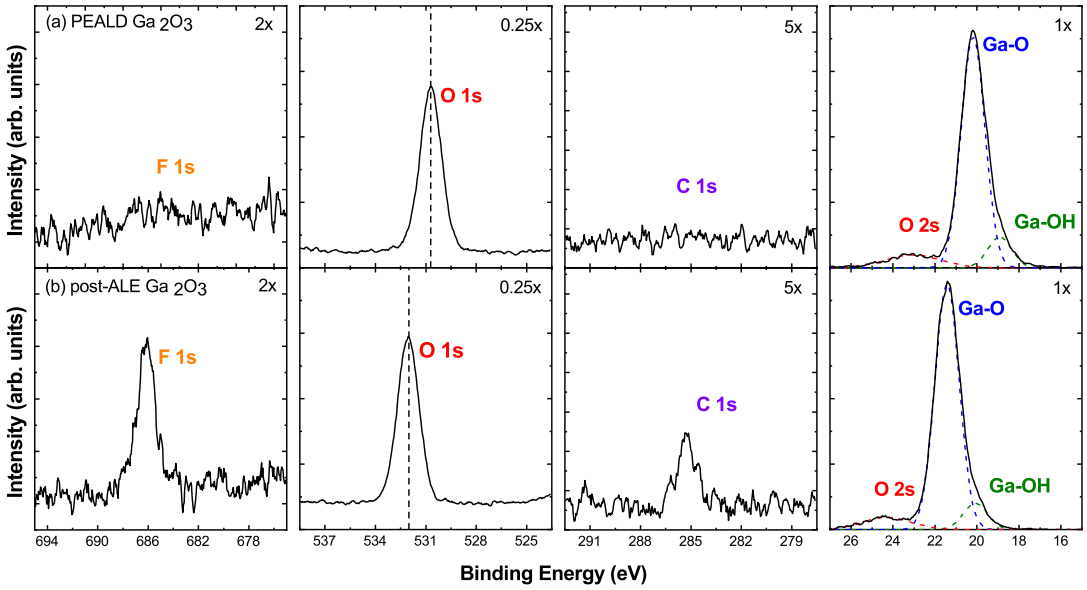

Figure 4.3 – XPS scans of F 1s, O 1s, C 1s, and Ga 3d core levels in Ga_2O_3 film (a) after PEALD of 20 nm at 250 °C, and (b) after etching of 2 nm by ALE.

Fig. 4.3(b) shows the XPS scans of the Ga 3d core level of a Ga_2O_3 film with fluorine termination, with spectral deconvolution indicated by dashed lines. An upward shift of 1.2 eV in binding energy may be observed in all peaks. Despite a binding energy shift, the energy splitting between the Ga-OH and Ga-O states remains consistent. Surface impurities of C and F were detected after ALE via XPS with similar concentrations of C and F, each accounting for up to 3 at. %. Surface atomic concentration of O was reduced to 53.0 ± 0.5% at the surface after ALE, while Ga content remained constant, indicating favorable substitution of oxygen by carbon and fluorine.

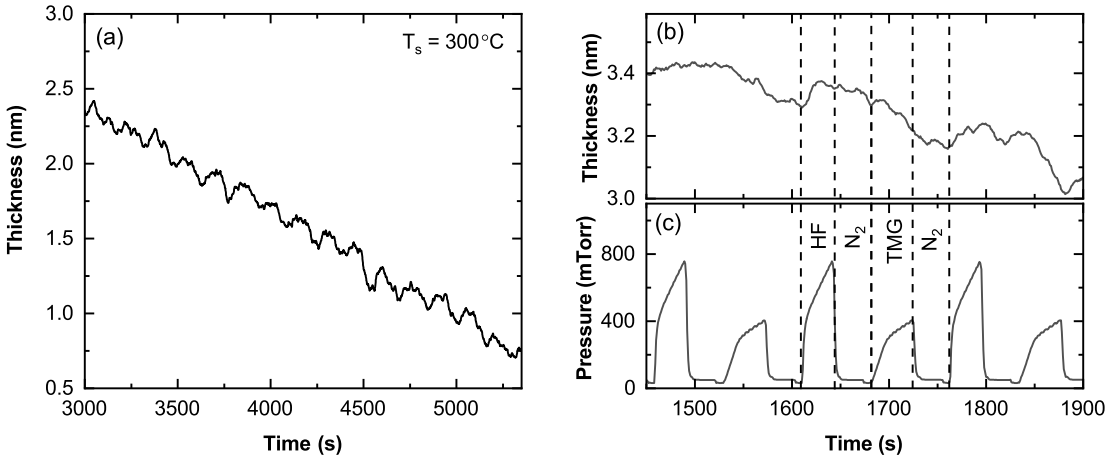

Figure 4.4 – Change of Ga_2O_3 thickness observed by *in situ* ellipsometry throughout (a) fifteen cycles, and (b) three cycles of HF (0.1 s pulse) and TMG (8 s pulse) exposures during ALE process. (c) Chamber pressure throughout three cycles of HF, TMG exposure, and N_2 purge with dashed lines and labels indicating individual exposures of reactants during one ALE cycle.

Thickness change per cycle remained approximately linear throughout the etching process. The linearity of the ALE process at 300 ºC can be seen in Fig. 4.4(a) throughout fifteen cycles of HF and TMG exposures on a Ga_2O_3 film. The ellipsometric response for three ALE cycles is shown in Fig. 4.4(b), with the process steps annotated for one cycle. One cycle of the process shown above consisted of a 0.1 s pulse of HF, followed by 30 s of exposure prior to a 30 s N_2 purge, and then a 8 s pulse of TMG, followed by 30 s of TMG exposure prior to another 30 s N_2 purge. The HF and TMG pulses and exposures have been highlighted in the plot. A slight increase in measured thickness is observed on each exposure. A decrease in thickness in observed during the TMG exposure as the ligand-exchange occurs and the resulting products desorb from the surface.

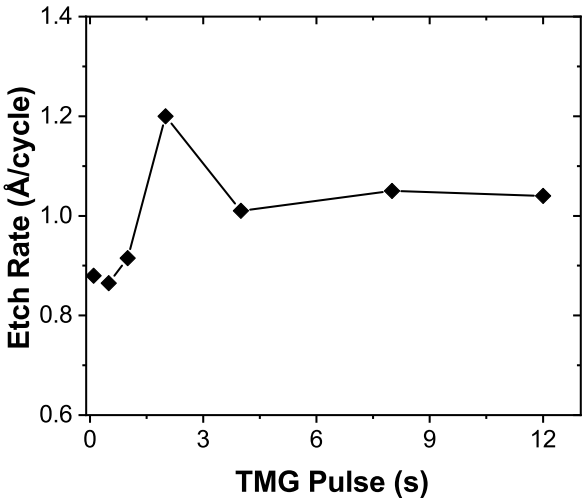

Figure 4.5 – Ga_2O_3 etch rate at 300 ºC vs TMG pulse time with HF pulse time fixed at 0.1 s.

Self-limiting behavior is an important aspect of ALE, indicating a process is restricted to affect only the surface atoms. The self-limiting behavior of the ALE process was determined by incrementing precursor exposure times prior to the N_2 chamber purge. Forty cycles of ALE were performed for each set of pulse times. The etch rates for each set of exposure times were taken as the average changes in thickness per cycle. As shown in Fig. 4.5, there is an increase in etch rate as the TMG pulse time is increased from 0.1 s to 4 s before the etch rate saturates at approximately 1.0 Å/cycle.

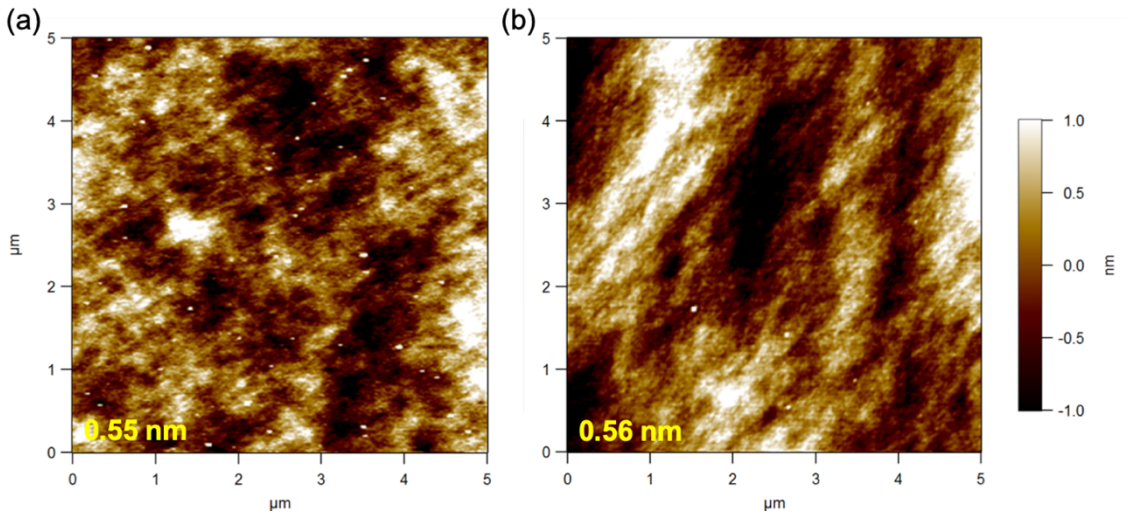

Figure 4.6 – (5.0-µm)^2 AFM images of (a) 10 nm of PEALD Ga_2O_3 on Si and (b) Ga_2O_3 after removal of 5 nm by ALE using HF and TMG at 300 ºC.

AFM images of a Ga_2O_3 film after deposition and after etching are shown in Fig. 4.6. A scan size of 25.0-um^2 was used to investigate the surface structure. An RMS surface roughness of 0.55 ± 0.05 nm was determined for 10 nm of PEALD Ga_2O_3 deposited at 250 ºC on Si (100). After removal of 5.0 nm by ALE at 300 ºC, the RMS roughness was 0.56 ± 0.05 nm, indicating uniform and conformal etching of the film.

4.4 Discussion

Thin films of Ga_2O_3 were deposited by PEALD using O_2 plasma as the oxidizing agent and TMG serving as the Ga source, then etched by thermal ALE using exposures of HF and TMG within the same reaction chamber.

During ALD, the TMG reaction step results in adsorbed precursor molecules on the substrate surface. The O_2 plasma exposure serves to both combust unreacted methyl groups at the surface, as well as oxidize the adsorbed Ga.

The proposed overall ALE reaction can be written as [40,46]

$$Ga_2O_{3(s)} + 6\,HF_{(g)} + 4\,Ga(CH_3)_{3(g)} \rightarrow 3\,H_2O_{(g)} + 6\,GaF(CH_3)_{2(g)}$$

which results in the production and desorption of H_2O and volatile $GaF(CH_3)_2$ species. This occurs through two discrete reactions at the surface, including fluorination with HF,

$$Ga_2O_{3(s)} + 6\,HF_{(g)} \rightarrow 2\,GaF_{3(ads)} + 3\,H_2O_{(g)},$$

and ligand exchange with TMG,

$$GaF_{3(ads)} + 2\,Ga(CH_3)_{3(g)} \rightarrow 3\,GaF(CH_3)_{2(g)}.$$

HF exposures result in the formation of a stable, non-volatile fluoride at the surface, as confirmed by XPS. Ellipsometry indicated that HF exposures does not spontaneously etch the Ga_2O_3 film at 300 ºC, as repeated exposures of HF without additional reactant exposures did not produce an evident change in film thickness. Ligand exchange between TMG and the fluorinated surface produces volatile $GaF_x(CH_3)_y$ species which desorb from the surface. Repeated TMG exposures did not etch Ga_2O_3 without prior fluorination, as ligand exchange with the fluorinated surface is necessary for volatile product formation and, therefore, vital for material removal.

Shorter N_2 purge times between precursor exposures resulted in unusually high deposition and etch rates for ALD and ALE. With an N_2 purge time 7.5 s, a deposition rate of 1.6 ± 0.2 Å/cycle and an etch rate of 2.0 ± 0.1 Å/cycle was observed, which are higher than typically reported values for ALD and ALE processes. This enhanced rate was attributed to residual reactants near the surface from incomplete purges producing non-ALD and non-ALE behavior.

TMA has previously been used for ALE of several other materials, but our literature search did not identify other reports of ALE using TMG for ligand-exchange. The viability for TMG to be used in etching processes of Ga_2O_3 when used with HF therefore expands the selection of precursors which may be used for ALE. The use of TMG as an ALE reactant also enables simple implementation of a single system for both ALD and ALE of Ga_2O_3. This requires only the addition of an HF source to an existing ALD system equipped with TMG and an oxygen source, such as O_2 plasma, O_3, or H_2O.

Gallium Nitride (GaN) is a related material which has also gained considerable interest recently due to favorable material properties which provide potential applications in power electronics and memory devices in addition to its currently realized applications in LEDs, lasers, and other photoelectronic devices. [47] As the native oxide of GaN is GaO_x, the ALE of Ga_2O_3 may provide a unique pathway for a conversion etch process. As others have reported, direct fluorination of GaN using HF is not a favorable process. [48] Therefore, oxidation of GaN could provide a pathway for fluorination and therefore a conversion etch method similar to those used for the ALE of Si, SiO_2, W, and other materials. [49–51]

4.5 Conclusions

PEALD of Ga_2O_3 was studied using TMG and O_2 plasma as precursors, and ALE of GaN was studied using TMG and HF. *In situ* multi-wavelength ellipsometry and x-ray photoelectron spectroscopy studies demonstrated both ALD and ALE of Ga_2O_3 was achieved, with a growth per cycle (GPC) of 0.9 ± 0.1 Å and an etch per cycle (EPC) of 1.0 ± 0.1 Å. HF was effective in the surface modification of Ga_2O_3, as it has been demonstrated

for ALE of Ga_2O_3 with various other precursors, including boron trichloride BCl_3, dimethyl aluminum chloride $AlCl(CH_3)_2$, trimethyl aluminum $Al(CH_3)_3$, titanium tetrachloride $TiCl_4$, and $Ga(N(CH_3)_2)_3$ as. [52] Ligand exchange using TMG as the metal precursor was demonstrated in this ALE process as well as this PEALD process. Previously reported demonstrations of ALE using TMG were not identified in our literature review, suggesting this as a new use of TMG as an effective metal precursor for ligand exchange in ALE.

Acknowledgements

This work was supported by Advanced Research Projects Agency-Energy under the PN-Diodes program through grant No. DE-AR0001691. We acknowledge the use of facilities within the John. M. Cowley Center for High Resolution Electron Microscopy and the NanoFab, at Arizona State University, supported in part by the NSF program NNCI-ECCS-1542160. We acknowledge Dr. Zhiyu Huang for performing ex situ spectroscopic ellipsometry measurements. We would like to thank Dr. Xingye Wang and Dr. Mei Hao for useful discussions.

REFERENCES

[1] M. Rebien, W. Henrion, M. Hong, J. P. Mannaerts, and M. Fleischer, *Optical Properties of Gallium Oxide Thin Films*, Applied Physics Letters **81**, 250 (2002).

[2] F.-P. Yu, S.-L. Ou, and D.-S. Wuu, *Pulsed Laser Deposition of Gallium Oxide Films for High Performance Solar-Blind Photodetectors*, Optical Materials Express **5**, 1240 (2015).

[3] X. Li, H. L. Lu, H. P. Ma, J. G. Yang, J. X. Chen, W. Huang, Q. Guo, J. J. Feng, and D. W. Zhang, *Chemical, Optical, and Electrical Characterization of Ga_2O_3 Thin Films Grown by Plasma-Enhanced Atomic Layer Deposition*, Current Applied Physics **19**, 72 (2019).

[4] M. Passlack, N. E. J. Hunt, E. F. Schubert, G. J. Zydzik, M. Hong, J. P. Mannaerts, R. L. Opila, and R. J. Fischer, *Dielectric Properties of Electron-Beam Deposited Ga_2O_3 Films*, Applied Physics Letters **64**, 2715 (1994).

[5] T. Yamada, J. Ito, R. Asahara, K. Watanabe, M. Nozaki, S. Nakazawa, Y. Anda, M. Ishida, T. Ueda, A. Yoshigoe, T. Hosoi, T. Shimura, and H. Watanabe, *Comprehensive Study on Initial Thermal Oxidation of GaN(0001) Surface and Subsequent Oxide Growth in Dry Oxygen Ambient*, Journal of Applied Physics **121**, (2017).

[6] G. X. Liu, F. K. Shan, J. J. Park, W. J. Lee, G. H. Lee, I. S. Kim, B. C. Shin, and S. G. Yoon, *Electrical Properties of Ga_2O_3-Based Dielectric Thin Films Prepared by Plasma Enhanced Atomic Layer Deposition (PEALD)*, Journal of Electroceramics **17**, 145 (2006).

[7] K. Sasaki, A. Kuramata, T. Masui, E. G. Víllora, K. Shimamura, and S.

Yamakoshi, *Device-Quality β-Ga_2O_3 Epitaxial Films Fabricated by Ozone Molecular Beam Epitaxy*, Applied Physics Express **5**, 8 (2012).

[8] G. Wagner, M. Baldini, D. Gogova, M. Schmidbauer, R. Schewski, M. Albrecht, Z. Galazka, D. Klimm, and R. Fornari, *Homoepitaxial Growth of β-Ga_2O_3 Layers by Metal-Organic Vapor Phase Epitaxy*, Physica Status Solidi (A) Applications and Materials Science **211**, 27 (2014).

[9] I. Donmez, C. Ozgit-Akgun, and N. Biyikli, *Low Temperature Deposition of Ga_2O_3 Thin Films Using Trimethylgallium and Oxygen Plasma*, Journal of Vacuum Science & Technology A: Vacuum, Surfaces, and Films **31**, 01A110 (2013).

[10] A. Mahmoodinezhad, C. Janowitz, F. Naumann, P. Plate, H. Gargouri, K. Henkel, D. Schmeißer, and J. I. Flege, *Low-Temperature Growth of Gallium Oxide Thin Films by Plasma-Enhanced Atomic Layer Deposition*, Journal of Vacuum Science & Technology A **38**, 022404 (2020).

[11] H. Lee, K. Kim, J. J. Woo, D. J. Jun, Y. Park, Y. Kim, H. W. Lee, Y. J. Cho, and H. M. Cho, *ALD and MOCVD of Ga_2O_3 Thin Films Using the New Ga Precursor Dimethylgallium Isopropoxide, Me_2GaO^iPr*, Chemical Vapor Deposition **17**, 191 (2011).

[12] M. Nieminen, L. Niinistö, and E. Rauhala, *Growth of Gallium Oxide Thin Films from Gallium Acetylacetonate by Atomic Layer Epitaxy*, Journal of Materials Chemistry **6**, 27 (1996).

[13] V. D. Wheeler, N. Nepal, D. R. Boris, S. B. Qadri, L. O. Nyakiti, A. Lang, A. Koehler, G. Foster, S. G. Walton, C. R. Eddy, and D. J. Meyer, *Phase Control of*

Crystalline Ga_2O_3 Films by Plasma-Enhanced Atomic Layer Deposition, Chemistry of Materials **32**, 1140 (2020).

[14] M. Passlack, E. F. Schubert, W. S. Hobson, M. Hong, N. Moriya, S. N. G. Chu, K. Konstadinidis, J. P. Mannaerts, M. L. Schnoes, and G. J. Zydzik, *Ga_2O_3 Films for Electronic and Optoelectronic Applications*, Journal of Applied Physics **77**, 686 (1995).

[15] L. Mazeina, F. K. Perkins, V. M. Bermudez, S. P. Arnold, and S. M. Prokes, *Functionalized Ga_2O_3 Nanowires as Active Material in Room Temperature Capacitance-Based Gas Sensors*, Langmuir **26**, 13722 (2010).

[16] A. V. Almaev, E. V. Chernikov, V. V. Novikov, B. O. Kushnarev, N. N. Yakovlev, E. V. Chuprakova, V. L. Oleinik, A. D. Lozinskaya, and D. S. Gogova, *Impact of Cr_2O_3 Additives on the Gas-Sensitive Properties of β-Ga_2O_3 Thin Films to Oxygen, Hydrogen, Carbon Monoxide, and Toluene Vapors*, Journal of Vacuum Science & Technology A **39**, 023405 (2021).

[17] H. Zhou, K. Maize, G. Qiu, A. Shakouri, and P. D. Ye, *β-Ga_2O_3 on Insulator Field-Effect Transistors with Drain Currents Exceeding 1.5 A/Mm and Their Self-Heating Effect*, Applied Physics Letters **111**, (2017).

[18] F. Ren, M. Hong, J. P. Mannaerts, J. R. Lothian, and A. Y. Cho, *Wet Chemical and Plasma Etching of $Ga_2O_3(Gd_2O_3)$*, Journal of the Electrochemical Society **144**, 239 (1997).

[19] T. Minami, Y. Nishi, T. Miyata, and J. I. Nomoto, *High-Efficiency Oxide Solar Cells with ZnO/Cu_2O Heterojunction Fabricated on Thermally Oxidized Cu_2O Sheets*, Applied Physics Express **4**, 2 (2011).

[20] A. K. Chandiran, N. Tetreault, R. Humphry-Baker, F. Kessler, E. Baranoff, C. Yi, M. K. Nazeeruddin, and M. Grätzel, *Subnanometer Ga_2O_3 Tunnelling Layer by Atomic Layer Deposition to Achieve 1.1 v Open-Circuit Potential in Dye-Sensitized Solar Cells*, Nano Letters **12**, 3941 (2012).

[21] H. Feng, W. Hao, C. Zhao, X. Xin, J. Cheng, Y. Cui, Y. Chen, and W. Wang, *Fabrication and UV-Sensing Properties of One-Dimensional β-Ga_2O_3 Nanomaterials*, Physica Status Solidi (A) Applications and Materials Science **210**, 1861 (2013).

[22] T. Oshima, T. Okuno, and S. Fujita, *Ga_2O_3 Thin Film Growth on c-Plane Sapphire Substrates by Molecular Beam Epitaxy for Deep-Ultraviolet Photodetectors*, Japanese Journal of Applied Physics, Part 1: Regular Papers and Short Notes and Review Papers **46**, 7217 (2007).

[23] T. Oshima, T. Okuno, N. Arai, N. Suzuki, S. Ohira, and S. Fujita, *Vertical Solar-Blind Deep-Ultraviolet Schottky Photodetectors Based on β-Ga_2O_3 Substrates*, Applied Physics Express **1**, (2008).

[24] D. W. Choi, K. B. Chung, and J. S. Park, *Low Temperature Ga_2O_3 Atomic Layer Deposition Using Gallium Tri-Isopropoxide and Water*, Thin Solid Films **546**, 31 (2013).

[25] Y. Zhou, C. Ahyi, T. Isaacs-Smith, M. Bozack, C. C. Tin, J. Williams, M. Park, A. jen Cheng, J. H. Park, D. J. Kim, D. Wang, E. A. Preble, A. Hanser, and K. Evans, *Formation, Etching and Electrical Characterization of a Thermally Grown Gallium Oxide on the Ga-Face of a Bulk GaN Substrate*, Solid-State Electronics **52**, 756 (2008).

[26] H. Liang, Y. Chen, X. Xia, C. Zhang, R. Shen, Y. Liu, Y. Luo, and G. Du, *A Preliminary Study of SF_6 Based Inductively Coupled Plasma Etching Techniques for Beta Gallium Trioxide Thin Film*, Materials Science in Semiconductor Processing **39**, 582 (2015).

[27] J. E. Hogan, S. W. Kaun, E. Ahmadi, Y. Oshima, and J. S. Speck, *Chlorine-Based Dry Etching of β-Ga_2O_3*, Semiconductor Science and Technology **31**, 065006 (2016).

[28] A. P. Shah and A. Bhattacharya, *Inductively Coupled Plasma Reactive-Ion Etching of β-Ga_2O_3: Comprehensive Investigation of Plasma Chemistry and Temperature*, Journal of Vacuum Science & Technology A: Vacuum, Surfaces, and Films **35**, 041301 (2017).

[29] J. Yang, S. Ahn, F. Ren, R. Khanna, K. Bevlin, D. Geerpuram, S. J. Pearton, and A. Kuramata, *Inductively Coupled Plasma Etch Damage in (-201) Ga_2O_3 Schottky Diodes*, Applied Physics Letters **110**, 1 (2017).

[30] Y. Kwon, G. Lee, S. Oh, J. Kim, S. J. Pearton, and F. Ren, *Tuning the Thickness of Exfoliated Quasi-Two-Dimensional β-Ga_2O_3 Flakes by Plasma Etching*, Applied Physics Letters **110**, (2017).

[31] R. Khanna, K. Bevlin, D. Geerpuram, J. Yang, F. Ren, and S. J. Pearton, *Dry Etching of Ga_2O_3*, Gallium Oxide 263 (2019).

[32] K. J. Kanarik, T. Lill, E. A. Hudson, S. Sriraman, S. Tan, J. Marks, V. Vahedi, and R. A. Gottscho, *Overview of Atomic Layer Etching in the Semiconductor Industry*, Journal of Vacuum Science & Technology A: Vacuum, Surfaces, and Films **33**, 020802 (2015).

[33] G. S. Oehrlein, D. Metzler, and C. Li, *Atomic Layer Etching at the Tipping Point: An Overview*, ECS Journal of Solid State Science and Technology **4**, N5041 (2015).

[34] K. Nojiri, K. J. Kanarik, S. Tan, E. A. Hudson, and R. A. Gottscho, *Atomic Layer Etching-Breaking Through the Limitation of Etch*, 1 (2018).

[35] C. T. Carver, J. J. Plombon, P. E. Romero, S. Suri, T. A. Tronic, and R. B. Turkot, *Atomic Layer Etching: An Industry Perspective*, ECS Journal of Solid State Science and Technology **4**, N5005 (2015).

[36] K. J. Kanarik, S. Tan, and R. A. Gottscho, *Atomic Layer Etching: Rethinking the Art of Etch*, Journal of Physical Chemistry Letters **9**, 4814 (2018).

[37] S. D. Athavale, *Realization of Atomic Layer Etching of Silicon*, Journal of Vacuum Science & Technology B: Microelectronics and Nanometer Structures **14**, 3702 (1996).

[38] K. J. Kanarik, S. Tan, W. Yang, T. Kim, T. Lill, A. Kabansky, E. A. Hudson, T. Ohba, K. Nojiri, J. Yu, R. Wise, I. L. Berry, Y. Pan, J. Marks, and R. A. Gottscho, *Predicting Synergy in Atomic Layer Etching*, Journal of Vacuum Science & Technology A: Vacuum, Surfaces, and Films **35**, 05C302 (2017).

[39] Y. Lee, J. W. Dumont, and S. M. George, *Atomic Layer Etching of Al_2O_3 Using Sequential, Self-Limiting Thermal Reactions with $Sn(Acac)_2$ and Hydrogen Fluoride*, Journal of Physical Chemistry C **119**, 25385 (2015).

[40] Y. Lee, J. W. Dumont, and S. M. George, *Trimethylaluminum as the Metal Precursor for the Atomic Layer Etching of Al_2O_3 Using Sequential, Self-Limiting Thermal Reactions*, Chemistry of Materials **28**, 2994 (2016).

[41] S. M. George and Y. Lee, *Prospects for Thermal Atomic Layer Etching Using Sequential, Self-Limiting Fluorination and Ligand-Exchange Reactions*, ACS Nano **10**, 4889 (2016).

[42] S. M. George, *Mechanisms of Thermal Atomic Layer Etching*, Accounts of Chemical Research **53**, 1151 (2020).

[43] Y. Lee, C. Huffman, and S. M. George, *Selectivity in Thermal Atomic Layer Etching Using Sequential, Self-Limiting Fluorination and Ligand-Exchange Reactions*, Chemistry of Materials **28**, 7657 (2016).

[44] S. Ohira and N. Arai, *Wet Chemical Etching Behavior of β-Ga_2O_3 Single Crystal*, Physica Status Solidi (C) Current Topics in Solid State Physics **5**, 3116 (2008).

[45] C. D. Wagner, *Sensitivity Factors for XPS Analysis of Surface Atoms*, Journal of Electron Spectroscopy and Related Phenomena **32**, 99 (1983).

[46] C. Fang, Y. Cao, D. Wu, and A. Li, *Thermal Atomic Layer Etching: Mechanism, Materials and Prospects*, Progress in Natural Science: Materials International **28**, 667 (2018).

[47] B. J. Baliga, *Gallium Nitride Devices for Power Electronic Applications*, Semiconductor Science and Technology **28**, (2013).

[48] N. R. Johnson, J. K. Hite, M. A. Mastro, C. R. Eddy, and S. M. George, *Thermal Atomic Layer Etching of Crystalline GaN Using Sequential Exposures of XeF_2 and BCl_3*, Applied Physics Letters **114**, (2019).

[49] A. I. Abdulagatov and S. M. George, *Thermal Atomic Layer Etching of Silicon Using O_2, HF, and $Al(CH_3)_3$ as the Reactants*, Chemistry of Materials **30**, 8465 (2018).

[50] R. Rahman, E. C. Mattson, J. P. Klesko, A. Dangerfield, S. Rivillon-Amy, D. C. Smith, D. Hausmann, and Y. J. Chabal, *Thermal Atomic Layer Etching of Silica and Alumina Thin Films Using Trimethylaluminum with Hydrogen Fluoride or Fluoroform*, ACS Applied Materials and Interfaces **10**, 31784 (2018).

[51] N. R. Johnson and S. M. George, *WO_3 and W Thermal Atomic Layer Etching Using "Conversion-Fluorination" and "Oxidation-Conversion-Fluorination" Mechanisms*, ACS Applied Materials and Interfaces **9**, 34435 (2017).

[52] Y. Lee, N. R. Johnson, and S. M. George, *Thermal Atomic Layer Etching of Gallium Oxide Using Sequential Exposures of HF and Various Metal Precursors*, Chemistry of Materials **32**, 5937 (2020).

CHAPTER V

ATOMIC LAYER ETCHING OF GALLIUM NITRIDE USING O_2 PLASMA OXIDATION, FLUORINATION, AND LIGAND-EXCHANGE

Research performed in collaboration with Daniel C. Messina, Saurabh Vishwakarma, Prudhvi Peri, David Smith, and Robert J. Nemanich

ABSTRACT

Conventional dry etching methods for GaN produce electrically active damage, which impacts device performance. Atomic layer etching (ALE) is a highly selective, self-limiting, and low-damage technique for material removal with atomic scale precision. Fluorination of GaN using HF has been shown to be insufficient for ALE. In this study, an oxidation, fluorination, and ligand-exchange mechanism is investigated for ALE of crystalline GaN. Oxidation by O_2 plasma exposure provides a pathway for surface fluorination by HF. This process was characterized using in situ x-ray photoelectron spectroscopy, in situ multi-wavelength ellipsometry, and transmission electron microscopy (TEM). Our results indicate this ALE process was less effective than anticipated, likely due to the crystallinity of the GaN substrates and the converted oxide surface.

5.1 Introduction

Development of GaN based electronic devices has been limited by the ability to achieve selective area doping and management of structural and point defects within GaN. [1] Dry etching of GaN, typically required for device fabrication, may introduce electrically active defects into the material. [2–4] Current leakage and high field

breakdown have been observed to be particularly affected in GaN-based devices prepared by reactive ion etching (RIE) or inductively coupled plasma (ICP) etching.

Atomic layer etching (ALE) is a self-limiting technique for material removal from wafer surfaces with atomic level precision. Sequential exposures of reactants are used to facilitate discrete half-reactions at the material surface. The half-reactions typically follow a modification-then-removal process to selectively etch material at an atomic scale. Due to the self-limiting nature of the ALE reactions, these etch methods produce little to no damage to the surface or underlying material.

ALE has been proposed as a method for removing damaged material produced by conventional dry etching methods. Etch-induced defects are most highly concentrated within a few nanometers within the surface and near-surface regions. However, deep damage may also occur, with reported damage extending beyond 50 nm from the wafer surface. [5] In Si, this damage has been found to be even deeper, with hydrogen found >30 nm from the substrate surface and deuterium >200 nm from the surface. [6] Although thermal annealing and N_2 plasma treatment has been shown to improve device performance, this is attributed primarily to recovery of damage limited to the first few nanometers from the surface. [7–9] Removal of deeper damage may prove necessary to achieve full realization of the potential performance of vertical GaN-based devices.

GaN ALE has previously been reported using plasma reactants common for conventional GaN dry etching techniques. ALE using surface modification by Cl_2 plasma followed by removal using a low energy Ar plasma was demonstrated by Kauppinen, *et al*.

using a conventional RIE reactor. [10] This enabled wide use of ALE for GaN fabrication with existing processing equipment.

In contrast to the prior research, our ALE process for GaN is informed by recent thermal ALE methods to limit the ion component of the etching process. In thermal ALE, removal of the modified surface typically occurs through a ligand-exchange mechanism in which a metal precursor exchanges a ligand with a molecule at the modified surface, producing stable and volatile complexes that desorb from the surface. [11] Fluorination and ligand-exchange is a commonly used method for thermal ALE of several oxide and nitride materials.

At this time, thermal ALE investigations have been performed primarily on amorphous materials prepared by atomic layer deposition (ALD). Thermal ALE of crystalline materials has been explored for several materials, including Al_2O_3, HfO_2, and ZnO_2. These materials were grown by ALD and annealed at high temperature to form polycrystalline films. [12,13] These studies have found that the etch rate of the crystalline material is reduced compared to the amorphous material under the same etch conditions. [12,13] For ALE of HfO_2, the etch rate decreased from 0.36 Å/cycle for the amorphous material to only 0.02 Å/cycle for crystalline HfO_2 using HF and $TiCl_4$ at 250 °C. [14] For crystalline Al_2O_3, etching was particularly diminished, with an etch rate of 0.76 Å/cycle for amorphous and 0.06 Å/cycle for the first 10 Å, followed by negligible etching of the remaining crystalline Al_2O_3 material. [15] These reductions in etch rates were attributed to higher density of the crystalline material.

Thermal ALE of crystalline GaN and AlN has also been reported. A fully thermal ALE process for crystalline GaN was reported by Johnson, *et al.*, involving the use of XeF_2 and BCl_3 with etch rates as high as 0.72 Å/cycle at 300°C. [16] However, this report also showed that HF and SF_6 proved to be ineffective ALE precursors as no etching was observed over 20 ALE reaction cycles. This report also demonstrated ALE of GaN using a combination of plasma and thermal reactions with NF_3 plasma for fluorination and BCl_3 for ligand-exchange.

Thermal ALE of crystalline AlN was performed using HF and tin acetylacetonate [$Sn(CH_3COCHCOCH_3)_2$, $Sn(acac)_2$] with an etch rate of 0.36 Å/cycle. [15] Etch rates were shown to improve when incorporating H_2 (1.96 Å/cycle) or Ar (0.66 Å/cycle) plasma exposure after $Sn(acac)_2$ exposure. Diminished etch rates were observed for a mixed AlO_xN_y layer at the surface, which was attributed to lower purity of the material.

We investigated an alternative etching pathway to accommodate the inability of HF to fluorinate the GaN surface. Our ALE process follows a plasma oxidation, fluorination, and ligand-exchange mechanism. The process begins with surface oxidation by a remote O_2 plasma. HF is then able to fluorinate the oxidized surface. After HF exposure, the resulting surface fluoride is stable and non-volatile at this temperature, so an additional step is required to remove the modified surface. Ligand-exchange with trimethylgallium [$Ga(CH_3)_3$, TMG] may then form $GaF(CH_3)_2$, which is volatile, and desorbs from the surface. A schematic of the ALE reactions is shown in Fig. 5.1. This method uses a limited ion component, to minimize plasma-induced damage, in which ions are not responsible for material removal.

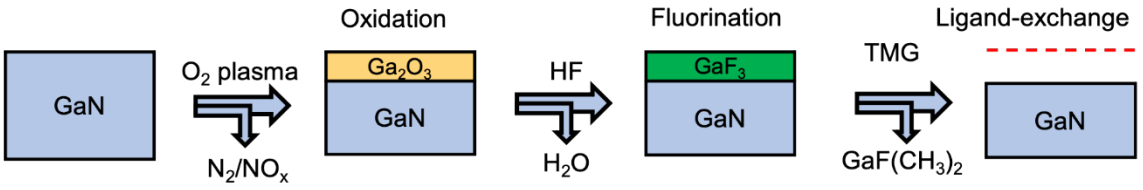

Figure 5.1 – Reaction schematic for plasma enhanced atomic layer etching of GaN using O_2 plasma for oxidation, HF for fluorination, and TMG for ligand-exchange.

5.2 Experimental Methods

ALE of GaN using O_2 plasma oxidation, HF fluorination, and ligand-exchange with trimethylgallium was investigated using in situ x-ray photoelectron spectroscopy (XPS), in situ multi-wavelength ellipsometry (MWE), and transmission electron microscopy (TEM).

Atomic layer etching was performed in a custom-built stainless-steel hot wall reactor. A turbomolecular pump backed by a roughing pump was used to reach a base pressure of 2 x 10^{-8} Torr for UHV sample transfer to XPS for sample characterization. A two-stage dry processing pump with a N_2 (99.999%, 14.2 SLM) dilution flow (Ebara, A70W) was used to reach a base pressure of 4 x 10^{-5} Torr during processing. Remote plasma generation occurred in a fused quartz tube using an inductively coupled 13.56 MHz RF generator (MKS, Elite 300), which was located approximately 25 cm above the wafer surface. The formation of a remote plasma limits the ion component of the plasma process, thereby reducing the plasma-related damage to the material. At this operating pressure, it is expected the O radicals will be fully thermalized. A bias was not applied to the grounded

substrate during the reactions. A C-type thermocouple, a proportional–integral–derivative (PID) controller (Eurotherm, 2216e), and a nichrome heating element behind the sample backside were used to radiatively heat the sample to 300 °C throughout the etching process. Chamber pressure was recorded at 1s intervals using a capacitance manometer (MKS, 627F) and a custom LabVIEW program.

HF vapor was derived from HF-pyridine ($(C_5H_5N)\cdot(HF)_x$, 70% HF by weight, Alfa-Aesar). The HF-pyridine was transferred into the precursor bubbler in a dry Ar filled PTFE glove bag. The HF-pyridine and TMG (99.998 wt%+, STREM Chemicals, Inc.) precursors were held at 30 ºC. Precursor vapor delivery occurred using ultra-high purity Ar (99.999%) carrier gas with flow rates of 5.0 standard cubic centimeters per minute (sccm) for TMG and 15.0 sccm for HF. Precursor exposure times of 30 seconds were used resulting in pressure transients of 600 – 800 mTorr and 200 – 400 mTorr for HF and TMG, respectively. A flow of N_2 at 30.0 sccm was used between reactant exposures to purge the system of unreacted precursor and byproducts. Multiple cycles of HF and TMG exposures were used between O_2 plasma exposures for removal of surface oxide formation.

Dynamic measurement of film thickness was made throughout the etching process using an *in situ* multi-wavelength ellipsometer (Film Sense, FS-1) mounted at 45° to the wafer surface. The ellipsometer used four light emitting diodes (LED) to produce light of wavelengths centered at 465 nm, 525 nm, 580 nm, and 635 nm. The polarization state of the reflected beam was determined using the division of amplitude polarimeter (DOAP) method. Data was collected at 1 s intervals using the manufacturer supplied software (Film Sense, desktop version 1.15).

This study was performed on GaN epitaxial layers grown by metal-organic chemical vapor deposition (MOCVD) using TMG and NH_3 as Ga and N sources, respectively, on a free-standing c-plane n^+ GaN substrate. Additionally, a study was performed on epitaxial GaN on Si supplied by Kyma Technologies. The GaN was grown using hydride vapor phase epitaxy (HVPE) with an intermediate AlN layer approximately 200 nm thick. Heteroepitaxial GaN was desired for resolution of GaN thickness using MWE.

In situ XPS (VG-Scienta, R3000) was performed using an Al K-α x-ray source with a photon energy of 1486.6 eV. The system was maintained at a base pressure of $5x10^{-10}$ Torr during measurements. XPS spectra were fit using Gaussian-Lorentzian line shapes after a standard Shirley background was subtracted. Spectral fitting enables resolution of peak binding energy to ± 0.1 eV. Empirically derived atomic sensitivity factors were used to determine surface stoichiometry. [17] The Ga 3d, N 1s, O 1s, C 1s, and F 1s XPS core level spectra were used for chemical state analysis at the wafer surface.

Samples were prepared for TEM by focused ion beam (FIB) (Thermo Fisher Scientific, Helios 5 UX dual beam system) initially operated at 30 kV, with further thinning at 5 kV, and a final cleaning at 2 kV. Field emission analytical electron microscopy (JOEL, JEM 2010F) operated at 200 kV and an aberration corrected TEM (Thermo Fisher Scientific, FEI Titan) operated at 300 kV were used to obtain high-resolution cross sectional images.

5.3 Results

In situ XPS, *in situ* MWE, and TEM were used to characterize ALE of GaN using O_2 plasma, HF, and TMG. XPS measurements were taken after each individual exposure for one cycle of ALE to study the surface reactions, as well as after multiple cycles of ALE.

Characterization of individual ALE reactions was performed using XPS between exposures of O_2 plasma, HF, and TMG. After O_2 plasma exposure, a reduction of intensity is observed for Ga 3d and N 1s, while a significant oxygen peak is observed in the O 1s spectrum. HF exposure resulted in an incomplete reduction of the O 1s signal as well as the identification of a F 1s peak. It is also noted a binding energy shift is observed for both the Ga 3d peak and the N 1s peak. This is attributed to adsorption-induced band bending at the surface from the chemisorption of fluorine. After TMG exposure, nearly complete removal of the F 1s peak is observed, as well as the formation of a small C 1s peak, indicating removal of fluoride and adsorption of methyl groups from TMG. These spectra are shown in Fig. 5.2.

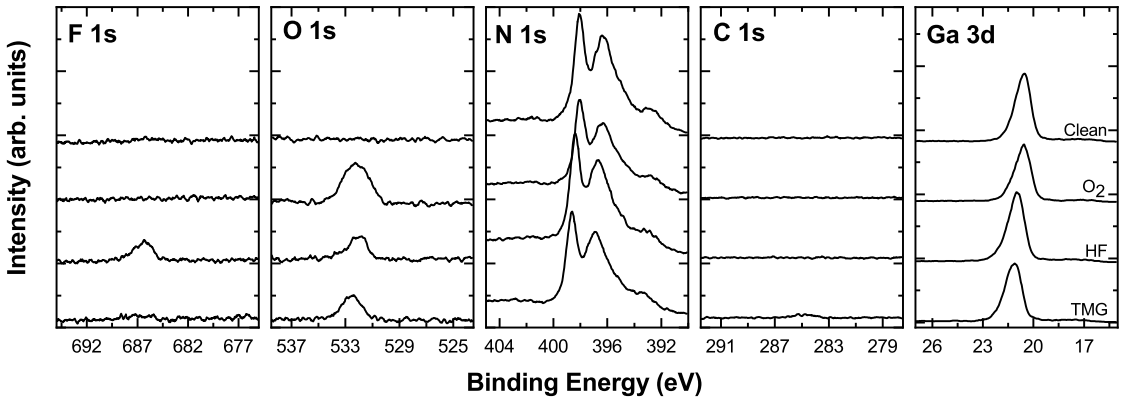

Figure 5.2 – XPS core level spectra of clean GaN and after individual ALE reactions, including; O_2 plasma, HF, and TMG.

Thickness measurements using *in situ* MWE were unable to resolve the GaN homoepitaxial interface or the wafer backside. Consequently, the MWE was used to measure formation of the oxide forming at the GaN surface using optical parameters for Ga_2O_3. XPS suggested single exposures of HF and TMG were not able to remove the oxidized surface. To fully remove the oxide, multiple alternating exposures of HF and TMG were employed. Thickness measurements of the surface oxide on GaN are shown in Fig. 5.3 during five ALE "supercycles" of O_2 plasma and alternating HF and TMG exposures. Using three alternating exposures of HF and TMG between O_2 plasma exposures resulted in a gradual increase in thickness, indicating oxide accumulation. When five alternating exposures of HF and TMG were employed, oxide thickness was not observed to increase over multiple cycles. The large spikes observed in the thickness measurements occurred during O_2 plasma exposures and are attributed to signal interference from the plasma ignition and birefringence of the quartz viewports on the chamber through which the MWE signal traverses.

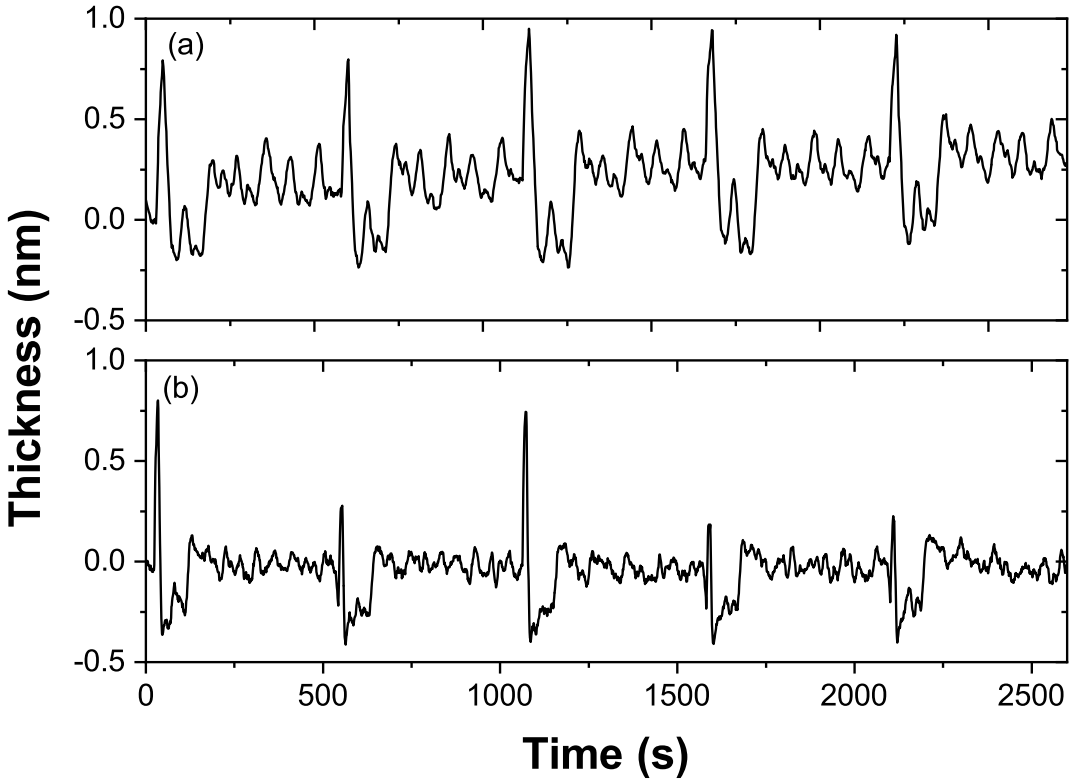

Figure 5.3 – Thickness of surface oxide measured using *in situ* MWE of GaN throughout five ALE supercycles consisting of (a) one O_2 plasma exposure followed by three alternating exposures of HF and TMG, and (b) one O_2 plasma exposure followed by five alternating exposures of HF and TMG.

To directly measure GaN thickness using in situ MWE, ALE was performed on 200 nm GaN on sapphire with an AlN buffer layer. A decrease in thickness was observed throughout one supercycle of O_2 plasma exposure and five alternating exposures of HF and TMG, as shown in Fig. 5.4. XPS scans were acquired after 10 supercycles of ALE indicated O, F, and C impurities remained at the surface. Only a small C 1s peak was observed, indicating very low C impurities. However, F impurities accounted for ~3 at. % of surface species within the XPS detection region.

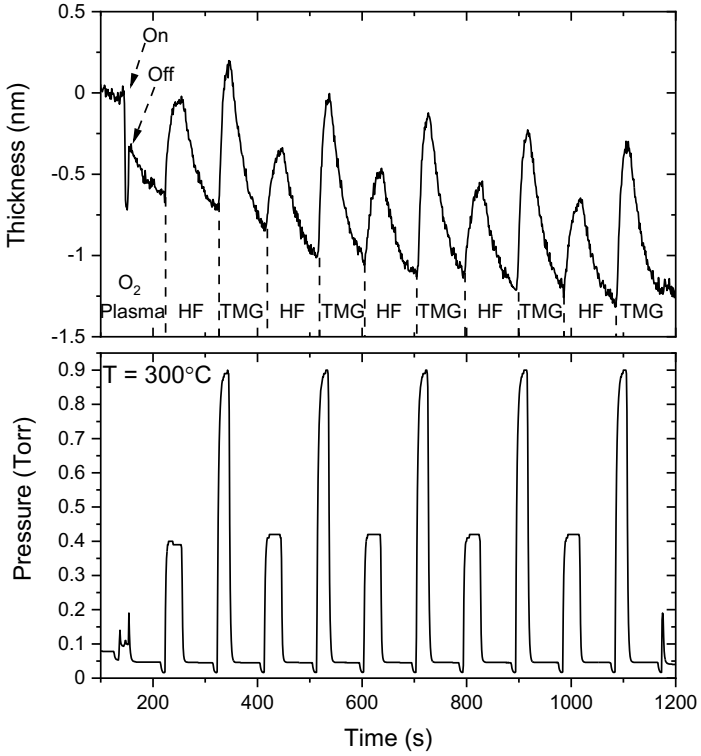

Figure 5.4 – Thickness change of 200 nm GaN film on sapphire, with chamber pressure during one supercycle of ALE using one O_2 plasma exposure and five alternating exposures of HF and TMG.

Metal contacts (Ti(50nm)/Au(100nm)) were patterned on GaN for characterization of the ALE process by TEM. A lithographic lift-off process was employed. ALE was performed on the sample to etch a thickness of 5 nm. This was compared to a non-patterned, non-etched control sample. The control sample is shown in Fig. 5.5(a,b) and the patterned and etched sample is shown in Fig. 5.5(c,d). Surface fringes are observed in Fig. 5.5(b) and (d), indicating some surface roughness. The Ti/Au metal contact is shown in Fig. 5.5(c) with the exposed and atomic layer etched surface to the right. The difference of GaN

thickness observed in the ALE exposed surface was less than anticipated and estimated to be <2 nm.

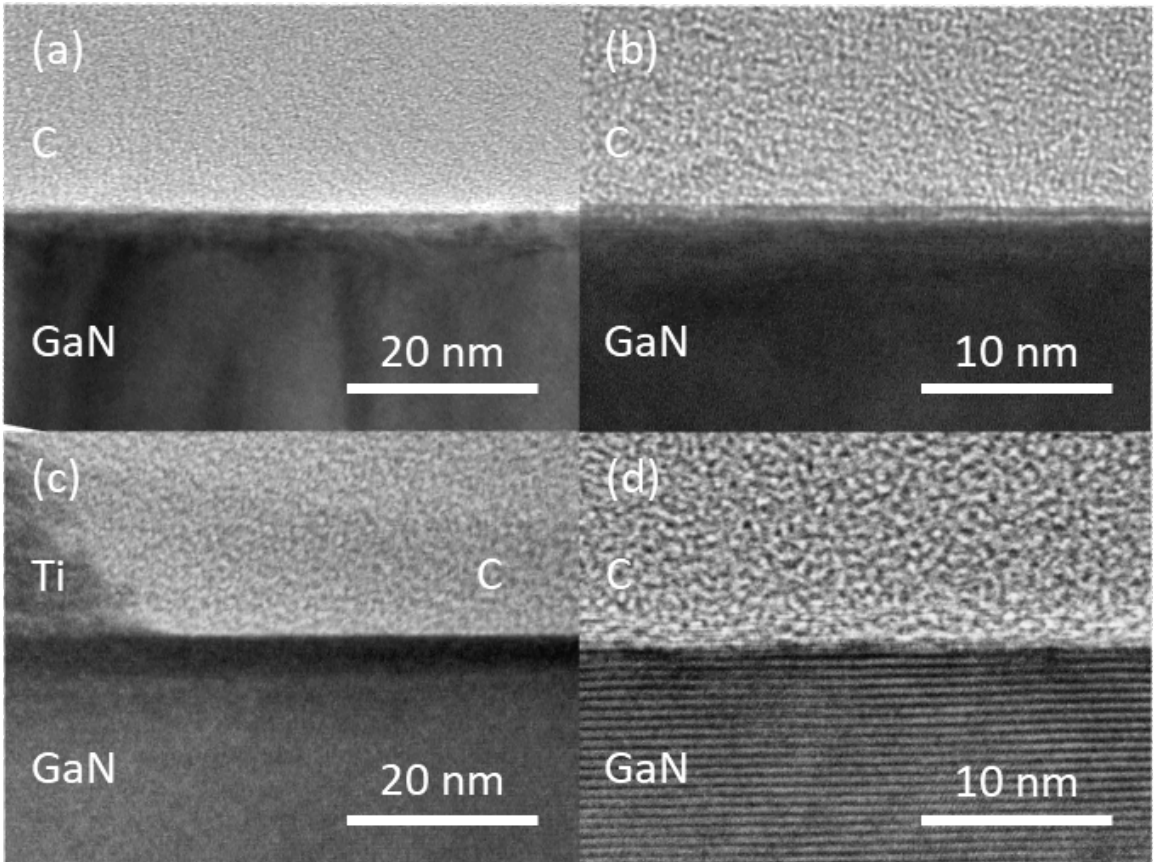

Figure 5.5 – Cross sectional images by TEM of (a,b) non-patterned and non-etched GaN, and (c,d) patterned GaN samples etched by ALE using O_2 plasma, fluorination, and ligand-exchange, (c) including the metal contact and (d) away from the metal contact.

5.4 Discussion

XPS measurements indicated O_2 plasma resulted in oxidation of ~1.0 nm of the GaN surface, and HF exposure reduced the oxide while fluorinating the surface, as expected. However, reduction of the oxide was not complete as O was still observed in the XPS measurements. XPS and ellipsometry measurements indicated an oxidized surface

remained after one cycle of O_2 plasma, HF, and TMG exposures, and repeated cycles produced oxide accumulation at the GaN surface. To compensate for this, multiple exposures of HF and TMG were employed to remove the oxide formed at the surface. The application of five alternating exposures of HF and TMG per each plasma oxidation prevented oxide accumulation, allowing for ALE supercycles to effectively etch GaN.

The thickness of MOCVD GaN samples obscured MWE measurement of the etch removal thickness. Instead, dynamic measurement of the thickness of the surface oxide was used to monitor the etching behavior. Increases in thickness of the surface oxide were indicative of oxide accumulation, as confirmed by XPS. Increased exposures of HF and TMG prevented oxide accumulation, resulting in a constant thin oxide layer as observed by MWE over multiple supercycles.

Surface fringes observed in TEM of the ALE GaN suggested lower surface roughness than the control sample, indicating ALE produced smoothing of the GaN surface. However, TEM results also indicated etch rate by ALE was lower than anticipated with only <2 nm removed from the surface over five ALE supercycles.

These results suggest the converted oxide could not be effectively etched using HF and TMG. This may be due to crystallinity of the oxide as Dycus, *et al.* [18] has shown that the native oxide on GaN (0001) is highly ordered in an arrangement similar to β-Ga_2O_3. Additionally, Hao, *et al.* [19] showed that crystalline β-Ga_2O_3 can be grown on GaN by plasma enhanced atomic layer deposition (PEALD) at only 250 °C. Similarly, PEALD Ga_2O_3 on GaN grown in our reaction chamber at 250 °C using TMG and O_2 plasma produced an ordered film for the first ~2 nm, as observed in TEM. A cross sectional image

of this PEALD Ga_2O_3 on GaN is shown in Fig. 5.6. A periodic structure is observed for the first ~2 nm above the interface.

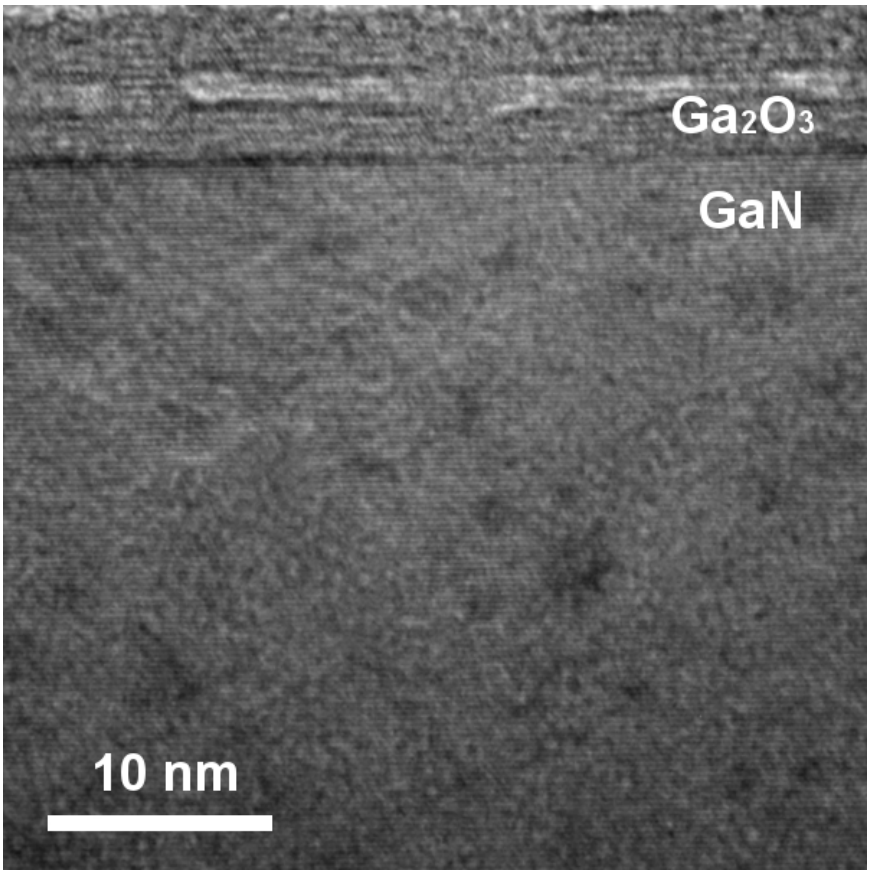

Figure 5.6 – Cross sectional TEM image of ~7 nm PEALD Ga_2O_3 on GaN.

HF and TMG have been shown to be effective for ALE of Ga_2O_3,[ref, my Ga_2O_3 paper] however, studies of ALE of crystalline AlN and Al_2O_3 suggest the crystalline III-nitrides and III-oxides may be more difficult to etch thermally using HF. Johnson, *et al*., reported a method for thermal ALE of crystalline AlN using HF and $Sn(acac)_2$. [15] In the study, wurtzite AlN (0001) was etched using HF and $Sn(acac)_2$. An XPS depth profile indicated the presence of a 4 nm AlO_xN_y layer at the AlN surface. Thermal ALE produced an etch rate of only 0.07 Å/cycle for the AlO_xN_y layer compared to 0.36 Å/cycle for the

underlying AlN. Murdzek, *et al*. showed that negligible etching of crystalline Al_2O_3 occurred beyond the initial 10 Å from the surface, when using HF and trimethylaluminum (TMA). [13]

ALE using O_2 plasma has recently been reported in a fully plasma-based ALE process of GaN using BCl_3 plasma as the other reactant, which indicates removal of the converted oxide is possible. [20] Although, it remains to be seen if there is a thermal pathway for removal. Future studies could investigate ALE of crystalline β-Ga_2O_3 using HF and TMG, as well as other thermal chemistries, as successful thermal ALE processes for crystalline Ga_2O_3 may prove effective in etching the converted oxide on GaN. Oxidation at other temperatures may also produce a less ordered oxide surface which may improve thermal reactions for ALE.

5.5 Conclusions

This study investigated oxidation as a pathway for ALE of GaN using O_2 plasma, HF, and TMG. Etching was characterized using *in situ* XPS, *in situ* MWE, and TEM. Multiple cycles of HF and TMG were necessary to remove the surface oxide formed during O_2 plasma exposure. TEM results indicated ALE produced smoothing of the surface, however, the etch rate using this method was smaller than predicted. This is attributed to a highly ordered native oxide formation on GaN producing decreased etch activity from thermal reactions. Alternative oxidation methods or different substrate temperatures during oxidation may be investigated to produce a less ordered surface oxide for improved ALE reactions.

Acknowledgements

This work was supported by the Advanced Research Projects Agency-Energy through the PN-Diodes program under grant No. DE-AR0000868. We acknowledge the use of facilities within the John M. Cowley Center for High Resolution Electron Microscopy, and the NanoFab, at Arizona State University, supported in part by the NSF program, NNCI-ECCS-1542160. We acknowledge Dr. Houqiang Fu and Dr. Kai Fu for deposition of MOCVD GaN, Kari Slotten for patterning of GaN samples, and Dr. Martha McCartney for their aid in performing SEM and TEM of the etched GaN. We would also like to thank Dr. Yuji Zhao, Dr. Fernando Ponce, Dr. Stephen Goodnick, Dr. Shanthan Alugubelli, Dr. Xingye Wang, and Dr. Mei Hao for their useful discussions.

REFERENCES

[1] H. Fu, K. Fu, C. Yang, H. Liu, K. A. Hatch, P. Peri, D. Herath Mudiyanselage, B. Li, T. H. Kim, S. R. Alugubelli, P. Y. Su, D. C. Messina, X. Deng, C. Y. Cheng, R. Vatan Meidanshahi, X. Huang, H. Chen, T. H. Yang, J. Zhou, A. M. Armstrong, A. A. Allerman, E. T. Yu, J. Han, S. M. Goodnick, D. J. Smith, R. J. Nemanich, F. A. Ponce, and Y. Zhao, *Selective Area Regrowth and Doping for Vertical Gallium Nitride Power Devices: Materials Challenges and Recent Progress*, Materials Today **xxx**, 1 (2021).

[2] Z. Mouffak, A. Bensaoula, and L. Trombetta, *The Effects of Nitrogen Plasma on Reactive-Ion Etching Induced Damage in GaN*, Journal of Applied Physics **95**, 727 (2004).

[3] R. J. Shul, L. Zhang, A. G. Baca, C. G. Willison, J. Han, S. J. Pearton, K. P. Lee, and F. Ren, *Inductively Coupled High-Density Plasma-Induced Etch Damage of GaN MESFETs*, Solid-State Electronics **45**, 13 (2001).

[4] J. M. Lee, K. M. Chang, S. W. Kim, C. Huh, I. H. Lee, and S. J. Park, *Dry Etch Damage in N-Type GaN and Its Recovery by Treatment with an N_2 Plasma*, Journal of Applied Physics **87**, 7667 (2000).

[5] X. A. Cao, H. Cho, S. J. Pearton, G. T. Dang, A. P. Zhang, F. Ren, R. J. Shul, L. Zhang, R. Hickman, and J. M. Van Hove, *Depth and Thermal Stability of Dry Etch Damage in GaN Schottky Diodes*, Applied Physics Letters **75**, 232 (1999).

[6] G. S. Oehrlein, *Dry Etching Damage of Silicon: A Review*, Materials Science and Engineering B **4**, 441 (1989).

[7] X. Wang, G. Yu, B. Lei, X. Wang, C. Lin, Y. Sui, S. Meng, M. Qi, and A. Li, *Recovery of Dry Etching-Induced Damage in n-GaN by Nitrogen Plasma Treatment at Growth Temperature*, Journal of Electronic Materials **36**, 697 (2007).

[8] D. G. Kent, K. P. Lee, A. P. Zhang, B. Luo, M. E. Overberg, C. R. Abernathy, F. Ren, K. D. Mackenzie, S. J. Pearton, and Y. Nakagawa, *Electrical Effects of N_2 Plasma Exposure on Dry-Etch Damage in p- and n-GaN Schottky Diodes*, Solid-State Electronics **45**, 1837 (2001).

[9] L. Ji-Myon, H. Chul, K. Dong-Joon, and P. Seong-Ju, *Dry-Etch Damage and Its Recovery in InGaN/GaN Multi-Quantum-Well Light-Emitting Diodes*, Semiconductor Science and Technology **18**, 530 (2003).

[10] C. Kauppinen, S. A. Khan, J. Sundqvist, D. B. Suyatin, S. Suihkonen, E. I. Kauppinen, and M. Sopanen, *Atomic Layer Etching of Gallium Nitride (0001)*, Journal of Vacuum Science & Technology A: Vacuum, Surfaces, and Films **35**, 060603 (2017).

[11] S. M. George, *Mechanisms of Thermal Atomic Layer Etching*, Accounts of Chemical Research **53**, 1151 (2020).

[12] J. A. Murdzek and S. M. George, *Effect of Crystallinity on Thermal Atomic Layer Etching of Hafnium Oxide, Zirconium Oxide, and Hafnium Zirconium Oxide*, Journal of Vacuum Science & Technology A **38**, 022608 (2020).

[13] J. A. Murdzek, A. Rajashekhar, R. S. Makala, and S. M. George, *Thermal Atomic Layer Etching of Amorphous and Crystalline Al_2O_3 Films*, Journal of Vacuum Science & Technology A **39**, 042602 (2021).

[14] J. A. Murdzek and S. M. George, *Thermal Atomic Layer Etching of Amorphous and Crystalline Hafnium Oxide, Zirconium Oxide, and Hafnium Zirconium Oxide*, 2019 International Symposium on VLSI Technology, Systems and Application (VLSI-TSA) **38**, 1 (2019).

[15] N. R. Johnson, H. Sun, K. Sharma, and S. M. George, *Thermal Atomic Layer Etching of Crystalline Aluminum Nitride Using Sequential, Self-Limiting Hydrogen Fluoride and $Sn(Acac)_2$ Reactions and Enhancement by H_2 and Ar Plasmas*, Journal of Vacuum Science & Technology A: Vacuum, Surfaces, and Films **34**, 050603 (2016).

[16] N. R. Johnson, J. K. Hite, M. A. Mastro, C. R. Eddy, and S. M. George, *Thermal Atomic Layer Etching of Crystalline GaN Using Sequential Exposures of XeF_2 and BCl_3*, Applied Physics Letters **114**, (2019).

[17] C. D. Wagner, *Sensitivity Factors for XPS Analysis of Surface Atoms*, Journal of Electron Spectroscopy and Related Phenomena **32**, 99 (1983).

[18] J. H. Dycus, K. J. Mirrielees, E. D. Grimley, R. Kirste, S. Mita, Z. Sitar, R. Collazo, D. L. Irving, and J. M. LeBeau, *Structure of Ultrathin Native Oxides on III–Nitride Surfaces*, ACS Applied Materials & Interfaces **10**, 10607 (2018).

[19] H. Hao, X. Chen, Z. Li, Y. Shen, H. Wang, Y. Zhao, R. Huang, T. Liu, J. Liang, Y. An, Q. Peng, and S. Ding, *Remote Plasma-Enhanced Atomic Layer Deposition*

of Gallium Oxide Thin Films with NH3 Plasma Pretreatment, Journal of Semiconductors **40**, 0 (2019).

[20] I. H. Hwang, H. Y. Cha, and K. S. Seo, *Low-damage and Self-limiting (Al)Gan Etching Process through Atomic Layer Etching Using O_2 and BCl_3 Plasma*, Coatings **11**, 1 (2021).

CHAPTER VI

EXTERNAL CHARGE COMPENSATION IN ETCHED GALLIUM NITRIDE MEASURED BY X-RAY PHOTOELECTRON SPECTROSCOPY

Research performed in collaboration with D. C. Messina, K. Fu, H. Fu, Y. Zhao, and R. J. Nemanich

ABSTRACT

Electronic states at GaN surfaces and at regrowth and heteroepitaxy interfaces inhibit electronic device performance. Understanding electronic state configuration at the GaN surface is therefore crucial for the development of GaN-based devices, which are currently of considerable interest in power electronic applications. GaN and other wurtzite III-nitrides possess a large spontaneous polarization along the c-axis, producing a bound sheet charge at the surface which affects the electronic state configuration through the formation of internal and external compensation charges. Defects induced by conventional plasma-based dry etching methods may inhibit internal screening of this bound charge and thus increase the concentration of external charged states. The surface band bending of n-type Ga-face GaN (0001) was measured with x-ray photoelectron spectroscopy after inductively coupled plasma (ICP) etching to investigate the impact of dry etching on external charge compensation. GaN samples were etched using inductively coupled plasma with varying RF power and a novel plasma enhanced atomic layer etching method using an oxidation, fluorination, and ligand-exchange mechanism. The band bending varied from 0.0 to 0.8 ± 0.1 eV for the samples measured.

6.1 Introduction

GaN is a wide bandgap semiconductor of considerable interest in the development of power electronics due to its superior chemical and physical properties. GaN-based devices exhibit improvements in power per unit width, energy conversion efficiency, switching frequency, and lower on-resistance over conventional Si devices. [1–3] Electronic state configuration at GaN surfaces and interfaces have been shown to greatly affect device performance, primarily in gate leakage, current collapse, and voltage breakdown. [4–6] The failure mechanisms associated with these issues aren't fully understood, but studies have suggested the defect states reduce drain current and provide a pathway for rapidly increasing excess gain current in a reverse polarization effect. [4–6] Piezoelectric and spontaneous polarization effects have also been shown to be of great importance in GaN/AlGaN heterostructures. [1,4,7–12]

There's a fundamental difference in the band bending of wurtzite group-III nitride (III-N) surfaces when compared to Si, diamond, zinc-blende, and traditional III-V and II-VI structures, which arises from the spontaneous polarization, the bound charge at the surface and interfaces, and the compensating charged states. Compensation of the bound charge arises from a combination of internal screening through formation of a surface charge region composed of electrons and ionized donors, and external screening through external surface charged states. The distribution of these compensation charges affects the internal electric field which ultimately affects device performance.

Conventional dry etching techniques such as inductively coupled plasma (ICP) etching and reactive ion etching (RIE) are essential in forming device structures. However, these etch

processes are known to introduce electrically active defects which hinder device performance. [13–20] The ion component of these methods rely on physical interaction with the surface through momentum transfer with surface atoms. This may introduce significant defect concentration in the surface and near-surface regions, as well as deeper electrically active damage which may propagate more than 50 nm into the material. [21] Surface defects induced by these dry etch methods may inhibit internal compensation of the polarization bound charge, resulting in larger concentration of external charged states. ICP etching allows for mitigation of defect formation through greater control of ion energy and flux, compared to RIE, by adjusting radio frequency (rf) bias and ICP power. [22–26] Several studies have also found high temperature annealing and N_2 plasma treatment to be effective in recovery of etch-induced damage with improvement in surface roughness and optical and electrical performance. [14–17,27]

Atomic layer etching (ALE) processes produce comparatively low damage as the active region is limited to surface groups. [28–31] ALE has also been proposed as a method for removing material from the surface and near-surface regions where significant defects are present. [31] Our ALE process may be considered a conversion-etch method which is a mechanism recently introduced in the development of thermal ALE methods for the etching of ZnO and SiO_2. [32–34] Firstly, the GaN surface is oxidized by a remote O_2 plasma which produces ~1 nm of oxide at the wafer surface, as measured by XPS and ellipsometry. Then, the oxide is fluorinated by HF exposure. The initial plasma oxidation is necessary to provide a pathway for fluorination by HF, as Johnson, *et al*. have found that HF does not sufficiently fluorinate the GaN surface for ALE. [35] And lastly, the fluorinated surface is removed through the formation of stable but volatile complexes

through ligand exchange with trimethylgallium (TMG). A schematic of this etch process is shown in Fig. 6.4. Fluorination and ligand exchange is a commonly used method for newly developed thermal ALE processes. [32,36,37] Several cycles of sequential HF and TMG exposures are required between each plasma oxidation to remove the surface oxide and complete one ALE "supercycle". The use of HF and TMG thermal reactions limits the ion component of this etch method which is expected to reduce damage to the surface and near-surface regions.

Measurements of band bending by photoelectron spectroscopy (PES) have been shown to depend on ambient conditions. Porsgaard, *et al.* [38] showed surface band bending of TiO_2 (110) varied with ambient O_2 pressure by 0.4 eV between UHV and atmospheric pressure (1 atm). To remove excess adsorbates and maintain consistent surface conditions for comparison of band bending measurements, *in situ* cleaning in NH_3 at 800 °C was used to prepare surfaces. A thin surface oxide remained on all samples which is representative of typical device interface.

X-ray photoelectron spectroscopy (XPS) is a widely used surface characterization technique for chemical state analysis to determine chemical composition and bonding, but has also been used for determination of surface band bending. [4,39–41] Band bending of GaN has shown to be of particular significance in representing surface quality after various processing methods. [4,39–44] This study compares band bending, measured by XPS, of GaN prepared by various processing methods and after various ICP etch conditions, to investigate the impact of dry etching on internal charge compensation and external charged states.

6.2 Polarization and Bound Charge in (0001) Gallium Nitride

The total polarization of a material is the sum of the spontaneous polarization of the equilibrium structure and the piezoelectric polarization induced by strain,

$$\vec{P} = \vec{P}_{pz} + \vec{P}_{sp}.$$

Restricting this along the c-axis, which is the direction of both the spontaneous polarization and in which standard bulk crystals are grown, the component of piezoelectric polarization for GaN along this direction is,

$$\vec{P}_{pz} = 2\left(\frac{a-a_0}{a_0}\right)\left(e_{31} - e_{33}\frac{C_{13}}{C_{33}}\right)\hat{c},$$

where a and a_0 are lattice constants, C_{13} and C_{33} are elastic constants, and e_{31} and e_{33} are piezoelectric coefficients. The piezoelectric polarization varies between samples and depends on growth conditions, substrate material, and external temperature and pressure. Although larger than in other compound materials, the piezoelectric polarization in relaxed GaN is negligible compared to the large spontaneous polarization. [4,45,46] The crystal structure and spontaneous polarization of GaN are shown in Fig. 6.1.

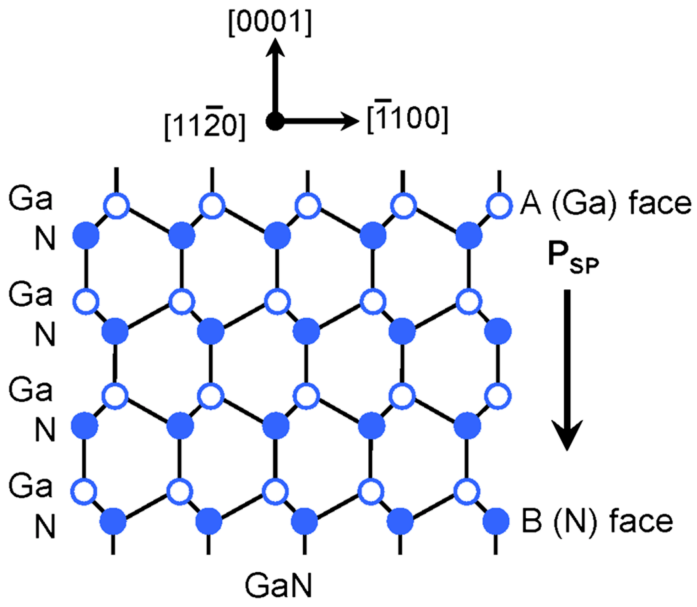

Figure 6.1 – Two dimensional projection of wurtzite GaN structure with spontaneous polarization. Reprinted with permission from Eller, *et al*. [4] Copyright © 2014, Springer Nature

The spontaneous polarization of wurtzite GaN has been calculated using the Berry-phase approach and local density or generalized gradient approximations to be -0.029 C/m^2 for Ga-face (0001). [10,47] The polarization is directed toward the N-face (000-1), as shown in Fig. 6.1. Experimental measurements of this polarization have produced a slightly lower value than theoretically predicted. One method reported by Yan, *et al.* found a polarization of approximately -0.022 C/m^2 using a thermodynamic model to indirectly determine the polarization from the GaN high-pressure phase transition. [48] Lähnemann, *et al.* also yielded a value of -0.022 ± 0.007 C/m^2 using microphotoluminescence and cathodoluminescence to determine emission energies of excitons bound to intrinsic stacking faults. [49]

This macroscopic polarization produces a negative bound sheet charge at the Ga-face (0001),

$$\sigma_b = \vec{P} \cdot \hat{c},$$

of $1.81 * 10^{13}$ charges/cm^2, using the theoretically predicted polarization of -0.029 C/m^2. A corresponding positive bound sheet charge is also produced at the N-face (000-1).

6.3 Charge Compensation and Band Bending

Gauss' Law and charge neutrality require that surface charges are compensated as the internal electric field of a wide bandgap semiconductor is equal to or approximately zero. Compensation of this large bound charge at the surface arises from a combination of external screening by external charged surface states and internal screening by the formation of a space charge region, as shown in Fig. 6.2. The densities of these compensation charges are therefore inversely related.

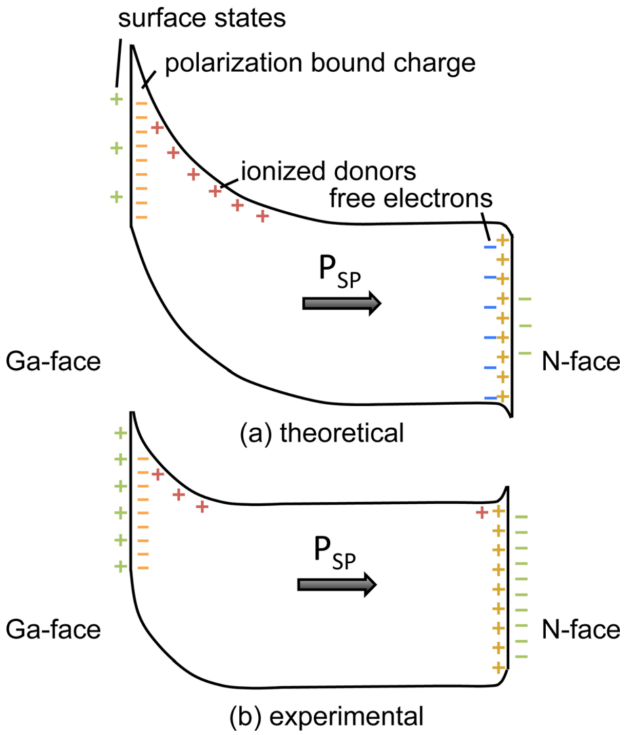

Figure 6.2 – (a) theoretical and (b) experimental band bending schematic for Ga- and N-face GaN. Reprinted with permission from Eller, *et al*. [4] Copyright © 2014, Springer Nature

An internal space charge region of ionized donors is formed at the surface to compensate the bound sheet charge. Band bending is a direct consequence of this internal screening and thus provides a method to measure this internal surface screening. However, dry etching and other processing methods may introduce defects into the material which inhibit the formation of this space charge region. The result is formation of external charge states to compensate the bound sheet charge.

Total compensation of the bound surface charge by internal screening would require a space charge region with upward band bending of 420 eV. However, the large internal field

results in inversion or accumulation. Band bending is therefore confined to the GaN bandgap, although experimental measurements on n-type GaN have been smaller, as shown in Fig. 6.2(b). Surface band bending of n-type GaN have been experimentally measured by various methods including XPS, [4] UPS, [50] scanning Kelvin probe microscopy, [44] and surface potential electric force microscopy (SP-EFM) [43] Experimental measurements of band bending in n-type GaN have yielded values ranging between -0.1 eV to 1.6 eV in various studies. [4,39,41,43,44,51]

Band bending is determined by the density of internal screening charge,

$$\phi_S = \frac{qN_{SS}^2}{2\epsilon\epsilon_0 N_D},$$

where q is the electron charge, N_{SS} is the surface state density, $\epsilon = 9.5$ is the relative permittivity of GaN, $\epsilon = 8.85 * 10^{-12} C/(V \cdot m)$ and $N_D = 1 * 10^{17} cm^{-3}$ is the donor density.

It then follows, changes in the relative density of surface states may be found from band bending measurements by the relation,

$$N_{SS} = \sqrt{2\epsilon\epsilon_0 N_D \left(\frac{\phi_S}{q}\right)}.$$

For GaN with a donor density of $N_D = 10^{17} cm^{-3}$, this suggests a change in band bending of 0.1 eV therefore corresponds to a reduction of surface state density by $3.2 * 10^{11}\ cm^{-2}$.

The samples in this study exhibited band bending varying from 0.0 eV to 0.8 eV. This is in agreement with previous studies which have found a likely Fermi level pinning state approximately 0.4 eV to 0.8 eV below the conduction band minimum. [4,50,52] This

pinning state has previously been attributed to a nitrogen vacancy or gallium dangling bond with agreement in experimental and theoretical results. The band bending response to various etch and processing methods is therefore limited by this pinning state.

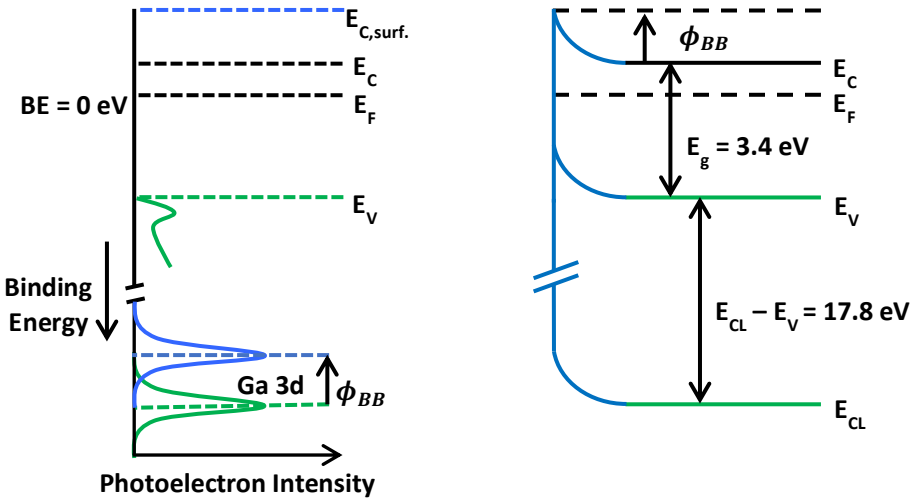

Figure 6.3 – GaN energy band diagram with surface band bending derived from the Ga 3d core level position measured by XPS.

Band bending may be determined from core levels measured by XPS using a method determined by Waldrop and Grant [53] and Kraut, *et al.*, [54] with the relation,

$$\phi_{BB} = (E_{CL} - E_V)_{bulk} + E_g - E_C - E_{CL,XPS}$$

where E_g is the band gap energy of GaN, taken to be 3.4 eV, [1–3] E_C is the conduction band level relative to the fermi level which was determined from the doping concentration to be 0.1 eV, [55] $(E_{CL} - E_V)_{bulk}$ is the energy spacing of the valence band from the Ga 3d core level in bulk GaN and is taken to be 17.8 eV as found in previous electronic state studies of GaN. [56–58]

Fermi level E_F position may be determined from the doping concentration N_D of a nondegenerate semiconductor from the relation, [55]

$$(E_C - E_F) = kT \ln (\mathrm{N_C}/\mathrm{N_D}),$$

where k is the Boltzmann constant and N_C is the effective density of states at the conduction band, which is 2.6 x 10^{18} cm^{-3} for n-type GaN. From this relation, it is estimated the Fermi level is ~0.1 eV below the conduction band for the measured samples.

6.4 Experimental Methods

XPS was used to study the impact of GaN dry etching on the surface band bending and external compensation charge. XPS measurements were performed using an Omicron-Scienta R3000 with an Al Kα x-ray source and a monochromatic photon energy of 1482.35 eV. The system is maintained at a base pressure of 7 x 10^{-10} Torr and is connected to a UHV transfer system with a base pressure of 3 x 10^{-9} Torr to minimize contamination exposure between processing and characterization. Using an analyzer slit size of 0.2 mm and a pass energy of 100 eV for this system, measured binding energies may be resolved to ± 0.1 eV. Calibration of XPS peak position was determined using a gold foil. XPS peak fitting was performed using a Gaussian-Lorentz peak shape and a standard Shirley background was subtracted prior to spectral fitting. The Ga 3d, N 1s, C 1s, O 1s, and F 1s XPS core level spectra were used for chemical state analysis at the wafer surface. Atomic sensitivity factors were used to determine surface composition. [59]

This study was performed on homoepitaxially grown GaN by metal-organic chemical vapor deposition (MOCVD) on a c-plane n^+ GaN substrate using trimethylgallium (TMG) and NH_3 at a growth temperature of 1050°C. The epitaxial GaN was n-type with a Si donor

concentration of 10^{17} cm^{-3}. The Fermi level was determined to be ~ 0.1 eV below the conduction band at this doping density. [55]

The samples were then transferred to UHV (~10^{-9} Torr) for XPS characterization and *in situ* processing. Initial XPS measurements were taken for all samples prior to *in situ* processing. *In situ* cleaning methods were performed by high temperature annealing in NH_3 ambient in a molecular beam epitaxy (MBE) chamber with a base pressure of <1*10^{-9} Torr. The GaN substrate was heated to 800 °C using a tungsten filament positioned under the back of the sample for 30 min. An NH_3 flux with a flow rate of 10 sccm maintained the chamber pressure at 1 x 10^{-5} Torr throughout heating, annealing, and cool-down phases. NH_3 annealing has previously been reported to produce atomically clean and stoichiometric GaN. [60]

ICP etching was performed using Cl_2 (flow rate = 30 sccm) and BCl_3 (flow rate = 8 sccm) with an ICP power of 400 W at a pressure of 5 mTorr. The substrates were maintained at 23 °C using He cooling during the etch process. The RF power was varied between samples from 5 W to 70 W for "slow" and "rapid" ICP etch conditions, respectively. Samples were etched for 2 minutes.

ALE was performed in a custom-built reactor using a novel method for GaN ALE using a conversion etch mechanism at a sample temperature of 300°C. Remote radio frequency (rf) plasma was generated using a 13.56 MHz rf generator (MKS, Elite 300), a 50 Ω impedance matching network (MKS, MWH-05), and a 13-turn copper coil wound around a 32 mm diameter fused quartz tube. O_2 plasma was ignited at 100 W for 20 s. The quartz tube extended ~25 cm above the wafer surface, limiting the ion component of the plasma

process and thereby reducing plasma-related damage. The etching process was characterized by *in situ* ellipsometry using a Film Sense FS-1 multi wavelength ellipsometer and the manufacturer supplied software (Film Sense, Desktop v. 1.15).

Precursors used in ALE reactions were trimethylgallium ($Ga(CH_3)_3$, TMG) (STREM Chemicals, 97%) and hydrogen fluoride-pyridine ($(C_5H_5N)\cdot(HF)_x$, HF-P) (Alfa-Aeser, 70 % HF by weight). The use of HF-P enables safe delivery of HF into the reaction chamber. Ar carrier gas (Matheson Tri-gas, 99.9999%) at a flow rate of 5.0 sccm was used for precursor delivery into the reaction chamber. N_2 gas (Matheson Tri-gas, 99.9999%) was used between O_2 plasma and precursor exposures for 30 s to purge the chamber of reaction byproducts and unreacted precursor. "Supercycles" of five sequential HF and TMG exposures were used between each O_2 plasma exposure. This etching process is discussed further in a report by Messina, *et al*. [61]

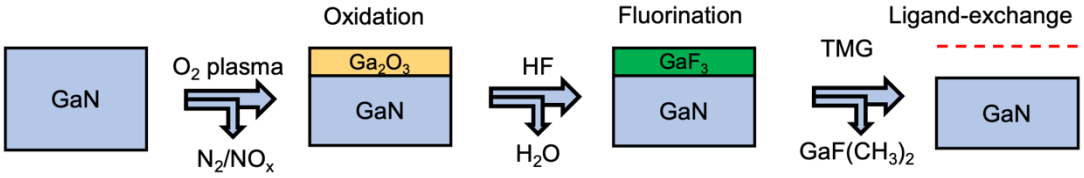

Figure 6.4 - Schematic of discrete reactions used in novel plasma-enhanced atomic layer etching (PEALE) process for GaN. Etching occurred through oxidation by O_2 plasma, followed by fluorination through HF exposure, and modified surface removal through a ligand-exchange with trimethylgallium (TMG). N_2 purge was used between reactions to remove reaction byproducts and unreacted precursor.

N_2 plasma formation occurred using a microwave electron cyclotron resonance (ECR) plasma generator. N_2 gas (Matheson Tri-gas, 99.9999%) with a flow rate of 20 sccm and

H_2 gas (Matheson Tri-gas, 99.9999%) with a flow rate of 10 sccm maintained a pressure of 1.0 x 10^{-4} Torr throughout 15 min of plasma exposure and 15 min of sample cool down. A tungsten filament located behind the sample backside was used to heat the samples to 700 °C and an infrared pyrometer (Mikron, M90-0) was used to measure surface temperature. A microwave power of 300 W was used to ignite the ECR plasma.

6.5 Results

In this study, we determine the concentrations of external charged surface states from experimentally measured band bending of various Ga-face GaN samples following several dry etch and sample preparation methods.

Samples with no clean prior to XPS measurement exhibited similar band bending measurements of +0.2 ± 0.1 eV regardless of etch process or preparation method. This is attributed to surface adsorbates compensating surface charges and thus adsorption-induced band bending dominating the surface. Oxygen and carbon were detected on all surfaces prior to surface cleaning. To remove excessive surface contaminants and produce consistent surface conditions for XPS measurement, samples were cleaned using an *in situ* NH_3 clean at 800 °C for 30 min. XPS measurements for all samples after NH_3 surface clean showed increased intensity in Ga 3d and N 1s spectra while O 1s and C 1s intensity decreased. This is shown for the non-etched and rapid ICP etched GaN in Fig. 6.5. A Ga LMM Auger peak is also observed to overlap with the N 1s spectra, as indicated in the figure. C 1s intensity was reduced to below the XPS detection limit for some samples.

Intensity of the Ga 3d and N 1s core level XPS peaks of the ICP etched samples were reduced relative to the non-etched GaN. This is attributed to increased surface adsorbates

caused by more active surface sites produced by the ICP etch process. *In situ* NH_3 cleaning reduced surface contaminants to levels consistent with other samples. Significant increase in Ga 3d and N 1s intensities were observed in the ICP etched as shown in the rapid ICP etch spectra shown in Fig. 6.5.

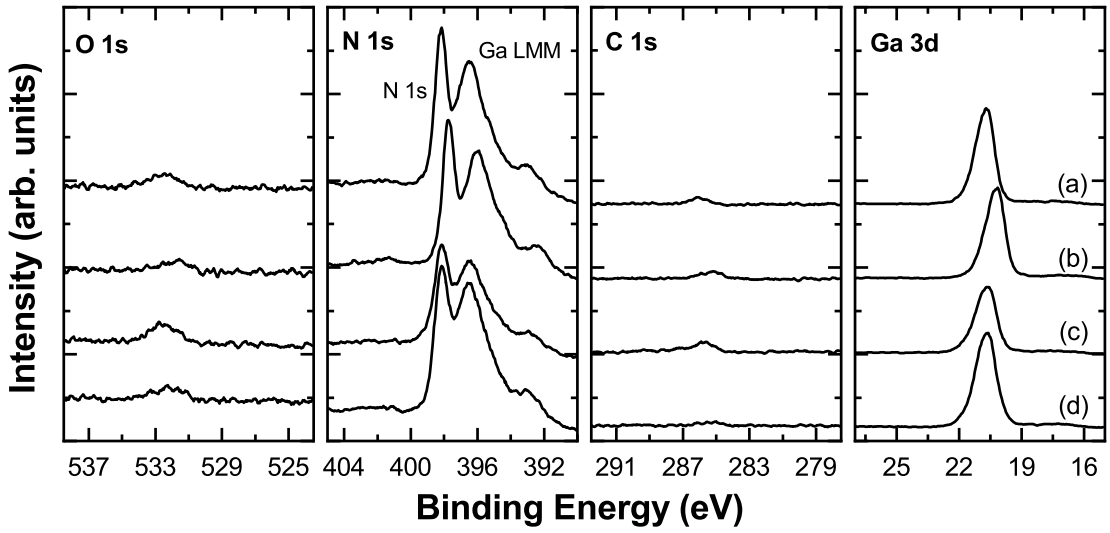

Figure 6.5 – O 1s, N 1s, C 1s, and Ga 3d XPS scans of GaN under various preparations; including (a) non-etched, (b) *in situ* NH_3 cleaned, (c) rapid ICP etch, and (d) rapid ICP etch with *in situ* NH_3 clean. Ga LMM Auger peaks are also observed to overlap with N 1s.

Oxygen coverage at the wafer surfaces was defined as the number of adsorbed oxygen atoms at the (0001) surface, where one monolayer (ml) corresponds to one oxygen atom per surface lattice site. The oxygen coverage was calculated from XPS intensities using the following relation, [62]

$$\Theta_O = \frac{I_O S_{Ga}}{S_0 I_{Ga}} \sum_{n=0}^{\infty} \exp\left[-\frac{n d_{GaN}}{\lambda_{Ga}\, cos[\phi]}\right],$$

where I_O and I_{Ga} are the integrated intensity of the O 1s and Ga 3d core level peaks, S_O and S_{Ga} are the atomic sensitivity factors for O 1s and Ga 3d electrons (0.66 and 0.31), [59] d_{GaN} is the distance between two GaN planes (2.6 Å), $\lambda_{Ga} = 2.4\ nm$ is the inelastic mean free path of Ga 3d electrons with kinetic energies ~1450 eV.

The change in O coverage is shown in Table 6.1 for GaN following *in situ* NH_3 clean. The rapid ICP etch and ALE processes exhibited the highest initial O coverage, but were consistent with other O-terminated samples following *in situ* cleaning. Additionally, a change in O content was observed in the FWHM of the Ga 3d spectra. The Ga 3d peak in GaN XPS measurements is broadened when surface oxides are present due to a Ga-O component at the higher binding energy side of the Ga 3d peak. Reduction of the surface oxide results in lower intensity of the Ga-O component and a corresponding reduction of the Ga 3d FWHM. Due to this "shoulder", deconvolution of the Ga 3d spectra was used to identify the Ga-N 3d peak for band bending calculations.

Table 6.1 - Change in O coverage and band bending of non-etched and etched GaN following *in situ* NH_3 cleaning.

	O Coverage (ml)		Band Bending Shift After Cleaning (eV)
	Initial	Cleaned	
Air exposed	1.2	0.9	+0.6
Rapid ICP etch	2.3	1.1	+0.2
Slow ICP etch	1.8	1.1	+0.3
ALE	2.0	1.3	+0.4

In addition to O and C, samples etched by ALE also exhibited F at the surface, observed by F 1s and F KLL Auger peaks. ALE samples also exhibited the lowest initial band bending of +0.0 ± 0.1 eV prior to *in situ* cleaning. Band bending of the ALE samples increased to +0.4 ± 0.1 eV following *in situ* cleaning.

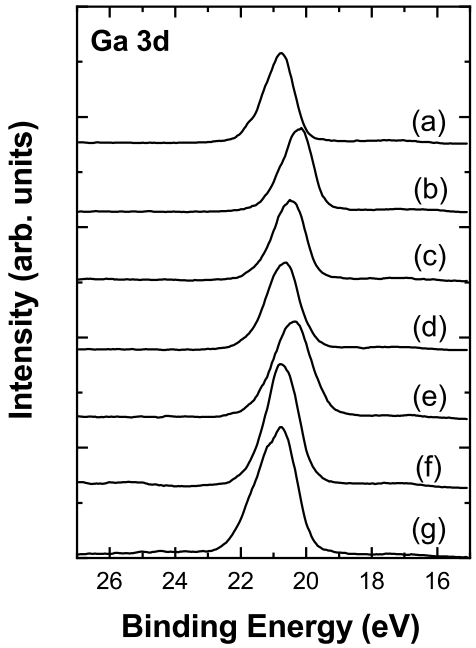

Figure 6.6 – Band bending was measured using the Ga 3d XPS scans of GaN after various preparations; including (a) air exposed, (b) *in situ* NH_3 cleaned, (c) slow ICP etch, (d) rapid ICP etch, (e) rapid ICP etch and N_2 plasma treatment, (f) rapid ICP etch and ALE, and (g) ALE.

The Ga 3d XPS scans are shown in Fig. 6.6 for *in situ* cleaned, O-terminated surfaces following the various etch and processing methods, as well as non-etched, as-received GaN prior to *in situ* cleaning. The non-etched and rapid ICP etch with N_2 plasma treatment

exhibited the lowest binding energy indicating larger upward band bending. The Ga 3d peak of the GaN etched by ALE, shown in Fig 6.6(g), exhibited the largest FWHM which is attributed to broadening by Ga-O and Ga-F peaks at the higher binding energy side.

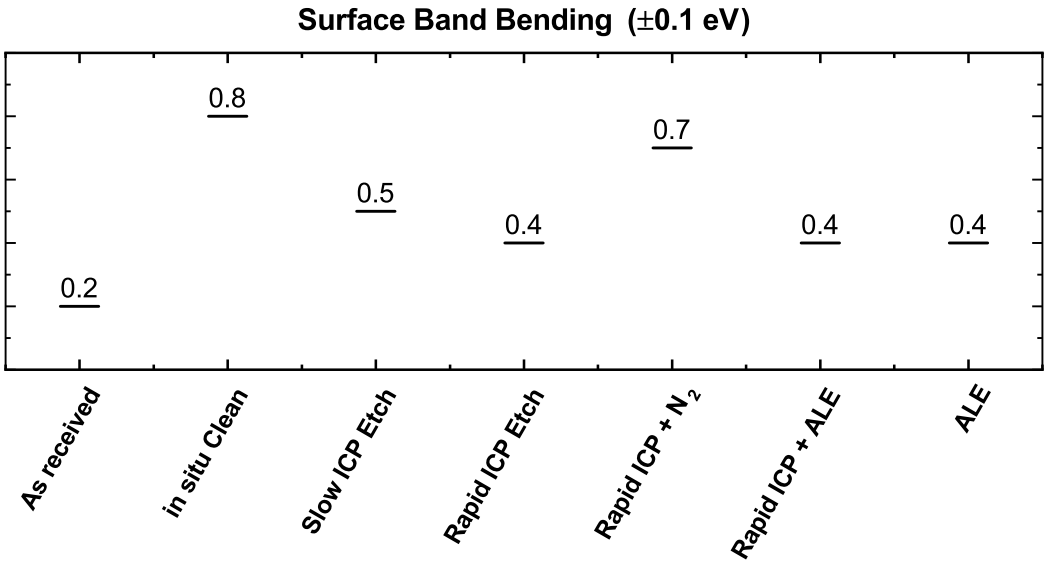

Figure 6.7 - Band bending measurements of GaN after various ICP etch conditions and surface processing techniques; including as-received (non-etched), in situ NH_3 cleaned (non-etched), slow ICP etched, rapid ICP etched, rapid ICP etch with N_2 plasma treatment, rapid ICP etch and ALE, and ALE.

The band bending determined from XPS measurements are shown in Fig. 6.7 and Table 6.2. External charge compensation determined using Eq. 4 with a GaN donor density of $1 * 10^{17} cm^{-3}$ from XPS measurements and is also shown in Table 6.2.

Table 6.2 – Band bending and external charge concentration of Ga-face GaN (0001) after various etch and surface preparation processes as determined from XPS.

	Band Bending (± 0.1 eV)	External Charge Concentration (*10^{13} e/cm^2)
Air exposed	+0.2	+1.8
In situ NH_3 clean	+0.8	+1.5
Slow ICP etch	+0.5	+1.6
Rapid ICP etch	+0.4	+1.7
Rapid etch + N_2 plasma	+0.7	+1.5
Rapid etch + ALE	+0.4	+1.7
ALE	+0.4	+1.7

6.6 Discussion

Correlation between etching and surface processing methods with measured band bending was observed. However, due to a likely Fermi level pinning state located 0.4 to 0.8 eV below the conduction band, the measured band bending response is limited. This is attributed to a pinning state able to compensate positive and negative charges.

The largest band bending was observed for non-etched GaN after *in situ* NH_3 cleaning, which we attribute to lower defect concentration in the surface region, allowing for internal charge compensation, and therefore, lower external surface state formation relative to etched samples. The “slow ICP etch” GaN exhibited higher band bending than the “rapid ICP etch” indicating the lower RF power produced less ion-related damage to the surface

and reduced surface state formation in agreement with previous studies of ICP etch-induced damage. [22–26] A large increase in band bending was observed after N_2 plasma exposure for rapid ICP etch GaN. This suggests a decrease in surface state density which is also in agreement with previous results indicating N_2 plasma treatment is effective in the recovery of damage produced by dry etching of GaN. [14–17,27]

GaN samples etched by a novel ALE method using an oxidation, fluorination, ligand-exchange mechanism exhibited the lowest band bending of +0.0 eV prior to *in situ* cleaning. After cleaning, the ALE samples exhibited band bending of $+0.4 \pm 0.1$ eV, which is lower than expected and attributed to adsorbed surface contaminants inhibiting upward band bending. Fluorine was observed in XPS measurements accounting for ~3% of surface composition within the XPS detection volume. A slight reduction in F 1s intensity was observed after *in situ* cleaning, however complete removal of F impurities was not achieved. The residual F adsorbates produced surfaces inconsistent with other O-terminated samples in this study. Post-ALE impurities at the surface may be mitigated by optimization of the etch parameters (particularly substrate temperature and exposure times), but are an expected byproduct of ALE processes involving thermal reaction mechanisms. However, these impurities are limited to the surface and should be less damaging to the material due to the limited ion component.

6.7 Conclusions

XPS core level measurements were used to determine surface band bending of n-type Ga-face GaN (0001) after various dry etching and *in situ* surface preparation methods. External surface charge density arising from compensation of intrinsic spontaneous polarization of

GaN was then deduced from band bending measurements. *In situ* cleaning using high temperature NH_3 exposure was used to remove surface contaminants resulting from sample transfer, leaving a thin oxide for consistent surface conditions necessary for band bending comparisons. Increased surface charge density was observed in ICP etched GaN, with surface charge density reduced for GaN etched with lower RF power. N_2 plasma treatment after ICP etching showed increase in band bending and a reduction of the surface charge density, in agreement with previous studies of N_2 plasma treatment effects on etch damage.

ACKNOWLEDGEMENTS

This work was supported by the Advanced Research Projects Agency-Energy through the PN-Diodes program under grant no. DE-AR0000868. We acknowledge Dr. David Smith, Dr. Fernando Ponce, Dr. Stephen Goodnick, Dr. Xingye Wang, Dr. Mei Hao, Dr. Shanthan Alugubelli, Dr. Hanxiao Liu, and Jesse Brown for their useful discussions. We also acknowledge Dr. Brianna Eller and Dr. Jialing Yang for their initial work in this area.

REFERENCES

[1] U. K. Mishra, P. Parikh, and Y. F. Wu, *AlGaN/GaN HEMTs - An Overview of Device Operation and Applications*, Proceedings of the IEEE **90**, 1022 (2002).

[2] B. J. Baliga, *Gallium Nitride Devices for Power Electronic Applications*, Semiconductor Science and Technology **28**, (2013).

[3] E. A. Jones, F. F. Wang, and D. Costinett, *Review of Commercial GaN Power Devices and GaN-Based Converter Design Challenges*, IEEE Journal of Emerging and Selected Topics in Power Electronics **4**, 707 (2016).

[4] B. S. Eller, J. Yang, and R. J. Nemanich, *Polarization Effects of GaN and AlGaN: Polarization Bound Charge, Band Bending, and Electronic Surface States*, Journal of Electronic Materials **43**, 4560 (2014).

[5] J. A. del Alamo and J. Joh, *GaN HEMT Reliability*, Microelectronics Reliability **49**, 1200 (2009).

[6] G. Meneghesso, G. Verzellesi, F. Danesin, F. Rampazzo, F. Zanon, A. Tazzoli, M. Meneghini, and E. Zanoni, *Reliability of GaN High-Electron-Mobility Transistors: State of the Art and Perspectives*, IEEE Transactions on Device and Materials Reliability **8**, 332 (2008).

[7] O. Ambacher, *Polarization Induced Effects in AlGaN/GaN Heterostructures*, Acta Physica Polonica A **98**, 195 (2000).

[8] E. T. Yu, X. Z. Dang, P. M. Asbeck, S. S. Lau, and G. J. Sullivan, *Spontaneous and Piezoelectric Polarization Effects in III–V Nitride Heterostructures*, Journal of Vacuum Science & Technology B: Microelectronics and Nanometer Structures **17**, 1742 (1999).

[9] S. H. Park and S. L. Chuang, *Spontaneous Polarization Effects in Wurtzite GaN/AlGaN Quantum Wells and Comparison with Experiment*, Applied Physics Letters **76**, 1981 (2000).

[10] F. Bernardini, V. Fiorentini, and D. Vanderbilt, *Spontaneous Polarization and Piezoelectric Constants of III-V Nitrides*, Physical Review B - Condensed Matter and Materials Physics **56**, R10024 (1997).

[11] J. Yang, Interface Electronic State Characterization of Plasma Enchanced Atomic Layer Deposited Dielectrics on GaN, Arizona State University, 2014.

[12] B. S. Eller, J. Yang, and R. J. Nemanich, *Electronic Surface and Dielectric Interface States on GaN and AlGaN*, Journal of Vacuum Science & Technology A: Vacuum, Surfaces, and Films **31**, 050807 (2013).

[13] K. C. Huang, W. H. Lan, and K. F. Huang, *Inductively Coupled Plasma Reactive Ion Etching-Induced GaN Defect Studied by Schottky Current Transport Analysis*, Japanese Journal of Applied Physics, Part 1: Regular Papers and Short Notes and Review Papers **43**, 82 (2004).

[14] B. Rong, R. J. Reeves, S. A. Brown, M. M. Alkaisi, E. Van Der Drift, R. Cheung, and W. G. Sloof, *A Study of Reactive Ion Etching Damage Effects in GaN*, Microelectronic Engineering **57**–**58**, 585 (2001).

[15] Z. Mouffak, A. Bensaoula, and L. Trombetta, *A Photoluminescence Study of Plasma Reactive Ion Etching-Induced Damage in GaN*, Journal of Semiconductors **35**, 3 (2014).

[16] J. M. Lee, K. M. Chang, S. W. Kim, C. Huh, I. H. Lee, and S. J. Park, *Dry Etch Damage in N-Type GaN and Its Recovery by Treatment with an N_2 Plasma*,

Journal of Applied Physics **87**, 7667 (2000).

[17] Z. Mouffak, A. Bensaoula, and L. Trombetta, *The Effects of Nitrogen Plasma on Reactive-Ion Etching Induced Damage in GaN*, Journal of Applied Physics **95**, 727 (2004).

[18] L. Ji-Myon, H. Chul, K. Dong-Joon, and P. Seong-Ju, *Dry-Etch Damage and Its Recovery in InGaN/GaN Multi-Quantum-Well Light-Emitting Diodes*, Semiconductor Science and Technology **18**, 530 (2003).

[19] C. R. Eddy and B. Molnar, *Plasma Etch-Induced Conduction Changes in Gallium Nitride*, Journal of Electronic Materials **28**, 314 (1999).

[20] Z. Mouffak, Plasma Reactive Ion Etching-Induced Damage in GaN, 2003.

[21] X. A. Cao, H. Cho, S. J. Pearton, G. T. Dang, A. P. Zhang, F. Ren, R. J. Shul, L. Zhang, R. Hickman, and J. M. Van Hove, *Depth and Thermal Stability of Dry Etch Damage in GaN Schottky Diodes*, Applied Physics Letters **75**, 232 (1999).

[22] R. J. Shul, L. Zhang, A. G. Baca, C. G. Willison, J. Han, S. J. Pearton, F. Ren, J. C. Zolper, and L. F. Lester, *High-Density Plasma-Induced Etch Damage*, Materials Research Society Symposium - Proceedings **573**, 271 (1999).

[23] R. J. Shul, L. Zhang, A. G. Baca, C. G. Willison, J. Han, S. J. Pearton, K. P. Lee, and F. Ren, *Inductively Coupled High-Density Plasma-Induced Etch Damage of GaN MESFETs*, Materials Research Society Symposium-Proceedings **622**, T751 (2000).

[24] Y. B. Hahn, R. J. Choi, J. H. Hong, H. J. Park, C. S. Choi, and H. J. Lee, *High-Density Plasma-Induced Etch Damage of InGaN/GaN Multiple Quantum Well Light-Emitting Diodes*, Journal of Applied Physics **92**, 1189 (2002).

[25] R. Qiu, H. Lu, D. Chen, R. Zhang, and Y. Zheng, *Optimization of Inductively Coupled Plasma Deep Etching of GaN and Etching Damage Analysis*, Applied Surface Science **257**, 2700 (2011).

[26] R. J. Shul, L. Zhang, A. G. Baca, C. G. Willison, J. Han, S. J. Pearton, K. P. Lee, and F. Ren, *Inductively Coupled High-Density Plasma-Induced Etch Damage of GaN MESFETs*, Solid-State Electronics **45**, 13 (2001).

[27] D. G. Kent, K. P. Lee, A. P. Zhang, B. Luo, M. E. Overberg, C. R. Abernathy, F. Ren, K. D. Mackenzie, S. J. Pearton, and Y. Nakagawa, *Effect of N_2 Plasma Treatments on Dry Etch Damage in n- and p-Type GaN*, Materials Research Society Symposium - Proceedings **45**, 467 (2001).

[28] K. J. Kanarik, T. Lill, E. A. Hudson, S. Sriraman, S. Tan, J. Marks, V. Vahedi, and R. A. Gottscho, *Overview of Atomic Layer Etching in the Semiconductor Industry*, Journal of Vacuum Science & Technology A: Vacuum, Surfaces, and Films **33**, 020802 (2015).

[29] K. Nojiri, K. J. Kanarik, S. Tan, E. A. Hudson, and R. A. Gottscho, *Atomic Layer Etching-Breaking Through the Limitation of Etch*, 1 (2018).

[30] G. S. Oehrlein, D. Metzler, and C. Li, *Atomic Layer Etching at the Tipping Point: An Overview*, ECS Journal of Solid State Science and Technology **4**, N5041 (2015).

[31] S. M. George and Y. Lee, *Prospects for Thermal Atomic Layer Etching Using Sequential, Self-Limiting Fluorination and Ligand-Exchange Reactions*, ACS Nano **10**, 4889 (2016).

[32] S. M. George, *Mechanisms of Thermal Atomic Layer Etching*, Accounts of

Chemical Research **53**, 1151 (2020).

[33] D. R. Zywotko and S. M. George, *Thermal Atomic Layer Etching of ZnO by a "Conversion-Etch" Mechanism Using Sequential Exposures of Hydrogen Fluoride and Trimethylaluminum*, Chemistry of Materials **29**, 1183 (2017).

[34] J. W. DuMont, A. E. Marquardt, A. M. Cano, and S. M. George, *Thermal Atomic Layer Etching of SiO_2 by a "Conversion-Etch" Mechanism Using Sequential Reactions of Trimethylaluminum and Hydrogen Fluoride*, ACS Applied Materials and Interfaces **9**, 10296 (2017).

[35] N. R. Johnson, J. K. Hite, M. A. Mastro, C. R. Eddy, and S. M. George, *Thermal Atomic Layer Etching of Crystalline GaN Using Sequential Exposures of XeF_2 and BCl_3*, Applied Physics Letters **114**, (2019).

[36] Y. Lee, J. W. Dumont, and S. M. George, *Atomic Layer Etching of Al_2O_3 Using Sequential, Self-Limiting Thermal Reactions with $Sn(Acac)_2$ and Hydrogen Fluoride*, Journal of Physical Chemistry C **119**, 25385 (2015).

[37] Y. Lee, J. W. Dumont, and S. M. George, *Trimethylaluminum as the Metal Precursor for the Atomic Layer Etching of Al_2O_3 Using Sequential, Self-Limiting Thermal Reactions*, Chemistry of Materials **28**, 2994 (2016).

[38] S. Porsgaard, P. Jiang, F. Borondics, S. Wendt, Z. Liu, H. Bluhm, F. Besenbacher, and M. Salmeron, *Charge State of Gold Nanoparticles Supported on Titania under Oxygen Pressure*, Angewandte Chemie - International Edition **50**, 2266 (2011).

[39] J. P. Long and V. M. Bermudez, *Band Bending and Photoemission-Induced Surface Photovoltages on Clean n- and p-GaN (0001) Surfaces*, Physical Review B - Condensed Matter and Materials Physics **66**, 1 (2002).

[40] I. Bartoš, O. Romanyuk, J. Houdkova, P. P. Paskov, T. Paskova, and P. Jiříček, *Electron Band Bending of Polar, Semipolar and Non-Polar GaN Surfaces*, Journal of Applied Physics **119**, (2016).

[41] R. Huang, T. Liu, Y. Zhao, Y. Zhu, Z. Huang, F. Li, J. Liu, L. Zhang, S. Zhang, A. Dingsun, and H. Yang, *Angular Dependent XPS Study of Surface Band Bending on Ga-Polar n-GaN*, Applied Surface Science **440**, 637 (2018).

[42] Y. Zhao, H. Gao, R. Huang, Z. Huang, F. Li, J. Feng, Q. Sun, A. Dingsun, and H. Yang, *Precise Determination of Surface Band Bending in Ga-Polar n-GaN Films by Angular Dependent X-Ray Photoemission Spectroscopy*, Scientific Reports **9**, 1 (2019).

[43] S. J. Cho, S. Dogan, S. Sabuktagin, M. A. Reshchikov, D. K. Johnstone, and H. Morkoc, *Surface Band Bending in As-Grown and Plasma-Treated n-Type GaN Films Using Surface Potential Electric Force Microscopy*, Applied Physics Letters **84**, 3070 (2004).

[44] S. Chevtchenko, X. Ni, Q. Fan, A. A. Baski, and H. Morkọ, *Surface Band Bending of a -Plane GaN Studied by Scanning Kelvin Probe Microscopy*, Applied Physics Letters **88**, (2006).

[45] U. Karrer, O. Ambacher, and M. Stutzmann, *Influence of Crystal Polarity on the Properties of Pt/GaN Schottky Diodes*, Applied Physics Letters **77**, 2012 (2000).

[46] O. Ambacher, R. Dimitrov, M. Stutzmann, B. E. Foutz, M. J. Murphy, J. A. Smart, J. R. Shealy, N. G. Weimann, K. Chu, M. Chumbes, B. Green, A. J. Sierakowski, W. J. Schaff, and L. F. Eastman, *Role of Spontaneous and Piezoelectric Polarization Induced Effects in Group-III Nitride Based Heterostructures and*

Devices, Physica Status Solidi (B) Basic Research **216**, 381 (1999).

[47] F. Bernardini, V. Fiorentini, and D. Vanderbilt, *Accurate Calculation of Polarization-Related Quantities in Semiconductors*, Physical Review B - Condensed Matter and Materials Physics **63**, 1 (2001).

[48] W. S. Yan, R. Zhang, Z. L. Xie, X. Q. Xiu, P. Han, H. Lu, P. Chen, S. L. Gu, Y. Shi, Y. D. Zheng, and Z. G. Liu, *A Thermodynamic Model and Estimation of the Experimental Value of Spontaneous Polarization in a Wurtzite GaN*, Applied Physics Letters **94**, 1 (2009).

[49] J. Lähnemann, O. Brandt, U. Jahn, C. Pfüller, C. Roder, P. Dogan, F. Grosse, A. Belabbes, F. Bechstedt, A. Trampert, and L. Geelhaar, *Direct Experimental Determination of the Spontaneous Polarization of GaN*, Physical Review B - Condensed Matter and Materials Physics **86**, 1 (2012).

[50] D. Segev and C. G. Van De Walle, *Origins of Fermi-Level Pinning on GaN and InN Polar and Nonpolar Surfaces*, Europhysics Letters **76**, 305 (2006).

[51] J. Yang, B. S. Eller, and R. J. Nemanich, *Surface Band Bending and Band Alignment of Plasma Enhanced Atomic Layer Deposited Dielectrics on Ga- and N-Face Gallium Nitride*, Journal of Applied Physics **116**, 1 (2014).

[52] T. Hashizume and H. Hasegawa, *Effects of Nitrogen Deficiency on Electronic Properties of AlGaN Surfaces Subjected to Thermal and Plasma Processes*, Applied Surface Science **234**, 387 (2004).

[53] J. R. Waldrop and R. W. Grant, *Measurement of AlN/GaN (0001) Heterojunction Band Offsets by x-Ray Photoemission Spectroscopy*, Applied Physics Letters **68**, 2879 (1995).

[54] E. A. Kraut, R. W. Grant, J. R. Waldrop, and S. P. Kowalczyk, *Heterojunction Band Discontinuities: Physics and Device Applications* (Elsevier, New York, 1987).

[55] O. Ambacher, *Growth and Applications of Group III-Nitrides*, Journal of Physics D: Applied Physics **31**, 2653 (1998).

[56] J. Hedman and N. Martensson, *Gallium Nitride Studied by Electron Spectroscopy*, Physica Scripta **22**, 176 (1980).

[57] J. R. Waldrop and R. W. Grant, *Measurement of AlN/GaN (0001) Heterojunction Band Offsets by x-Ray Photoemission Spectroscopy*, Applied Physics Letters **68**, 2879 (1996).

[58] T. E. Cook, C. C. Fulton, W. J. Mecouch, R. F. Davis, G. Lucovsky, and R. J. Nemanich, *Band Offset Measurements of the GaN (0001)/HfO_2 Interface*, Journal of Applied Physics **94**, 7155 (2003).

[59] C. D. Wagner, *Sensitivity Factors for XPS Analysis of Surface Atoms*, Journal of Electron Spectroscopy and Related Phenomena **32**, 99 (1983).

[60] S. W. King, J. P. Barnak, M. D. Bremser, K. M. Tracy, C. Ronning, R. F. Davis, and R. J. Nemanich, *Cleaning of AlN and GaN Surfaces*, Journal of Applied Physics **84**, 5248 (1998).

[61] D. C. Messina, K. A. Hatch, and R. J. Nemanich, *Atomic Layer Etching of Gallium Nitride Enabled by Water Vapor and O_2-Plasma Oxidation*, Unpublished (n.d.).

[62] V. M. Bermudez, *Study of Oxygen Chemisorption on the GaN(0001)-(1x1) Surface*, Journal of Applied Physics **80**, 1190 (1996).

CHAPTER VII

OVERVIEW AND FUTURE WORK

7.1 Atomic Layer Etching of Crystalline Gallium Oxide

In chapter 5 of this dissertation, thermal atomic layer etching (ALE) of Ga_2O_3 was reported using HF and trimethylgallium ($Ga(CH_3)_3$, TMG) to produce a self-limiting, low-damage etching method. This study was performed on amorphous Ga_2O_3 grown on Si by plasma enhanced atomic layer deposition (PEALD). Another report has recently presented thermal ALE of amorphous Ga_2O_3 grown by ALD. [1] Amorphous Ga_2O_3 has proven to be effective in applications of photovoltaics and solar-blind ultraviolet (UV) photodetectors. [2,3] However, crystalline Ga_2O_3, especially monoclinic β-Ga_2O_3 has gained interest as an ultrawide bandgap (UWBG) material for potential applications in power electronics. [4–6] Thermal ALE of β-Ga_2O_3 has yet to be demonstrated and may be of interest due to its expanding potential applications.

Most reports of thermal ALE have been performed on amorphous materials grown by ALD. [7,8] However, thermal ALE has been reported for some crystalline materials, including HfO_2, ZrO_2, Al_2O_3, GaN, and AlN. [9–12] Murdzek, *et al*. showed that etch rates from thermal ALE were much lower for polycrystalline HfO_2 and ZrO_2 compared to the amorphous materials. [9] Using HF and $TiCl_4$, the etch rate decreased from 0.61 Å/cycle for amorphous ZrO_2 to 0.26 Å/cycle for polycrystalline ZrO_2. For HfO_2, this effect was more pronounced with a decrease in etch rate from 0.36 Å/cycle to 0.02 Å/cycle between the amorphous and polycrystalline materials.

Crystallinity was demonstrated to have an even more profound effect in thermal ALE of Al_2O_3. [10] Etching of Al_2O_3 using HF and trimethylaluminum (TMA) is considered to be the model system for thermal ALE. [8] However, ALE of crystalline Al_2O_3, annealed at 1000 °C, using these reactants produced an etch rate of 0.06 Å/cycle for the first 10 Å and then negligible etching was observed for the deeper material. [10] In this study, multiple annealing temperatures were used prior to ALE, and the measured etch rates decreased with higher annealing temperatures. This was attributed to greater density in the more crystalline films and suggested kinetic factors may be significant to fluorination of Al_2O_3.

Crystallinity has been shown to be a significant factor in etch rates using thermal ALE processes. The Ga_2O_3 ALE process demonstrated in this dissertation was performed on amorphous material grown by PEALD. Thermal ALE of crystalline Ga_2O_3 has yet to be demonstrated and therefore may be of interest for applications in β-Ga_2O_3 processing techniques.

7.2 Oxidation as a Pathway for Gallium Nitride Atomic Layer Etching

Although HF has proven to be effective for fluorination processes for ALE of other materials, it does not sufficiently fluorinate GaN for ALE. An ALE method for GaN was investigated in Chapter 6 using O_2 plasma oxidation to produce a pathway for ALE using HF and TMG. These results indicated that this ALE method was less effective than expected. The low efficiency of this etch method was attributed to crystallinity of the converted oxide surface layer. Other reports have shown that the native oxide on GaN is

highly ordered in a configuration similar to β-Ga_2O_3. [13] Crystallinity has been shown to hinder etch rates in thermal ALE of HfO_2, ZrO_2, and Al_2O_3.

The structure of ultrathin native oxides on c-plane GaN has been directly observed using aberration corrected scanning transmission electron microscopy (STEM). [13] The oxide observed at the surface was highly ordered in an arrangement similar to β-Ga_2O_3, and is shown in Fig. 7.1. Density functional theory (DFT) calculations were also used in this reported study to investigate stable oxidation conditions at the surface of GaN. These calculations support an energetically favorable mixing of octahedral and tetrahedral bonding observed in the STEM images. The observed structure was found to be more stable than previously proposed surface oxide models.

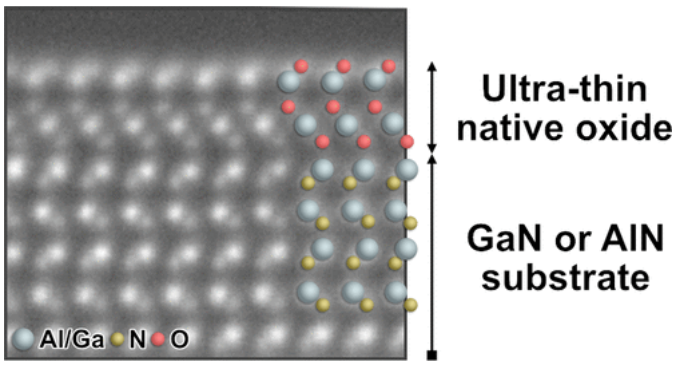

Figure 7.1 – An ultrathin (~6 Å) native oxide layer on GaN/AlN observed by aberration corrected scanning transmission electron microscopy (STEM). Reprinted with permission from Houston Dycus, *et al*. [13]

ALE of GaN using oxidation by O_2 plasma has recently been demonstrated in a fully plasma-based process with BCl_3 plasma used as the other reactant. [14] This indicates an oxidized GaN surface may be removed in an ALE process. However, this method still

includes an ion component for removal of the oxidized surface, and it remains to be determined if oxidation can be used in a thermal ALE process.

Thermal ALE of crystalline AlN showed that a mixed AlO_xN_y surface layer significantly hindered the etch rate using HF and tin acetylacetonate ($Sn(CH_3COCHCOCH_3)_2$, $Sn(acac)_2$). The etch rate of crystalline AlN was shown to be 0.36 Å/cycle, while an etch rate of 0.07 Å/cycle was observed for the AlO_xN_y surface layer. These results suggests that etching of crystalline GaN using an oxidation and HF mechanism may also be hindered by the formation of GaO_xN_y layers.

Further investigation of oxidation methods using different substrate temperatures and reactants may produce a surface that is more reactive for removal through thermal ALE processes. Furthermore, more chemistries may be investigated to remove the oxidized GaN surface for thermal ALE.

7.3 Characterization of Band Bending and External Charge Compensation in Gallium Nitride Using X-ray Photoelectron Spectroscopy

Conventional dry etching methods have been shown to produce electrically active damage in GaN, particularly in the surface region. [15–17] These surface defects may inhibit internal screening of a bound sheet charge that arises due to the large spontaneous polarization of GaN. In Chapter 6, x-ray photoelectron spectroscopy (XPS) was used to determine band bending and deduce external surface charge concentration of GaN after various etch and surface processing conditions.

This method could be applied to investigate surface state concentrations produced by other commonly used dry etching processes such as reactive ion etching (RIE) where

the etch damage is expected to be greater due to less control of ion energy compared to inductively coupled plasma (ICP) etching. [18] Other reported methods of GaN ALE could be used to investigate changes in surface state concentration via removal of material near the surface where dry etching-induced damage is expected to be most highly concentrated. [11,14,19]

The effective depth of emitted electrons in XPS is dependent upon scattering processes of the excited photoelectrons. Core level energies measured by XPS are therefore an average over the XPS measurement depth. Angle dependent x-ray photoelectron spectroscopy enables depth sensitive measurements because the high angle measurements are more sensitive to the surface layer. Consequently, angle dependent XPS may be used to improve upon standard XPS by measurement of core levels at different depths within GaN. Combining the angle dependent XPS measurements with a quadratic depletion model may produce improved characterization of the depletion region. Additionally, the screening depth in semiconductors is a consequence of electric field screening. Varying the free charge concentration through different doping densities would effectively change the depletion length at the surface. Further study of charge compensation at the GaN surface may employ different doping densities to characterize the depth of internal charge compensation.

REFERENCES

[1] Y. Lee, N. R. Johnson, and S. M. George, *Thermal Atomic Layer Etching of Gallium Oxide Using Sequential Exposures of HF and Various Metal Precursors*, Chemistry of Materials **32**, 5937 (2020).

[2] S. Han, M. Fang, X. Huang, M. Fang, W. Zhao, S. Xu, D. Zhu, W. Xu, W. Liu, P. Cao, and Y. Lu, *High-Performance UV Detectors Based on Room-Temperature Deposited Amorphous Ga2O3 Thin Films by RF Magnetron Sputtering*, Journal of Materials Chemistry C **7**, 11834 (2019).

[3] Y. S. Lee, D. Chua, R. E. Brandt, S. C. Siah, J. V. Li, J. P. Mailoa, S. W. Lee, R. G. Gordon, and T. Buonassisi, *Atomic Layer Deposited Gallium Oxide Buffer Layer Enables 1.2 v Open-Circuit Voltage in Cuprous Oxide Solar Cells*, Advanced Materials **26**, 4704 (2014).

[4] J. Y. Tsao, S. Chowdhury, M. A. Hollis, D. Jena, N. M. Johnson, K. A. Jones, R. J. Kaplar, S. Rajan, C. G. Van de Walle, E. Bellotti, C. L. Chua, R. Collazo, M. E. Coltrin, J. A. Cooper, K. R. Evans, S. Graham, T. A. Grotjohn, E. R. Heller, M. Higashiwaki, M. S. Islam, P. W. Juodawlkis, M. A. Khan, A. D. Koehler, J. H. Leach, U. K. Mishra, R. J. Nemanich, R. C. N. Pilawa-Podgurski, J. B. Shealy, Z. Sitar, M. J. Tadjer, A. F. Witulski, M. Wraback, and J. A. Simmons, *Ultrawide-Bandgap Semiconductors: Research Opportunities and Challenges*, Advanced Electronic Materials **4**, (2018).

[5] K. Sasaki, M. Higashiwaki, A. Kuramata, T. Masui, and S. Yamakoshi, *MBE Grown Ga_2O_3 and Its Power Device Applications*, Journal of Crystal Growth **378**,

591 (2013).

[6] S. J. Pearton, J. Yang, P. H. Cary, F. Ren, J. Kim, M. J. Tadjer, and M. A. Mastro, *A Review of Ga_2O_3 Materials, Processing, and Devices*, Applied Physics Reviews **5**, (2018).

[7] Y. Lee, J. W. Dumont, and S. M. George, *Atomic Layer Etching of Al_2O_3 Using Sequential, Self-Limiting Thermal Reactions with $Sn(Acac)_2$ and Hydrogen Fluoride*, Journal of Physical Chemistry C **119**, 25385 (2015).

[8] S. M. George, *Mechanisms of Thermal Atomic Layer Etching*, Accounts of Chemical Research **53**, 1151 (2020).

[9] J. A. Murdzek and S. M. George, *Effect of Crystallinity on Thermal Atomic Layer Etching of Hafnium Oxide, Zirconium Oxide, and Hafnium Zirconium Oxide*, Journal of Vacuum Science & Technology A **38**, 022608 (2020).

[10] J. A. Murdzek, A. Rajashekhar, R. S. Makala, and S. M. George, *Thermal Atomic Layer Etching of Amorphous and Crystalline Al_2O_3 Films*, Journal of Vacuum Science & Technology A **39**, 042602 (2021).

[11] N. R. Johnson, J. K. Hite, M. A. Mastro, C. R. Eddy, and S. M. George, *Thermal Atomic Layer Etching of Crystalline GaN Using Sequential Exposures of XeF_2 and BCl_3*, Applied Physics Letters **114**, (2019).

[12] N. R. Johnson, H. Sun, K. Sharma, and S. M. George, *Thermal Atomic Layer Etching of Crystalline Aluminum Nitride Using Sequential, Self-Limiting Hydrogen Fluoride and $Sn(Acac)_2$ Reactions and Enhancement by H_2 and Ar*

Plasmas, Journal of Vacuum Science & Technology A: Vacuum, Surfaces, and Films **34**, 050603 (2016).

[13] J. H. Dycus, K. J. Mirrielees, E. D. Grimley, R. Kirste, S. Mita, Z. Sitar, R. Collazo, D. L. Irving, and J. M. LeBeau, *Structure of Ultrathin Native Oxides on III–Nitride Surfaces*, ACS Applied Materials & Interfaces **10**, 10607 (2018).

[14] I. H. Hwang, H. Y. Cha, and K. S. Seo, *Low-damage and Self-limiting (Al)Gan Etching Process through Atomic Layer Etching Using O_2 and BCl_3 Plasma*, Coatings **11**, 1 (2021).

[15] R. J. Shul, L. Zhang, A. G. Baca, C. G. Willison, J. Han, S. J. Pearton, K. P. Lee, and F. Ren, *Inductively Coupled High-Density Plasma-Induced Etch Damage of GaN MESFETs*, Solid-State Electronics **45**, 13 (2001).

[16] Z. Mouffak, Plasma Reactive Ion Etching-Induced Damage in GaN, 2003.

[17] X. A. Cao, H. Cho, S. J. Pearton, G. T. Dang, A. P. Zhang, F. Ren, R. J. Shul, L. Zhang, R. Hickman, and J. M. Van Hove, *Depth and Thermal Stability of Dry Etch Damage in GaN Schottky Diodes*, Applied Physics Letters **75**, 232 (1999).

[18] S. J. Pearton, R. J. Shul, and F. Ren, *A Review of Dry Etching of GaN and Related Materials*, MRS Internet Journal of Nitride Semiconductor Research **5**, 1 (2000).

[19] C. Kauppinen, S. A. Khan, J. Sundqvist, D. B. Suyatin, S. Suihkonen, E. I. Kauppinen, and M. Sopanen, *Atomic Layer Etching of Gallium Nitride (0001)*, Journal of Vacuum Science & Technology A: Vacuum, Surfaces, and Films **35**, 060603 (2017).

REFERENCES

[1] J. A. del Alamo and J. Joh, *GaN HEMT Reliability*, Microelectronics Reliability **49**, 1200 (2009).

[2] G. Meneghesso, G. Verzellesi, F. Danesin, F. Rampazzo, F. Zanon, A. Tazzoli, M. Meneghini, and E. Zanoni, *Reliability of GaN High-Electron-Mobility Transistors: State of the Art and Perspectives*, IEEE Transactions on Device and Materials Reliability **8**, 332 (2008).

[3] J. Yang, S. Ahn, F. Ren, S. Pearton, R. Khanna, K. Bevlin, D. Geerpuram, and A. Kuramata, *Inductively Coupled Plasma Etching of Bulk, Single-Crystal Ga_2O_3*, Journal of Vacuum Science & Technology B, Nanotechnology and Microelectronics: Materials, Processing, Measurement, and Phenomena **35**, 031205 (2017).

[4] J. Yang, F. Ren, R. Khanna, K. Bevlin, D. Geerpuram, L.-C. Tung, J. Lin, H. Jiang, J. Lee, E. Flitsiyan, L. Chernyak, S. J. Pearton, and A. Kuramata, *Annealing of Dry Etch Damage in Metallized and Bare (-201) Ga_2O_3*, Journal of Vacuum Science & Technology B **35**, 051201 (2017).

[5] J. Y. Tsao, S. Chowdhury, M. A. Hollis, D. Jena, N. M. Johnson, K. A. Jones, R. J. Kaplar, S. Rajan, C. G. Van de Walle, E. Bellotti, C. L. Chua, R. Collazo, M. E. Coltrin, J. A. Cooper, K. R. Evans, S. Graham, T. A. Grotjohn, E. R. Heller, M. Higashiwaki, M. S. Islam, P. W. Juodawlkis, M. A. Khan, A. D. Koehler, J. H. Leach, U. K. Mishra, R. J. Nemanich, R. C. N. Pilawa-Podgurski, J. B. Shealy, Z. Sitar, M. J. Tadjer, A. F. Witulski, M. Wraback, and J. A. Simmons, *Ultrawide-Bandgap Semiconductors: Research Opportunities and Challenges*, Advanced Electronic Materials **4**, (2018).

[6] B. J. Baliga, *Gallium Nitride Devices for Power Electronic Applications*, Semiconductor Science and Technology **28**, (2013).

[7] U. K. Mishra, L. Shen, T. E. Kazior, and Y. F. Wu, *GaN-Based RF Power Devices and Amplifiers*, Proceedings of the IEEE **96**, 287 (2008).

[8] S. J. Pearton, J. Yang, P. H. Cary, F. Ren, J. Kim, M. J. Tadjer, and M. A. Mastro, *A Review of Ga_2O_3 Materials, Processing, and Devices*, Applied Physics Reviews **5**, (2018).

[9] H. P. Maruska, W. C. Rhines, and D. A. Stevenson, *Preparation of Mg-Doped GaN Diodes Exhibiting Violet Electroluminescence*, Materials Research Bulletin **7**, 777 (1972).

[10] H. Amano, N. Sawaki, I. Akasaki, and Y. Toyoda, *Metalorganic Vapor Phase Epitaxial Growth of a High Quality GaN Film Using an AlN Buffer Layer*, Applied

Physics Letters **48**, 353 (1986).

[11] S. Nakamura, M. Senoh, and T. Mukai, *P-GaN / N-InGaN / N-GaN Double-Heterostructure Blue-Light-Emitting Diodes*, Japanese Journal of Applied Physics **32**, 8 (1993).

[12] S. Nakamura, *Background Story of the Invention of Efficient Blue InGaN Light Emitting Diodes (Nobel Lecture)*, Reviews of Modern Physics **87**, 1139 (2015).

[13] F. Ren, M. Hong, J. P. Mannaerts, J. R. Lothian, and A. Y. Cho, *Wet Chemical and Plasma Etching of $Ga_2O_3(Gd_2O_3)$*, Journal of the Electrochemical Society **144**, 239 (1997).

[14] F. Ren, M. Hong, W. S. Hobson, J. M. Kuo, J. R. Lothian, J. P. Mannaerts, J. Kwo, S. N. G. Chu, Y. K. Chen, and A. Y. Cho, *Demonstration of Enhancement-Mode p- and n-Channel GaAs MOSFETs with $Ga_2O_3(Gd_2O_3)$ as Gate Oxide*, Solid-State Electronics **41**, 1751 (1997).

[15] Y. C. Wang, M. Hong, J. M. Kuo, J. P. Mannaerts, J. Kwo, H. S. Tsai, J. J. Krajewski, J. S. Weiner, Y. K. Chen, and A. Y. Cho, *Advances in GaAs MOSFETs Using $Ga_2O_3(Gd_2O_3)$ as Gate Oxide*, Materials Research Society Symposium - Proceedings **573**, 219 (1999).

[16] L. Mazeina, F. K. Perkins, V. M. Bermudez, S. P. Arnold, and S. M. Prokes, *Functionalized Ga_2O_3 Nanowires as Active Material in Room Temperature Capacitance-Based Gas Sensors*, Langmuir **26**, 13722 (2010).

[17] A. V. Almaev, E. V. Chernikov, V. V. Novikov, B. O. Kushnarev, N. N. Yakovlev, E. V. Chuprakova, V. L. Oleinik, A. D. Lozinskaya, and D. S. Gogova, *Impact of Cr_2O_3 Additives on the Gas-Sensitive Properties of β-Ga_2O_3 Thin Films to Oxygen, Hydrogen, Carbon Monoxide, and Toluene Vapors*, Journal of Vacuum Science & Technology A **39**, 023405 (2021).

[18] H. Zhou, K. Maize, G. Qiu, A. Shakouri, and P. D. Ye, *β-Ga_2O_3 on Insulator Field-Effect Transistors with Drain Currents Exceeding 1.5 A/Mm and Their Self-Heating Effect*, Applied Physics Letters **111**, (2017).

[19] M. Higashiwaki, K. Sasaki, A. Kuramata, T. Masui, and S. Yamakoshi, *Gallium Oxide (Ga_2O_3) Metal-Semiconductor Field-Effect Transistors on Single-Crystal β-Ga_2O_3 (010) Substrates*, Applied Physics Letters **100**, 1 (2012).

[20] M. Higashiwaki, K. Sasaki, T. Kamimura, M. Hoi Wong, D. Krishnamurthy, A. Kuramata, T. Masui, and S. Yamakoshi, *Depletion-Mode Ga_2O_3 Metal-Oxide-Semiconductor Field-Effect Transistors on β-Ga_2O_3 (010) Substrates and Temperature Dependence of Their Device Characteristics*, Applied Physics Letters **103**, 1 (2013).

[21] T. Minami, Y. Nishi, T. Miyata, and J. I. Nomoto, *High-Efficiency Oxide Solar Cells with ZnO/Cu_2O Heterojunction Fabricated on Thermally Oxidized Cu_2O Sheets*, Applied Physics Express **4**, 2 (2011).

[22] A. K. Chandiran, N. Tetreault, R. Humphry-Baker, F. Kessler, E. Baranoff, C. Yi, M. K. Nazeeruddin, and M. Grätzel, *Subnanometer Ga_2O_3 Tunnelling Layer by Atomic Layer Deposition to Achieve 1.1 v Open-Circuit Potential in Dye-Sensitized Solar Cells*, Nano Letters **12**, 3941 (2012).

[23] H. Feng, W. Hao, C. Zhao, X. Xin, J. Cheng, Y. Cui, Y. Chen, and W. Wang, *Fabrication and UV-Sensing Properties of One-Dimensional β-Ga_2O_3 Nanomaterials*, Physica Status Solidi (A) Applications and Materials Science **210**, 1861 (2013).

[24] T. Oshima, T. Okuno, and S. Fujita, *Ga_2O_3 Thin Film Growth on c-Plane Sapphire Substrates by Molecular Beam Epitaxy for Deep-Ultraviolet Photodetectors*, Japanese Journal of Applied Physics, Part 1: Regular Papers and Short Notes and Review Papers **46**, 7217 (2007).

[25] T. Oshima, T. Okuno, N. Arai, N. Suzuki, S. Ohira, and S. Fujita, *Vertical Solar-Blind Deep-Ultraviolet Schottky Photodetectors Based on β-Ga_2O_3 Substrates*, Applied Physics Express **1**, (2008).

[26] J. K. Sheu and G. C. Chi, *The Doping Process and Dopant Characteristics of GaN*, Journal of Physics Condensed Matter **14**, (2002).

[27] C. G. Van De Walle, *Defects and Doping in GaN*, Brazilian Journal of Physics **27**, 74 (1997).

[28] H. J. Hrostowski and R. H. Kaiser, *Infrared Spectra of Group III Acceptors in Silicon*, Journal of Physics and Chemistry of Solids **4**, 148 (1958).

[29] Y. P. Qian, D. Y. Guo, X. L. Chu, H. Z. Shi, W. K. Zhu, K. Wang, X. K. Huang, H. Wang, S. L. Wang, P. G. Li, X. H. Zhang, and W. H. Tang, *Mg-Doped p-Type β-Ga_2O_3 Thin Film for Solar-Blind Ultraviolet Photodetector*, Materials Letters **209**, 558 (2017).

[30] E. Chikoidze, C. Sartel, H. Mohamed, I. Madaci, T. Tchelidze, M. Modreanu, P. Vales-Castro, C. Rubio, C. Arnold, V. Sallet, Y. Dumont, and A. Perez-Tomas, *Enhancing the Intrinsic P-Type Conductivity of the Ultra-Wide Bandgap Ga_2O_3 Semiconductor*, Journal of Materials Chemistry C **7**, 10231 (2019).

[31] A. Kyrtsos, M. Matsubara, and E. Bellotti, *On the Feasibility of P-Type Ga_2O_3*, Applied Physics Letters **112**, (2018).

[32] J. Ma, J. Lin, J. Liu, F. Li, Y. Liu, and G. Yang, *Achieving High Conductivity P-Type Ga_2O_3 through Al-N and In-N Co-Doping*, Chemical Physics Letters **746**,

137308 (2020).

[33] S. J. Pearton, R. J. Shul, and F. Ren, *A Review of Dry Etching of GaN and Related Materials*, MRS Internet Journal of Nitride Semiconductor Research **5**, 1 (2000).

[34] S. Zhou, B. Cao, and S. Liu, *Dry Etching Characteristics of GaN Using Cl_2/BCl_3 Inductively Coupled Plasmas*, Applied Surface Science **257**, 905 (2010).

[35] Y. J. Han, S. Xue, W. P. Guo, C. Z. Sun, Z. B. Hao, and Y. Luo, *Characteristics of N-GaN after Cl_2/Ar and Cl_2/N_2 Inductively Coupled Plasma Etching*, Japanese Journal of Applied Physics, Part 1: Regular Papers and Short Notes and Review Papers **42**, 6409 (2003).

[36] T. Sreenidhi, K. Baskar, A. Dasgupta, and N. Dasgupta, *Reactive Ion Etching of GaN in SF_6 + Ar and SF_6 + N_2 Plasma*, Semiconductor Science and Technology **23**, (2008).

[37] M. E. Lin, Z. F. Fan, Z. Ma, L. H. Allen, and H. Morkoç, *Reactive Ion Etching of GaN Using BCl_3*, Applied Physics Letters **64**, 887 (1994).

[38] R. J. Shul, C. I. . Ashby, D. J. Rieger, A. J. Howard, S. J. Pearton, C. R. Abernathy, C. B. Vartuli, P. A. Barnes, and P. Davis, *Plasma Chemsitry Dependent ECR Etching of GaN*, Materials Research Society Symposium - Proceedings **395**, 751 (1996).

[39] H. Liang, Y. Chen, X. Xia, C. Zhang, R. Shen, Y. Liu, Y. Luo, and G. Du, *A Preliminary Study of SF_6 Based Inductively Coupled Plasma Etching Techniques for Beta Gallium Trioxide Thin Film*, Materials Science in Semiconductor Processing **39**, 582 (2015).

[40] J. Yang, S. Ahn, F. Ren, R. Khanna, K. Bevlin, D. Geerpuram, S. J. Pearton, and A. Kuramata, *Inductively Coupled Plasma Etch Damage in (-201) Ga_2O_3 Schottky Diodes*, Applied Physics Letters **110**, 1 (2017).

[41] J. E. Hogan, S. W. Kaun, E. Ahmadi, Y. Oshima, and J. S. Speck, *Chlorine-Based Dry Etching of β-Ga_2O_3*, Semiconductor Science and Technology **31**, 065006 (2016).

[42] Y. Kwon, G. Lee, S. Oh, J. Kim, S. J. Pearton, and F. Ren, *Tuning the Thickness of Exfoliated Quasi-Two-Dimensional β-Ga_2O_3 Flakes by Plasma Etching*, Applied Physics Letters **110**, (2017).

[43] X. A. Cao, H. Cho, S. J. Pearton, G. T. Dang, A. P. Zhang, F. Ren, R. J. Shul, L. Zhang, R. Hickman, and J. M. Van Hove, *Depth and Thermal Stability of Dry Etch Damage in GaN Schottky Diodes*, Applied Physics Letters **75**, 232 (1999).

[44] G. S. Oehrlein, *Dry Etching Damage of Silicon: A Review*, Materials Science and

Engineering B **4**, 441 (1989).

[45] J. M. Lee, K. M. Chang, S. W. Kim, C. Huh, I. H. Lee, and S. J. Park, *Dry Etch Damage in N-Type GaN and Its Recovery by Treatment with an N_2 Plasma*, Journal of Applied Physics **87**, 7667 (2000).

[46] F. Ren, J. R. Lothian, S. J. Pearton, C. R. Abernathy, C. B. Vartuli, J. D. Mackenzie, R. G. Wilson, and R. F. Karlicek, *Effect of Dry Etching on Surface Properties of III-Nitrides*, Journal of Electronic Materials **26**, 1287 (1997).

[47] R. Khanna, K. Bevlin, D. Geerpuram, J. Yang, F. Ren, and S. J. Pearton, *Dry Etching of Ga_2O_3*, Gallium Oxide 263 (2019).

[48] S. J. Pearton and R. J. Shul, *Etching of III Nitrides*, **50**, 103 (1997).

[49] Z. Mouffak, A. Bensaoula, and L. Trombetta, *The Effects of Nitrogen Plasma on Reactive-Ion Etching Induced Damage in GaN*, Journal of Applied Physics **95**, 727 (2004).

[50] Z. Mouffak, A. Bensaoula, and L. Trombetta, *A Photoluminescence Study of Plasma Reactive Ion Etching-Induced Damage in GaN*, Journal of Semiconductors **35**, 3 (2014).

[51] L. Ji-Myon, H. Chul, K. Dong-Joon, and P. Seong-Ju, *Dry-Etch Damage and Its Recovery in InGaN/GaN Multi-Quantum-Well Light-Emitting Diodes*, Semiconductor Science and Technology **18**, 530 (2003).

[52] D. G. Kent, K. P. Lee, A. P. Zhang, B. Luo, M. E. Overberg, C. R. Abernathy, F. Ren, K. D. Mackenzie, S. J. Pearton, and Y. Nakagawa, *Effect of N_2 Plasma Treatments on Dry Etch Damage in n- and p-Type GaN*, Materials Research Society Symposium - Proceedings **45**, 467 (2001).

[53] D. G. Kent, K. P. Lee, A. P. Zhang, B. Luo, M. E. Overberg, C. R. Abernathy, F. Ren, K. D. Mackenzie, S. J. Pearton, and Y. Nakagawa, *Electrical Effects of N_2 Plasma Exposure on Dry-Etch Damage in p- and n-GaN Schottky Diodes*, Solid-State Electronics **45**, 1837 (2001).

[54] H. K. Lee, H. J. Yun, K. H. Shim, H. G. Park, T. H. Jang, S. N. Lee, and C. J. Choi, *Improvement of Dry Etch-Induced Surface Roughness of Single Crystalline β-Ga_2O_3 Using Post-Wet Chemical Treatments*, Applied Surface Science **506**, 144673 (2020).

[55] X. Wang, G. Yu, B. Lei, X. Wang, C. Lin, Y. Sui, S. Meng, M. Qi, and A. Li, *Recovery of Dry Etching-Induced Damage in n-GaN by Nitrogen Plasma Treatment at Growth Temperature*, Journal of Electronic Materials **36**, 697 (2007).

[1] S. M. George, *Atomic Layer Deposition: An Overview*, Chemical Reviews **110**,

111 (2010).

[2] H. Kim and I. K. Oh, *Review of Plasma-Enhanced Atomic Layer Deposition: Technical Enabler of Nanoscale Device Fabrication*, Japanese Journal of Applied Physics **53**, 0 (2014).

[3] K. Nojiri, K. J. Kanarik, S. Tan, E. A. Hudson, and R. A. Gottscho, *Atomic Layer Etching-Breaking Through the Limitation of Etch*, 1 (2018).

[4] K. J. Kanarik, T. Lill, E. A. Hudson, S. Sriraman, S. Tan, J. Marks, V. Vahedi, and R. A. Gottscho, *Overview of Atomic Layer Etching in the Semiconductor Industry*, Journal of Vacuum Science & Technology A: Vacuum, Surfaces, and Films **33**, 020802 (2015).

[5] G. S. Oehrlein, D. Metzler, and C. Li, *Atomic Layer Etching at the Tipping Point: An Overview*, ECS Journal of Solid State Science and Technology **4**, N5041 (2015).

[6] S. M. George and Y. Lee, *Prospects for Thermal Atomic Layer Etching Using Sequential, Self-Limiting Fluorination and Ligand-Exchange Reactions*, ACS Nano **10**, 4889 (2016).

[7] M. Kariniemi, J. Niinistö, M. Vehkamäki, M. Kemell, M. Ritala, M. Leskelä, and M. Putkonen, *Conformality of Remote Plasma-Enhanced Atomic Layer Deposition Processes: An Experimental Study*, Journal of Vacuum Science & Technology A: Vacuum, Surfaces, and Films **30**, 01A115 (2012).

[8] S. M. George, *Mechanisms of Thermal Atomic Layer Etching*, Accounts of Chemical Research **53**, 1151 (2020).

[9] S. E. Potts, L. Schmalz, M. Fenker, B. Díaz, J. Światowska, V. Maurice, A. Seyeux, P. Marcus, G. Radnóczi, L. Tóth, and W. M. M. Kessels, *Ultra-Thin Aluminium Oxide Films Deposited by Plasma-Enhanced Atomic Layer Deposition for Corrosion Protection*, Journal of The Electrochemical Society **158**, C132 (2011).

[10] T. Lee, J. Ahn, J. Oh, Y. Kim, Y. B. Kim, D. K. Choi, and J. Jung, *Characterization of Ultra-Thin HfO_2 Gate Oxide Prepared by Using Atomic Layer Deposition*, Journal of the Korean Physical Society **42**, 272 (2003).

[11] P. D. Ye, G. D. Wilk, J. Kwo, B. Yang, H. J. L. Gossmann, M. Frei, S. N. G. Chu, J. P. Mannaerts, M. Sergent, M. Hong, K. K. Ng, and J. Bude, *GaAs MOSFET with Oxide Gate Dielectric Grown by Atomic Layer Deposition*, IEEE Electron Device Letters **24**, 209 (2003).

[12] Z. Ren, G. Yuan, J. Zhang, L. Xu, J. Zhang, W. Chen, and Y. Hao, *Hydrogen-Terminated Polycrystalline Diamond MOSFETs with Al_2O_3 Passivation Layers*

Grown by Atomic Layer Deposition at Different Temperatures, AIP Advances **8**, 1 (2018).

[13] J. W. Elam, Z. A. Sechrist, and S. M. George, *ZnO/Al_2O_3 Nanolaminates Fabricated by Atomic Layer Deposition: Growth and Surface Roughness Measurements*, Thin Solid Films **414**, 43 (2002).

[14] H. Zhang and R. Solanki, *Atomic Layer Deposition of High Dielectric Constant Nanolaminates*, Journal of The Electrochemical Society **148**, F63 (2001).

[15] R. Zazpe, M. Ungureanu, F. Golmar, P. Stoliar, R. Llopis, F. Casanova, D. F. Pickup, C. Rogero, and L. E. Hueso, *Resistive Switching Dependence on Atomic Layer Deposition Parameters in HfO_2-Based Memory Devices*, Journal of Materials Chemistry C **2**, 3204 (2014).

[16] D. J. Lee, S. S. Yim, K. S. Kim, S. H. Kim, and K. B. Kim, *Nonvolatile Memory Characteristics of Atomic Layer Deposited Ru Nanocrystals with a SiO_2/Al_2O_3 Bilayered Tunnel Barrier*, Journal of Applied Physics **107**, (2010).

[17] K. J. Kanarik, S. Tan, and R. A. Gottscho, *Atomic Layer Etching: Rethinking the Art of Etch*, Journal of Physical Chemistry Letters **9**, 4814 (2018).

[18] K. J. Kanarik, S. Tan, J. Holland, A. Eppler, V. Vahedi, J. Marks, and R. A. Gottscho, *Moving Atomic Layer Etch from Lab to Fab*, Solid State Technology **56**, 14 (2013).

[19] Y. Lee, J. W. Dumont, and S. M. George, *Atomic Layer Etching of Al_2O_3 Using Sequential, Self-Limiting Thermal Reactions with $Sn(Acac)_2$ and Hydrogen Fluoride*, Journal of Physical Chemistry C **119**, 25385 (2015).

[20] H. B. Profijt, S. E. Potts, M. C. M. van de Sanden, and W. M. M. Kessels, *Plasma-Assisted Atomic Layer Deposition: Basics, Opportunities, and Challenges*, Journal of Vacuum Science & Technology A: Vacuum, Surfaces, and Films **29**, 050801 (2011).

[21] H. Kim, *Characteristics and Applications of Plasma Enhanced-Atomic Layer Deposition*, Thin Solid Films **519**, 6639 (2011).

[22] R. L. Puurunen, *Surface Chemistry of Atomic Layer Deposition: A Case Study for the Trimethylaluminum/Water Process*, Journal of Applied Physics **97**, (2005).

[23] R. L. Puurunen, T. A. Zeelie, and A. O. I. Krause, *Cobalt(III) Acetylacetonate Chemisorbed on Aluminum-Nitride-Modified Silica: Characteristics and Hydroformylation Activity*, Catalysis Letters **83**, 27 (2002).

[24] R. L. Puurunen, M. Lindblad, A. Rootc, and A. O. I. Krausea, *Successive Reactions of Gaseous Trimethylaluminium and Ammonia on Porous Alumina*,

Physical Chemistry Chemical Physics **3**, 1093 (2001).

[25] I. Donmez, C. Ozgit-Akgun, and N. Biyikli, *Low Temperature Deposition of Ga_2O_3 Thin Films Using Trimethylgallium and Oxygen Plasma*, Journal of Vacuum Science & Technology A: Vacuum, Surfaces, and Films **31**, 01A110 (2013).

[26] R. O'Donoghue, J. Rechmann, M. Aghaee, D. Rogalla, H. W. Becker, M. Creatore, A. D. Wieck, and A. Devi, *Low Temperature Growth of Gallium Oxide Thin Films via Plasma Enhanced Atomic Layer Deposition*, Dalton Transactions **46**, 16551 (2017).

[27] A. Mahmoodinezhad, C. Janowitz, F. Naumann, P. Plate, H. Gargouri, K. Henkel, D. Schmeißer, and J. I. Flege, *Low-Temperature Growth of Gallium Oxide Thin Films by Plasma-Enhanced Atomic Layer Deposition*, Journal of Vacuum Science & Technology A **38**, 022404 (2020).

[28] A. Singh, A. Mathur, D. Pal, A. Sengupta, R. Singh, and S. Chattopadhyay, *Near Room Temperature Atomic Layer Deposition of ZnO Thin Films on Poly (Methyl Methacrylate) (PMMA) Templates: A Study of Structure, Morphology and Photoluminescence of ZnO as an Effect of Template Confinement*, Vacuum **161**, 398 (2019).

[29] M. Kot, C. Das, Z. Wang, K. Henkel, Z. Rouissi, K. Wojciechowski, H. J. Snaith, and D. Schmeisser, *Room-Temperature Atomic Layer Deposition of Al_2O_3: Impact on Efficiency, Stability and Surface Properties in Perovskite Solar Cells*, ChemSusChem **9**, 3401 (2016).

[30] A. J. M. MacKus, D. Garcia-Alonso, H. C. M. Knoops, A. A. Bol, and W. M. M. Kessels, *Room-Temperature Atomic Layer Deposition of Platinum*, Chemistry of Materials **25**, 1769 (2013).

[31] H. Kim, *Atomic Layer Deposition of Metal and Nitride Thin Films: Current Research Efforts and Applications for Semiconductor Device Processing*, Journal of Vacuum Science & Technology B: Microelectronics and Nanometer Structures **21**, 2231 (2003).

[32] M. N. Yoder, *Atomic Layer Etching*, U.S. Patent No. 4756794 (1988).

[33] T. Ohba, W. Yang, S. Tan, K. J. Kanarik, and K. Nojiri, *Atomic Layer Etching of GaN and AlGaN Using Directional Plasma-Enhanced Approach*, Japanese Journal of Applied Physics **56**, (2017).

[34] N. R. Johnson, J. K. Hite, M. A. Mastro, C. R. Eddy, and S. M. George, *Thermal Atomic Layer Etching of Crystalline GaN Using Sequential Exposures of XeF_2 and BCl_3*, Applied Physics Letters **114**, (2019).

[35] C. T. Carver, J. J. Plombon, P. E. Romero, S. Suri, T. A. Tronic, and R. B. Turkot, *Atomic Layer Etching: An Industry Perspective*, ECS Journal of Solid State Science and Technology **4**, N5005 (2015).

[36] R. Rahman, E. C. Mattson, J. P. Klesko, A. Dangerfield, S. Rivillon-Amy, D. C. Smith, D. Hausmann, and Y. J. Chabal, *Thermal Atomic Layer Etching of Silica and Alumina Thin Films Using Trimethylaluminum with Hydrogen Fluoride or Fluoroform*, ACS Applied Materials and Interfaces **10**, 31784 (2018).

[37] Y. Lee, J. W. Dumont, and S. M. George, *Trimethylaluminum as the Metal Precursor for the Atomic Layer Etching of Al_2O_3 Using Sequential, Self-Limiting Thermal Reactions*, Chemistry of Materials **28**, 2994 (2016).

[38] J. W. DuMont and S. M. George, *Competition between Al_2O_3 Atomic Layer Etching and AlF_3 Atomic Layer Deposition Using Sequential Exposures of Trimethylaluminum and Hydrogen Fluoride*, Journal of Chemical Physics **146**, (2017).

[39] S. B. S. Heil, J. L. Van Hemmen, M. C. M. Van De Sanden, and W. M. M. Kessels, *Reaction Mechanisms during Plasma-Assisted Atomic Layer Deposition of Metal Oxides: A Case Study for Al_2O_3*, Journal of Applied Physics **103**, (2008).

[40] S. B. S. Heil, P. Kudlacek, E. Langereis, R. Engeln, M. C. M. Van De Sanden, and W. M. M. Kessels, *In Situ Reaction Mechanism Studies of Plasma-Assisted Atomic Layer Deposition of Al_2O_3*, Applied Physics Letters **89**, 1 (2006).

[41] D. N. Goldstein, J. A. McCormick, and S. M. George, *Al_2O_3 Atomic Layer Deposition with Trimethylaluminum and Ozone Studied by in Situ Transmission FTIR Spectroscopy and Quadrupole Mass Spectrometry*, Journal of Physical Chemistry C **112**, 19530 (2008).

[42] Y. Lee and S. M. George, *Thermal Atomic Layer Etching of Titanium Nitride Using Sequential, Self-Limiting Reactions: Oxidation to TiO_2 and Fluorination to Volatile TiF_4*, Chemistry of Materials **29**, 8202 (2017).

[43] M. Konh, C. He, X. Lin, X. Guo, V. Pallem, R. L. Opila, A. V. Teplyakov, Z. Wang, and B. Yuan, *Molecular Mechanisms of Atomic Layer Etching of Cobalt with Sequential Exposure to Molecular Chlorine and Diketones*, Journal of Vacuum Science & Technology A **37**, 021004 (2019).

[44] A. I. Abdulagatov and S. M. George, *Thermal Atomic Layer Etching of Silicon Using O_2, HF, and $Al(CH_3)_3$ as the Reactants*, Chemistry of Materials **30**, 8465 (2018).

[45] U. Kilic, A. Mock, D. Sekora, S. Gilbert, S. Valloppilly, N. Ianno, M. Langell, E. Schubert, and M. Schubert, *Precursor-Surface Interactions Revealed during Plasma-Enhanced Atomic Layer Deposition of Metal Oxide Thin Films by in-Situ*

Spectroscopic Ellipsometry, Scientific Reports **10**, 1 (2020).

[46] J. W. DuMont, A. E. Marquardt, A. M. Cano, and S. M. George, *Thermal Atomic Layer Etching of SiO_2 by a "Conversion-Etch" Mechanism Using Sequential Reactions of Trimethylaluminum and Hydrogen Fluoride*, ACS Applied Materials and Interfaces **9**, 10296 (2017).

[47] N. R. Johnson and S. M. George, *WO_3 and W Thermal Atomic Layer Etching Using "Conversion-Fluorination" and "Oxidation-Conversion-Fluorination" Mechanisms*, ACS Applied Materials and Interfaces **9**, 34435 (2017).

[48] N. Miyoshi, H. Kobayashi, K. Shinoda, M. Kurihara, T. Watanabe, Y. Kouzuma, K. Yokogawa, S. Sakai, and M. Izawa, *Atomic Layer Etching of Silicon Nitride Using Infrared Annealing for Short Desorption Time of Ammonium Fluorosilicate*, Japanese Journal of Applied Physics **56**, (2017).

[49] E. J. Song, J. H. Kim, J. D. Kwon, S. H. Kwon, and J. H. Ahn, *Silicon Atomic Layer Etching by Two-Step Plasma Process Consisting of Oxidation and Modification to Form $(NH_4)_2SiF_6$, and Its Sublimation*, Japanese Journal of Applied Physics **57**, (2018).

[50] H. Zhu, X. Qin, L. Cheng, A. Azcatl, J. Kim, and R. M. Wallace, *Remote Plasma Oxidation and Atomic Layer Etching of MoS_2*, ACS Applied Materials and Interfaces **8**, 19119 (2016).

[51] N. R. Johnson, H. Sun, K. Sharma, and S. M. George, *Thermal Atomic Layer Etching of Crystalline Aluminum Nitride Using Sequential, Self-Limiting Hydrogen Fluoride and $Sn(Acac)_2$ Reactions and Enhancement by H_2 and Ar Plasmas*, Journal of Vacuum Science & Technology A: Vacuum, Surfaces, and Films **34**, 050603 (2016).

[52] J. A. Murdzek and S. M. George, *Thermal Atomic Layer Etching of Amorphous and Crystalline Hafnium Oxide, Zirconium Oxide, and Hafnium Zirconium Oxide*, 2019 International Symposium on VLSI Technology, Systems and Application (VLSI-TSA) **38**, 1 (2019).

[53] J. A. Murdzek and S. M. George, *Effect of Crystallinity on Thermal Atomic Layer Etching of Hafnium Oxide, Zirconium Oxide, and Hafnium Zirconium Oxide*, Journal of Vacuum Science & Technology A **38**, 022608 (2020).

[1] H. Hertz, *Ueber Einen Einfluss Des Ultravioletten Lichtes Auf Die Electrische Entladung*, Annalen Der Physik **267**, 983 (1887).

[2] M. Planck, *On the Theory of the Energy Distribution Law of the Normal Spectrum*, Verh. Dtsch. Phys. Ges. Berlin **237**, 1 (1900).

[3] A. Einstein, *Über Einen Die Erzeuyunq Und Verwandlung Des Lichtes*

Betreffenden Heuristischen Gesichtspunkt, Annalen Der Physik **4**, 132 (1905).

[4] H. Y. Fan, *Theory of Photoelectric Emission from Metals*, Physical Review **68**, 43 (1945).

[5] W. E. Spicer, *Photoemissive, Photoconductive, and Optical Absorption Studies of Alkali-Antimony Compounds*, Physical Review **112**, 114 (1958).

[6] C. N. Berglund and W. E. Spicer, *Photoemission Studies of Copper and Silver: Theory*, Physical Review **136**, 1030 (1964).

[7] C. N. Berglund and W. E. Spicer, *Photoemission Studies of Copper and Silver: Experiment*, Physical Review **136**, (1964).

[8] A. Fahlman, C. Nordling, and K. Siegbahn, *ESCA : Atomic, Molecular and Solid State Structure Studied by Means of Electron Spectroscopy* (Uppsala : Almqvist and Wiksell, 1967).

[9] L. Meitner, *Über Die Entstehung Der β-Strahl-Spektren Radioaktiver Substanzen*, Zeitschrift Für Physik **9**, 131 (1922).

[10] L. Meitner, *Über Den Zusammenhang Zwischen β- Und γ-Strahlen*, Zeitschrift Für Physik **9**, 145 (1922).

[11] P. Auger, *Sur Les Rayons β Secondaires Produits Dans Un Gaz Par Des Rayons X*, Comptes Rendus Des Séances Hebdomadaires de l'Académie Des Sciences **177**, 169 (1923).

[12] L. Pauling, *The Nature of the Chemical Bond*, 3rd ed. (Cornell University Press, Ithaca, NY, 1960).

[13] Z. Zhang and J. T. Yates, *Band Bending in Semiconductors: Chemical and Physical Consequences at Surfaces and Interfaces*, Chemical Reviews **112**, 5520 (2012).

[14] J. R. Waldrop and R. W. Grant, *Measurement of AlN/GaN (0001) Heterojunction Band Offsets by x-Ray Photoemission Spectroscopy*, Applied Physics Letters **68**, 2879 (1995).

[15] E. A. Kraut, R. W. Grant, J. R. Waldrop, and S. P. Kowalczyk, *Heterojunction Band Discontinuities: Physics and Device Applications* (Elsevier, New York, 1987).

[16] O. Ambacher, *Growth and Applications of Group III-Nitrides*, Journal of Physics D: Applied Physics **31**, 2653 (1998).

[17] C. D. Wagner, *Sensitivity Factors for XPS Analysis of Surface Atoms*, Journal of

Electron Spectroscopy and Related Phenomena **32**, 99 (1983).

[18] C. D. Wagner, L. E. Davis, M. V. Zeller, J. A. Taylor, R. M. Raymond, and L. H. Gale, *Empirical Atomic Sensitivity Factors for Quantitative Analysis by Electron Spectroscopy for Chemical Analysis*, Surface Interface Analysis **3**, 1981 (1981).

[19] V. M. Bermudez, *Study of Oxygen Chemisorption on the GaN(0001)-(1x1) Surface*, Journal of Applied Physics **80**, 1190 (1996).

[20] C. Negara, Z. Li, T. Längle, and J. Beyerer, *Simplified Stokes Polarimeter Based on Division-of-Amplitude*, 44 (2019).

[21] E. Compain and B. Drevillon, *Broadband Division-of-Amplitude Polarimeter Based on Uncoated Prisms*, Applied Optics **37**, 5938 (1998).

[22] A. V. Tikhonravov, M. K. Trubetskov, E. Masetti, A. V. Krasilnikova, and I. V. Kochikov, *Sensitivity of the Ellipsometric Angles Psi and Delta to the Surface Inhomogeneity*, Advances in Optical Interference Coatings **3738**, 173 (1999).

[23] A. Y. Cho and J. R. Arthur, *Molecular Beam Epitaxy*, Solid-State Chemistry **10**, 157 (1975).

[24] C. Kauppinen, S. A. Khan, J. Sundqvist, D. B. Suyatin, S. Suihkonen, E. I. Kauppinen, and M. Sopanen, *Atomic Layer Etching of Gallium Nitride (0001)*, Journal of Vacuum Science & Technology A: Vacuum, Surfaces, and Films **35**, 060603 (2017).

[25] N. R. Johnson, J. K. Hite, M. A. Mastro, C. R. Eddy, and S. M. George, *Thermal Atomic Layer Etching of Crystalline GaN Using Sequential Exposures of XeF_2 and BCl_3*, Applied Physics Letters **114**, (2019).

[26] F. W. Amalraj, A. K. Dhasiyan, Y. Lu, N. Shimizu, O. Oda, K. Ishikawa, H. Kondo, M. Sekine, N. Ikarashi, and M. Hori, *Effect of N_2/H_2 Plasma on GaN Substrate Cleaning for Homoepitaxial GaN Growth by Radical-Enhanced Metalorganic Chemical Vapor Deposition (REMOCVD)*, AIP Advances **8**, (2018).

[27] X. A. Cao, A. P. Zhang, G. T. Dang, H. Cho, F. Ren, S. J. Pearton, R. J. Shul, L. Zhang, R. Hickman, and J. M. Van Hove, *Inductively Coupled Plasma Damage in GaN Schottky Diodes*, Journal of Vacuum Science & Technology B **17**, 1540 (1999).

[28] R. N. Tiwari and L. Chang, *Etching of GaN by Microwave Plasma of Hydrogen*, Semiconductor Science and Technology **25**, (2010).

[29] I. H. Hwang, H. Y. Cha, and K. S. Seo, *Low-damage and Self-limiting (Al)Gan Etching Process through Atomic Layer Etching Using O_2 and BCl_3 Plasma*, Coatings **11**, 1 (2021).

[30] S.-J. Park, C. P. Sun, J. T. Yeh, J. K. Cataldo, and N. Metropoulos, *Reactive Ion Etching of Molybdenum In CF4/O2 Plasma*, MRS Proceedings **68**, 65 (1986).

[31] S. Park, C. Sun, and R. J. Purtell, *A Mechanistic Study of SF_6/O_2 Reactive Ion Etching of Molybdenum*, Journal of Vacuum Science & Technology B **5**, 1372 (1987).

[32] T. P. Chow and A. J. Steckl, *Plasma Etching of Sputtered Mo and $MoSi_2$ Thin Films in NF_3 Gas Mixtures*, Journal of Applied Physics **53**, 5531 (1982).

[33] P. R. Peri, K. Hatch, D. Messina, K. Fu, Y. Zhao, R. Nemanich, and D. Smith, *Plasma Enhanced Atomic Layer-Etched and Regrown GaN-on-GaN High Power p-n Diodes*, Microscopy and Microanalysis **26**, 840 (2020).

[1] M. Rebien, W. Henrion, M. Hong, J. P. Mannaerts, and M. Fleischer, *Optical Properties of Gallium Oxide Thin Films*, Applied Physics Letters **81**, 250 (2002).

[2] F.-P. Yu, S.-L. Ou, and D.-S. Wuu, *Pulsed Laser Deposition of Gallium Oxide Films for High Performance Solar-Blind Photodetectors*, Optical Materials Express **5**, 1240 (2015).

[3] X. Li, H. L. Lu, H. P. Ma, J. G. Yang, J. X. Chen, W. Huang, Q. Guo, J. J. Feng, and D. W. Zhang, *Chemical, Optical, and Electrical Characterization of Ga_2O_3 Thin Films Grown by Plasma-Enhanced Atomic Layer Deposition*, Current Applied Physics **19**, 72 (2019).

[4] M. Passlack, N. E. J. Hunt, E. F. Schubert, G. J. Zydzik, M. Hong, J. P. Mannaerts, R. L. Opila, and R. J. Fischer, *Dielectric Properties of Electron-Beam Deposited Ga_2O_3 Films*, Applied Physics Letters **64**, 2715 (1994).

[5] T. Yamada, J. Ito, R. Asahara, K. Watanabe, M. Nozaki, S. Nakazawa, Y. Anda, M. Ishida, T. Ueda, A. Yoshigoe, T. Hosoi, T. Shimura, and H. Watanabe, *Comprehensive Study on Initial Thermal Oxidation of GaN(0001) Surface and Subsequent Oxide Growth in Dry Oxygen Ambient*, Journal of Applied Physics **121**, (2017).

[6] G. X. Liu, F. K. Shan, J. J. Park, W. J. Lee, G. H. Lee, I. S. Kim, B. C. Shin, and S. G. Yoon, *Electrical Properties of Ga_2O_3-Based Dielectric Thin Films Prepared by Plasma Enhanced Atomic Layer Deposition (PEALD)*, Journal of Electroceramics **17**, 145 (2006).

[7] K. Sasaki, A. Kuramata, T. Masui, E. G. Víllora, K. Shimamura, and S. Yamakoshi, *Device-Quality β-Ga_2O_3 Epitaxial Films Fabricated by Ozone Molecular Beam Epitaxy*, Applied Physics Express **5**, 8 (2012).

[8] G. Wagner, M. Baldini, D. Gogova, M. Schmidbauer, R. Schewski, M. Albrecht, Z. Galazka, D. Klimm, and R. Fornari, *Homoepitaxial Growth of β-Ga_2O_3 Layers*

by Metal-Organic Vapor Phase Epitaxy, Physica Status Solidi (A) Applications and Materials Science **211**, 27 (2014).

[9] I. Donmez, C. Ozgit-Akgun, and N. Biyikli, *Low Temperature Deposition of Ga_2O_3 Thin Films Using Trimethylgallium and Oxygen Plasma*, Journal of Vacuum Science & Technology A: Vacuum, Surfaces, and Films **31**, 01A110 (2013).

[10] A. Mahmoodinezhad, C. Janowitz, F. Naumann, P. Plate, H. Gargouri, K. Henkel, D. Schmeißer, and J. I. Flege, *Low-Temperature Growth of Gallium Oxide Thin Films by Plasma-Enhanced Atomic Layer Deposition*, Journal of Vacuum Science & Technology A **38**, 022404 (2020).

[11] H. Lee, K. Kim, J. J. Woo, D. J. Jun, Y. Park, Y. Kim, H. W. Lee, Y. J. Cho, and H. M. Cho, *ALD and MOCVD of Ga_2O_3 Thin Films Using the New Ga Precursor Dimethylgallium Isopropoxide, Me_2GaO^iPr*, Chemical Vapor Deposition **17**, 191 (2011).

[12] M. Nieminen, L. Niinistö, and E. Rauhala, *Growth of Gallium Oxide Thin Films from Gallium Acetylacetonate by Atomic Layer Epitaxy*, Journal of Materials Chemistry **6**, 27 (1996).

[13] V. D. Wheeler, N. Nepal, D. R. Boris, S. B. Qadri, L. O. Nyakiti, A. Lang, A. Koehler, G. Foster, S. G. Walton, C. R. Eddy, and D. J. Meyer, *Phase Control of Crystalline Ga_2O_3 Films by Plasma-Enhanced Atomic Layer Deposition*, Chemistry of Materials **32**, 1140 (2020).

[14] M. Passlack, E. F. Schubert, W. S. Hobson, M. Hong, N. Moriya, S. N. G. Chu, K. Konstadinidis, J. P. Mannaerts, M. L. Schnoes, and G. J. Zydzik, *Ga_2O_3 Films for Electronic and Optoelectronic Applications*, Journal of Applied Physics **77**, 686 (1995).

[15] L. Mazeina, F. K. Perkins, V. M. Bermudez, S. P. Arnold, and S. M. Prokes, *Functionalized Ga_2O_3 Nanowires as Active Material in Room Temperature Capacitance-Based Gas Sensors*, Langmuir **26**, 13722 (2010).

[16] A. V. Almaev, E. V. Chernikov, V. V. Novikov, B. O. Kushnarev, N. N. Yakovlev, E. V. Chuprakova, V. L. Oleinik, A. D. Lozinskaya, and D. S. Gogova, *Impact of Cr_2O_3 Additives on the Gas-Sensitive Properties of β-Ga_2O_3 Thin Films to Oxygen, Hydrogen, Carbon Monoxide, and Toluene Vapors*, Journal of Vacuum Science & Technology A **39**, 023405 (2021).

[17] H. Zhou, K. Maize, G. Qiu, A. Shakouri, and P. D. Ye, *β-Ga_2O_3 on Insulator Field-Effect Transistors with Drain Currents Exceeding 1.5 A/Mm and Their Self-Heating Effect*, Applied Physics Letters **111**, (2017).

[18] F. Ren, M. Hong, J. P. Mannaerts, J. R. Lothian, and A. Y. Cho, *Wet Chemical and*

Plasma Etching of $Ga_2O_3(Gd_2O_3)$, Journal of the Electrochemical Society **144**, 239 (1997).

[19] T. Minami, Y. Nishi, T. Miyata, and J. I. Nomoto, *High-Efficiency Oxide Solar Cells with ZnO/Cu_2O Heterojunction Fabricated on Thermally Oxidized Cu_2O Sheets*, Applied Physics Express **4**, 2 (2011).

[20] A. K. Chandiran, N. Tetreault, R. Humphry-Baker, F. Kessler, E. Baranoff, C. Yi, M. K. Nazeeruddin, and M. Grätzel, *Subnanometer Ga_2O_3 Tunnelling Layer by Atomic Layer Deposition to Achieve 1.1 v Open-Circuit Potential in Dye-Sensitized Solar Cells*, Nano Letters **12**, 3941 (2012).

[21] H. Feng, W. Hao, C. Zhao, X. Xin, J. Cheng, Y. Cui, Y. Chen, and W. Wang, *Fabrication and UV-Sensing Properties of One-Dimensional β-Ga_2O_3 Nanomaterials*, Physica Status Solidi (A) Applications and Materials Science **210**, 1861 (2013).

[22] T. Oshima, T. Okuno, and S. Fujita, *Ga_2O_3 Thin Film Growth on c-Plane Sapphire Substrates by Molecular Beam Epitaxy for Deep-Ultraviolet Photodetectors*, Japanese Journal of Applied Physics, Part 1: Regular Papers and Short Notes and Review Papers **46**, 7217 (2007).

[23] T. Oshima, T. Okuno, N. Arai, N. Suzuki, S. Ohira, and S. Fujita, *Vertical Solar-Blind Deep-Ultraviolet Schottky Photodetectors Based on β-Ga_2O_3 Substrates*, Applied Physics Express **1**, (2008).

[24] D. W. Choi, K. B. Chung, and J. S. Park, *Low Temperature Ga_2O_3 Atomic Layer Deposition Using Gallium Tri-Isopropoxide and Water*, Thin Solid Films **546**, 31 (2013).

[25] Y. Zhou, C. Ahyi, T. Isaacs-Smith, M. Bozack, C. C. Tin, J. Williams, M. Park, A. jen Cheng, J. H. Park, D. J. Kim, D. Wang, E. A. Preble, A. Hanser, and K. Evans, *Formation, Etching and Electrical Characterization of a Thermally Grown Gallium Oxide on the Ga-Face of a Bulk GaN Substrate*, Solid-State Electronics **52**, 756 (2008).

[26] H. Liang, Y. Chen, X. Xia, C. Zhang, R. Shen, Y. Liu, Y. Luo, and G. Du, *A Preliminary Study of SF_6 Based Inductively Coupled Plasma Etching Techniques for Beta Gallium Trioxide Thin Film*, Materials Science in Semiconductor Processing **39**, 582 (2015).

[27] J. E. Hogan, S. W. Kaun, E. Ahmadi, Y. Oshima, and J. S. Speck, *Chlorine-Based Dry Etching of β-Ga_2O_3*, Semiconductor Science and Technology **31**, 065006 (2016).

[28] A. P. Shah and A. Bhattacharya, *Inductively Coupled Plasma Reactive-Ion Etching of β-Ga_2O_3: Comprehensive Investigation of Plasma Chemistry and Temperature*,

Journal of Vacuum Science & Technology A: Vacuum, Surfaces, and Films **35**, 041301 (2017).

[29] J. Yang, S. Ahn, F. Ren, R. Khanna, K. Bevlin, D. Geerpuram, S. J. Pearton, and A. Kuramata, *Inductively Coupled Plasma Etch Damage in (-201) Ga_2O_3 Schottky Diodes*, Applied Physics Letters **110**, 1 (2017).

[30] Y. Kwon, G. Lee, S. Oh, J. Kim, S. J. Pearton, and F. Ren, *Tuning the Thickness of Exfoliated Quasi-Two-Dimensional β-Ga_2O_3 Flakes by Plasma Etching*, Applied Physics Letters **110**, (2017).

[31] R. Khanna, K. Bevlin, D. Geerpuram, J. Yang, F. Ren, and S. J. Pearton, *Dry Etching of Ga_2O_3*, Gallium Oxide 263 (2019).

[32] K. J. Kanarik, T. Lill, E. A. Hudson, S. Sriraman, S. Tan, J. Marks, V. Vahedi, and R. A. Gottscho, *Overview of Atomic Layer Etching in the Semiconductor Industry*, Journal of Vacuum Science & Technology A: Vacuum, Surfaces, and Films **33**, 020802 (2015).

[33] G. S. Oehrlein, D. Metzler, and C. Li, *Atomic Layer Etching at the Tipping Point: An Overview*, ECS Journal of Solid State Science and Technology **4**, N5041 (2015).

[34] K. Nojiri, K. J. Kanarik, S. Tan, E. A. Hudson, and R. A. Gottscho, *Atomic Layer Etching-Breaking Through the Limitation of Etch*, 1 (2018).

[35] C. T. Carver, J. J. Plombon, P. E. Romero, S. Suri, T. A. Tronic, and R. B. Turkot, *Atomic Layer Etching: An Industry Perspective*, ECS Journal of Solid State Science and Technology **4**, N5005 (2015).

[36] K. J. Kanarik, S. Tan, and R. A. Gottscho, *Atomic Layer Etching: Rethinking the Art of Etch*, Journal of Physical Chemistry Letters **9**, 4814 (2018).

[37] S. D. Athavale, *Realization of Atomic Layer Etching of Silicon*, Journal of Vacuum Science & Technology B: Microelectronics and Nanometer Structures **14**, 3702 (1996).

[38] K. J. Kanarik, S. Tan, W. Yang, T. Kim, T. Lill, A. Kabansky, E. A. Hudson, T. Ohba, K. Nojiri, J. Yu, R. Wise, I. L. Berry, Y. Pan, J. Marks, and R. A. Gottscho, *Predicting Synergy in Atomic Layer Etching*, Journal of Vacuum Science & Technology A: Vacuum, Surfaces, and Films **35**, 05C302 (2017).

[39] Y. Lee, J. W. Dumont, and S. M. George, *Atomic Layer Etching of Al_2O_3 Using Sequential, Self-Limiting Thermal Reactions with $Sn(Acac)_2$ and Hydrogen Fluoride*, Journal of Physical Chemistry C **119**, 25385 (2015).

[40] Y. Lee, J. W. Dumont, and S. M. George, *Trimethylaluminum as the Metal*

Precursor for the Atomic Layer Etching of Al_2O_3 Using Sequential, Self-Limiting Thermal Reactions, Chemistry of Materials **28**, 2994 (2016).

[41] S. M. George and Y. Lee, *Prospects for Thermal Atomic Layer Etching Using Sequential, Self-Limiting Fluorination and Ligand-Exchange Reactions*, ACS Nano **10**, 4889 (2016).

[42] S. M. George, *Mechanisms of Thermal Atomic Layer Etching*, Accounts of Chemical Research **53**, 1151 (2020).

[43] Y. Lee, C. Huffman, and S. M. George, *Selectivity in Thermal Atomic Layer Etching Using Sequential, Self-Limiting Fluorination and Ligand-Exchange Reactions*, Chemistry of Materials **28**, 7657 (2016).

[44] S. Ohira and N. Arai, *Wet Chemical Etching Behavior of β-Ga_2O_3 Single Crystal*, Physica Status Solidi (C) Current Topics in Solid State Physics **5**, 3116 (2008).

[45] C. D. Wagner, *Sensitivity Factors for XPS Analysis of Surface Atoms*, Journal of Electron Spectroscopy and Related Phenomena **32**, 99 (1983).

[46] C. Fang, Y. Cao, D. Wu, and A. Li, *Thermal Atomic Layer Etching: Mechanism, Materials and Prospects*, Progress in Natural Science: Materials International **28**, 667 (2018).

[47] B. J. Baliga, *Gallium Nitride Devices for Power Electronic Applications*, Semiconductor Science and Technology **28**, (2013).

[48] N. R. Johnson, J. K. Hite, M. A. Mastro, C. R. Eddy, and S. M. George, *Thermal Atomic Layer Etching of Crystalline GaN Using Sequential Exposures of XeF_2 and BCl_3*, Applied Physics Letters **114**, (2019).

[49] A. I. Abdulagatov and S. M. George, *Thermal Atomic Layer Etching of Silicon Using O_2, HF, and $Al(CH_3)_3$ as the Reactants*, Chemistry of Materials **30**, 8465 (2018).

[50] R. Rahman, E. C. Mattson, J. P. Klesko, A. Dangerfield, S. Rivillon-Amy, D. C. Smith, D. Hausmann, and Y. J. Chabal, *Thermal Atomic Layer Etching of Silica and Alumina Thin Films Using Trimethylaluminum with Hydrogen Fluoride or Fluoroform*, ACS Applied Materials and Interfaces **10**, 31784 (2018).

[51] N. R. Johnson and S. M. George, *WO_3 and W Thermal Atomic Layer Etching Using "Conversion-Fluorination" and "Oxidation-Conversion-Fluorination" Mechanisms*, ACS Applied Materials and Interfaces **9**, 34435 (2017).

[52] Y. Lee, N. R. Johnson, and S. M. George, *Thermal Atomic Layer Etching of Gallium Oxide Using Sequential Exposures of HF and Various Metal Precursors*, Chemistry of Materials **32**, 5937 (2020).

[1] H. Fu, K. Fu, C. Yang, H. Liu, K. A. Hatch, P. Peri, D. Herath Mudiyanselage, B. Li, T. H. Kim, S. R. Alugubelli, P. Y. Su, D. C. Messina, X. Deng, C. Y. Cheng, R. Vatan Meidanshahi, X. Huang, H. Chen, T. H. Yang, J. Zhou, A. M. Armstrong, A. A. Allerman, E. T. Yu, J. Han, S. M. Goodnick, D. J. Smith, R. J. Nemanich, F. A. Ponce, and Y. Zhao, *Selective Area Regrowth and Doping for Vertical Gallium Nitride Power Devices: Materials Challenges and Recent Progress*, Materials Today **xxx**, 1 (2021).

[2] Z. Mouffak, A. Bensaoula, and L. Trombetta, *The Effects of Nitrogen Plasma on Reactive-Ion Etching Induced Damage in GaN*, Journal of Applied Physics **95**, 727 (2004).

[3] R. J. Shul, L. Zhang, A. G. Baca, C. G. Willison, J. Han, S. J. Pearton, K. P. Lee, and F. Ren, *Inductively Coupled High-Density Plasma-Induced Etch Damage of GaN MESFETs*, Solid-State Electronics **45**, 13 (2001).

[4] J. M. Lee, K. M. Chang, S. W. Kim, C. Huh, I. H. Lee, and S. J. Park, *Dry Etch Damage in N-Type GaN and Its Recovery by Treatment with an N_2 Plasma*, Journal of Applied Physics **87**, 7667 (2000).

[5] X. A. Cao, H. Cho, S. J. Pearton, G. T. Dang, A. P. Zhang, F. Ren, R. J. Shul, L. Zhang, R. Hickman, and J. M. Van Hove, *Depth and Thermal Stability of Dry Etch Damage in GaN Schottky Diodes*, Applied Physics Letters **75**, 232 (1999).

[6] G. S. Oehrlein, *Dry Etching Damage of Silicon: A Review*, Materials Science and Engineering B **4**, 441 (1989).

[7] X. Wang, G. Yu, B. Lei, X. Wang, C. Lin, Y. Sui, S. Meng, M. Qi, and A. Li, *Recovery of Dry Etching-Induced Damage in n-GaN by Nitrogen Plasma Treatment at Growth Temperature*, Journal of Electronic Materials **36**, 697 (2007).

[8] D. G. Kent, K. P. Lee, A. P. Zhang, B. Luo, M. E. Overberg, C. R. Abernathy, F. Ren, K. D. Mackenzie, S. J. Pearton, and Y. Nakagawa, *Electrical Effects of N_2 Plasma Exposure on Dry-Etch Damage in p- and n-GaN Schottky Diodes*, Solid-State Electronics **45**, 1837 (2001).

[9] L. Ji-Myon, H. Chul, K. Dong-Joon, and P. Seong-Ju, *Dry-Etch Damage and Its Recovery in InGaN/GaN Multi-Quantum-Well Light-Emitting Diodes*, Semiconductor Science and Technology **18**, 530 (2003).

[10] C. Kauppinen, S. A. Khan, J. Sundqvist, D. B. Suyatin, S. Suihkonen, E. I. Kauppinen, and M. Sopanen, *Atomic Layer Etching of Gallium Nitride (0001)*, Journal of Vacuum Science & Technology A: Vacuum, Surfaces, and Films **35**, 060603 (2017).

[11] S. M. George, *Mechanisms of Thermal Atomic Layer Etching*, Accounts of Chemical Research **53**, 1151 (2020).

[12] J. A. Murdzek and S. M. George, *Effect of Crystallinity on Thermal Atomic Layer Etching of Hafnium Oxide, Zirconium Oxide, and Hafnium Zirconium Oxide*, Journal of Vacuum Science & Technology A **38**, 022608 (2020).

[13] J. A. Murdzek, A. Rajashekhar, R. S. Makala, and S. M. George, *Thermal Atomic Layer Etching of Amorphous and Crystalline Al_2O_3 Films*, Journal of Vacuum Science & Technology A **39**, 042602 (2021).

[14] J. A. Murdzek and S. M. George, *Thermal Atomic Layer Etching of Amorphous and Crystalline Hafnium Oxide, Zirconium Oxide, and Hafnium Zirconium Oxide*, 2019 International Symposium on VLSI Technology, Systems and Application (VLSI-TSA) **38**, 1 (2019).

[15] N. R. Johnson, H. Sun, K. Sharma, and S. M. George, *Thermal Atomic Layer Etching of Crystalline Aluminum Nitride Using Sequential, Self-Limiting Hydrogen Fluoride and $Sn(Acac)_2$ Reactions and Enhancement by H_2 and Ar Plasmas*, Journal of Vacuum Science & Technology A: Vacuum, Surfaces, and Films **34**, 050603 (2016).

[16] N. R. Johnson, J. K. Hite, M. A. Mastro, C. R. Eddy, and S. M. George, *Thermal Atomic Layer Etching of Crystalline GaN Using Sequential Exposures of XeF_2 and BCl_3*, Applied Physics Letters **114**, (2019).

[17] C. D. Wagner, *Sensitivity Factors for XPS Analysis of Surface Atoms*, Journal of Electron Spectroscopy and Related Phenomena **32**, 99 (1983).

[18] J. H. Dycus, K. J. Mirrielees, E. D. Grimley, R. Kirste, S. Mita, Z. Sitar, R. Collazo, D. L. Irving, and J. M. LeBeau, *Structure of Ultrathin Native Oxides on III–Nitride Surfaces*, ACS Applied Materials & Interfaces **10**, 10607 (2018).

[19] H. Hao, X. Chen, Z. Li, Y. Shen, H. Wang, Y. Zhao, R. Huang, T. Liu, J. Liang, Y. An, Q. Peng, and S. Ding, *Remote Plasma-Enhanced Atomic Layer Deposition of Gallium Oxide Thin Films with NH3 Plasma Pretreatment*, Journal of Semiconductors **40**, 0 (2019).

[20] I. H. Hwang, H. Y. Cha, and K. S. Seo, *Low-damage and Self-limiting (Al)Gan Etching Process through Atomic Layer Etching Using O_2 and BCl_3 Plasma*, Coatings **11**, 1 (2021).

[1] U. K. Mishra, P. Parikh, and Y. F. Wu, *AlGaN/GaN HEMTs - An Overview of Device Operation and Applications*, Proceedings of the IEEE **90**, 1022 (2002).

[2] B. J. Baliga, *Gallium Nitride Devices for Power Electronic Applications*, Semiconductor Science and Technology **28**, (2013).

[3] E. A. Jones, F. F. Wang, and D. Costinett, *Review of Commercial GaN Power Devices and GaN-Based Converter Design Challenges*, IEEE Journal of Emerging

and Selected Topics in Power Electronics **4**, 707 (2016).

[4] B. S. Eller, J. Yang, and R. J. Nemanich, *Polarization Effects of GaN and AlGaN: Polarization Bound Charge, Band Bending, and Electronic Surface States*, Journal of Electronic Materials **43**, 4560 (2014).

[5] J. A. del Alamo and J. Joh, *GaN HEMT Reliability*, Microelectronics Reliability **49**, 1200 (2009).

[6] G. Meneghesso, G. Verzellesi, F. Danesin, F. Rampazzo, F. Zanon, A. Tazzoli, M. Meneghini, and E. Zanoni, *Reliability of GaN High-Electron-Mobility Transistors: State of the Art and Perspectives*, IEEE Transactions on Device and Materials Reliability **8**, 332 (2008).

[7] O. Ambacher, *Polarization Induced Effects in AlGaN/GaN Heterostructures*, Acta Physica Polonica A **98**, 195 (2000).

[8] E. T. Yu, X. Z. Dang, P. M. Asbeck, S. S. Lau, and G. J. Sullivan, *Spontaneous and Piezoelectric Polarization Effects in III–V Nitride Heterostructures*, Journal of Vacuum Science & Technology B: Microelectronics and Nanometer Structures **17**, 1742 (1999).

[9] S. H. Park and S. L. Chuang, *Spontaneous Polarization Effects in Wurtzite GaN/AlGaN Quantum Wells and Comparison with Experiment*, Applied Physics Letters **76**, 1981 (2000).

[10] F. Bernardini, V. Fiorentini, and D. Vanderbilt, *Spontaneous Polarization and Piezoelectric Constants of III-V Nitrides*, Physical Review B - Condensed Matter and Materials Physics **56**, R10024 (1997).

[11] J. Yang, Interface Electronic State Characterization of Plasma Enchanced Atomic Layer Deposited Dielectrics on GaN, Arizona State University, 2014.

[12] B. S. Eller, J. Yang, and R. J. Nemanich, *Electronic Surface and Dielectric Interface States on GaN and AlGaN*, Journal of Vacuum Science & Technology A: Vacuum, Surfaces, and Films **31**, 050807 (2013).

[13] K. C. Huang, W. H. Lan, and K. F. Huang, *Inductively Coupled Plasma Reactive Ion Etching-Induced GaN Defect Studied by Schottky Current Transport Analysis*, Japanese Journal of Applied Physics, Part 1: Regular Papers and Short Notes and Review Papers **43**, 82 (2004).

[14] B. Rong, R. J. Reeves, S. A. Brown, M. M. Alkaisi, E. Van Der Drift, R. Cheung, and W. G. Sloof, *A Study of Reactive Ion Etching Damage Effects in GaN*, Microelectronic Engineering **57**–**58**, 585 (2001).

[15] Z. Mouffak, A. Bensaoula, and L. Trombetta, *A Photoluminescence Study of*

Plasma Reactive Ion Etching-Induced Damage in GaN, Journal of Semiconductors **35**, 3 (2014).

[16] J. M. Lee, K. M. Chang, S. W. Kim, C. Huh, I. H. Lee, and S. J. Park, *Dry Etch Damage in N-Type GaN and Its Recovery by Treatment with an N_2 Plasma*, Journal of Applied Physics **87**, 7667 (2000).

[17] Z. Mouffak, A. Bensaoula, and L. Trombetta, *The Effects of Nitrogen Plasma on Reactive-Ion Etching Induced Damage in GaN*, Journal of Applied Physics **95**, 727 (2004).

[18] L. Ji-Myon, H. Chul, K. Dong-Joon, and P. Seong-Ju, *Dry-Etch Damage and Its Recovery in InGaN/GaN Multi-Quantum-Well Light-Emitting Diodes*, Semiconductor Science and Technology **18**, 530 (2003).

[19] C. R. Eddy and B. Molnar, *Plasma Etch-Induced Conduction Changes in Gallium Nitride*, Journal of Electronic Materials **28**, 314 (1999).

[20] Z. Mouffak, Plasma Reactive Ion Etching-Induced Damage in GaN, 2003.

[21] X. A. Cao, H. Cho, S. J. Pearton, G. T. Dang, A. P. Zhang, F. Ren, R. J. Shul, L. Zhang, R. Hickman, and J. M. Van Hove, *Depth and Thermal Stability of Dry Etch Damage in GaN Schottky Diodes*, Applied Physics Letters **75**, 232 (1999).

[22] R. J. Shul, L. Zhang, A. G. Baca, C. G. Willison, J. Han, S. J. Pearton, F. Ren, J. C. Zolper, and L. F. Lester, *High-Density Plasma-Induced Etch Damage*, Materials Research Society Symposium - Proceedings **573**, 271 (1999).

[23] R. J. Shul, L. Zhang, A. G. Baca, C. G. Willison, J. Han, S. J. Pearton, K. P. Lee, and F. Ren, *Inductively Coupled High-Density Plasma-Induced Etch Damage of GaN MESFETs*, Materials Research Society Symposium-Proceedings **622**, T751 (2000).

[24] Y. B. Hahn, R. J. Choi, J. H. Hong, H. J. Park, C. S. Choi, and H. J. Lee, *High-Density Plasma-Induced Etch Damage of InGaN/GaN Multiple Quantum Well Light-Emitting Diodes*, Journal of Applied Physics **92**, 1189 (2002).

[25] R. Qiu, H. Lu, D. Chen, R. Zhang, and Y. Zheng, *Optimization of Inductively Coupled Plasma Deep Etching of GaN and Etching Damage Analysis*, Applied Surface Science **257**, 2700 (2011).

[26] R. J. Shul, L. Zhang, A. G. Baca, C. G. Willison, J. Han, S. J. Pearton, K. P. Lee, and F. Ren, *Inductively Coupled High-Density Plasma-Induced Etch Damage of GaN MESFETs*, Solid-State Electronics **45**, 13 (2001).

[27] D. G. Kent, K. P. Lee, A. P. Zhang, B. Luo, M. E. Overberg, C. R. Abernathy, F. Ren, K. D. Mackenzie, S. J. Pearton, and Y. Nakagawa, *Effect of N_2 Plasma*

Treatments on Dry Etch Damage in n- and p-Type GaN, Materials Research Society Symposium - Proceedings **45**, 467 (2001).

[28] K. J. Kanarik, T. Lill, E. A. Hudson, S. Sriraman, S. Tan, J. Marks, V. Vahedi, and R. A. Gottscho, *Overview of Atomic Layer Etching in the Semiconductor Industry*, Journal of Vacuum Science & Technology A: Vacuum, Surfaces, and Films **33**, 020802 (2015).

[29] K. Nojiri, K. J. Kanarik, S. Tan, E. A. Hudson, and R. A. Gottscho, *Atomic Layer Etching-Breaking Through the Limitation of Etch*, 1 (2018).

[30] G. S. Oehrlein, D. Metzler, and C. Li, *Atomic Layer Etching at the Tipping Point: An Overview*, ECS Journal of Solid State Science and Technology **4**, N5041 (2015).

[31] S. M. George and Y. Lee, *Prospects for Thermal Atomic Layer Etching Using Sequential, Self-Limiting Fluorination and Ligand-Exchange Reactions*, ACS Nano **10**, 4889 (2016).

[32] S. M. George, *Mechanisms of Thermal Atomic Layer Etching*, Accounts of Chemical Research **53**, 1151 (2020).

[33] D. R. Zywotko and S. M. George, *Thermal Atomic Layer Etching of ZnO by a "Conversion-Etch" Mechanism Using Sequential Exposures of Hydrogen Fluoride and Trimethylaluminum*, Chemistry of Materials **29**, 1183 (2017).

[34] J. W. DuMont, A. E. Marquardt, A. M. Cano, and S. M. George, *Thermal Atomic Layer Etching of SiO_2 by a "Conversion-Etch" Mechanism Using Sequential Reactions of Trimethylaluminum and Hydrogen Fluoride*, ACS Applied Materials and Interfaces **9**, 10296 (2017).

[35] N. R. Johnson, J. K. Hite, M. A. Mastro, C. R. Eddy, and S. M. George, *Thermal Atomic Layer Etching of Crystalline GaN Using Sequential Exposures of XeF_2 and BCl_3*, Applied Physics Letters **114**, (2019).

[36] Y. Lee, J. W. Dumont, and S. M. George, *Atomic Layer Etching of Al_2O_3 Using Sequential, Self-Limiting Thermal Reactions with $Sn(Acac)_2$ and Hydrogen Fluoride*, Journal of Physical Chemistry C **119**, 25385 (2015).

[37] Y. Lee, J. W. Dumont, and S. M. George, *Trimethylaluminum as the Metal Precursor for the Atomic Layer Etching of Al_2O_3 Using Sequential, Self-Limiting Thermal Reactions*, Chemistry of Materials **28**, 2994 (2016).

[38] S. Porsgaard, P. Jiang, F. Borondics, S. Wendt, Z. Liu, H. Bluhm, F. Besenbacher, and M. Salmeron, *Charge State of Gold Nanoparticles Supported on Titania under Oxygen Pressure*, Angewandte Chemie - International Edition **50**, 2266 (2011).

[39] J. P. Long and V. M. Bermudez, *Band Bending and Photoemission-Induced Surface Photovoltages on Clean n- and p-GaN (0001) Surfaces*, Physical Review B - Condensed Matter and Materials Physics **66**, 1 (2002).

[40] I. Bartoš, O. Romanyuk, J. Houdkova, P. P. Paskov, T. Paskova, and P. Jiříček, *Electron Band Bending of Polar, Semipolar and Non-Polar GaN Surfaces*, Journal of Applied Physics **119**, (2016).

[41] R. Huang, T. Liu, Y. Zhao, Y. Zhu, Z. Huang, F. Li, J. Liu, L. Zhang, S. Zhang, A. Dingsun, and H. Yang, *Angular Dependent XPS Study of Surface Band Bending on Ga-Polar n-GaN*, Applied Surface Science **440**, 637 (2018).

[42] Y. Zhao, H. Gao, R. Huang, Z. Huang, F. Li, J. Feng, Q. Sun, A. Dingsun, and H. Yang, *Precise Determination of Surface Band Bending in Ga-Polar n-GaN Films by Angular Dependent X-Ray Photoemission Spectroscopy*, Scientific Reports **9**, 1 (2019).

[43] S. J. Cho, S. Dogan, S. Sabuktagin, M. A. Reshchikov, D. K. Johnstone, and H. Morkoc, *Surface Band Bending in As-Grown and Plasma-Treated n-Type GaN Films Using Surface Potential Electric Force Microscopy*, Applied Physics Letters **84**, 3070 (2004).

[44] S. Chevtchenko, X. Ni, Q. Fan, A. A. Baski, and H. Morkǫ, *Surface Band Bending of a -Plane GaN Studied by Scanning Kelvin Probe Microscopy*, Applied Physics Letters **88**, (2006).

[45] U. Karrer, O. Ambacher, and M. Stutzmann, *Influence of Crystal Polarity on the Properties of Pt/GaN Schottky Diodes*, Applied Physics Letters **77**, 2012 (2000).

[46] O. Ambacher, R. Dimitrov, M. Stutzmann, B. E. Foutz, M. J. Murphy, J. A. Smart, J. R. Shealy, N. G. Weimann, K. Chu, M. Chumbes, B. Green, A. J. Sierakowski, W. J. Schaff, and L. F. Eastman, *Role of Spontaneous and Piezoelectric Polarization Induced Effects in Group-III Nitride Based Heterostructures and Devices*, Physica Status Solidi (B) Basic Research **216**, 381 (1999).

[47] F. Bernardini, V. Fiorentini, and D. Vanderbilt, *Accurate Calculation of Polarization-Related Quantities in Semiconductors*, Physical Review B - Condensed Matter and Materials Physics **63**, 1 (2001).

[48] W. S. Yan, R. Zhang, Z. L. Xie, X. Q. Xiu, P. Han, H. Lu, P. Chen, S. L. Gu, Y. Shi, Y. D. Zheng, and Z. G. Liu, *A Thermodynamic Model and Estimation of the Experimental Value of Spontaneous Polarization in a Wurtzite GaN*, Applied Physics Letters **94**, 1 (2009).

[49] J. Lähnemann, O. Brandt, U. Jahn, C. Pfüller, C. Roder, P. Dogan, F. Grosse, A. Belabbes, F. Bechstedt, A. Trampert, and L. Geelhaar, *Direct Experimental Determination of the Spontaneous Polarization of GaN*, Physical Review B -

Condensed Matter and Materials Physics **86**, 1 (2012).

[50] D. Segev and C. G. Van De Walle, *Origins of Fermi-Level Pinning on GaN and InN Polar and Nonpolar Surfaces*, Europhysics Letters **76**, 305 (2006).

[51] J. Yang, B. S. Eller, and R. J. Nemanich, *Surface Band Bending and Band Alignment of Plasma Enhanced Atomic Layer Deposited Dielectrics on Ga- and N-Face Gallium Nitride*, Journal of Applied Physics **116**, 1 (2014).

[52] T. Hashizume and H. Hasegawa, *Effects of Nitrogen Deficiency on Electronic Properties of AlGaN Surfaces Subjected to Thermal and Plasma Processes*, Applied Surface Science **234**, 387 (2004).

[53] J. R. Waldrop and R. W. Grant, *Measurement of AlN/GaN (0001) Heterojunction Band Offsets by x-Ray Photoemission Spectroscopy*, Applied Physics Letters **68**, 2879 (1995).

[54] E. A. Kraut, R. W. Grant, J. R. Waldrop, and S. P. Kowalczyk, *Heterojunction Band Discontinuities: Physics and Device Applications* (Elsevier, New York, 1987).

[55] O. Ambacher, *Growth and Applications of Group III-Nitrides*, Journal of Physics D: Applied Physics **31**, 2653 (1998).

[56] J. Hedman and N. Martensson, *Gallium Nitride Studied by Electron Spectroscopy*, Physica Scripta **22**, 176 (1980).

[57] J. R. Waldrop and R. W. Grant, *Measurement of AlN/GaN (0001) Heterojunction Band Offsets by x-Ray Photoemission Spectroscopy*, Applied Physics Letters **68**, 2879 (1996).

[58] T. E. Cook, C. C. Fulton, W. J. Mecouch, R. F. Davis, G. Lucovsky, and R. J. Nemanich, *Band Offset Measurements of the GaN (0001)/HfO_2 Interface*, Journal of Applied Physics **94**, 7155 (2003).

[59] C. D. Wagner, *Sensitivity Factors for XPS Analysis of Surface Atoms*, Journal of Electron Spectroscopy and Related Phenomena **32**, 99 (1983).

[60] S. W. King, J. P. Barnak, M. D. Bremser, K. M. Tracy, C. Ronning, R. F. Davis, and R. J. Nemanich, *Cleaning of AlN and GaN Surfaces*, Journal of Applied Physics **84**, 5248 (1998).

[61] D. C. Messina, K. A. Hatch, and R. J. Nemanich, *Atomic Layer Etching of Gallium Nitride Enabled by Water Vapor and O_2-Plasma Oxidation*, Unpublished (n.d.).

[62] V. M. Bermudez, *Study of Oxygen Chemisorption on the GaN(0001)-(1x1) Surface*, Journal of Applied Physics **80**, 1190 (1996).

[1] Y. Lee, N. R. Johnson, and S. M. George, *Thermal Atomic Layer Etching of Gallium Oxide Using Sequential Exposures of HF and Various Metal Precursors*, Chemistry of Materials **32**, 5937 (2020).

[2] S. Han, M. Fang, X. Huang, M. Fang, W. Zhao, S. Xu, D. Zhu, W. Xu, W. Liu, P. Cao, and Y. Lu, *High-Performance UV Detectors Based on Room-Temperature Deposited Amorphous Ga2O3 Thin Films by RF Magnetron Sputtering*, Journal of Materials Chemistry C **7**, 11834 (2019).

[3] Y. S. Lee, D. Chua, R. E. Brandt, S. C. Siah, J. V. Li, J. P. Mailoa, S. W. Lee, R. G. Gordon, and T. Buonassisi, *Atomic Layer Deposited Gallium Oxide Buffer Layer Enables 1.2 v Open-Circuit Voltage in Cuprous Oxide Solar Cells*, Advanced Materials **26**, 4704 (2014).

[4] J. Y. Tsao, S. Chowdhury, M. A. Hollis, D. Jena, N. M. Johnson, K. A. Jones, R. J. Kaplar, S. Rajan, C. G. Van de Walle, E. Bellotti, C. L. Chua, R. Collazo, M. E. Coltrin, J. A. Cooper, K. R. Evans, S. Graham, T. A. Grotjohn, E. R. Heller, M. Higashiwaki, M. S. Islam, P. W. Juodawlkis, M. A. Khan, A. D. Koehler, J. H. Leach, U. K. Mishra, R. J. Nemanich, R. C. N. Pilawa-Podgurski, J. B. Shealy, Z. Sitar, M. J. Tadjer, A. F. Witulski, M. Wraback, and J. A. Simmons, *Ultrawide-Bandgap Semiconductors: Research Opportunities and Challenges*, Advanced Electronic Materials **4**, (2018).

[5] K. Sasaki, M. Higashiwaki, A. Kuramata, T. Masui, and S. Yamakoshi, *MBE Grown Ga_2O_3 and Its Power Device Applications*, Journal of Crystal Growth **378**, 591 (2013).

[6] S. J. Pearton, J. Yang, P. H. Cary, F. Ren, J. Kim, M. J. Tadjer, and M. A. Mastro, *A Review of Ga_2O_3 Materials, Processing, and Devices*, Applied Physics Reviews **5**, (2018).

[7] Y. Lee, J. W. Dumont, and S. M. George, *Atomic Layer Etching of Al_2O_3 Using Sequential, Self-Limiting Thermal Reactions with $Sn(Acac)_2$ and Hydrogen Fluoride*, Journal of Physical Chemistry C **119**, 25385 (2015).

[8] S. M. George, *Mechanisms of Thermal Atomic Layer Etching*, Accounts of Chemical Research **53**, 1151 (2020).

[9] J. A. Murdzek and S. M. George, *Effect of Crystallinity on Thermal Atomic Layer Etching of Hafnium Oxide, Zirconium Oxide, and Hafnium Zirconium Oxide*, Journal of Vacuum Science & Technology A **38**, 022608 (2020).

[10] J. A. Murdzek, A. Rajashekhar, R. S. Makala, and S. M. George, *Thermal Atomic Layer Etching of Amorphous and Crystalline Al_2O_3 Films*, Journal of Vacuum Science & Technology A **39**, 042602 (2021).

[11] N. R. Johnson, J. K. Hite, M. A. Mastro, C. R. Eddy, and S. M. George, *Thermal*

Atomic Layer Etching of Crystalline GaN Using Sequential Exposures of XeF_2 and BCl_3, Applied Physics Letters **114**, (2019).

[12] N. R. Johnson, H. Sun, K. Sharma, and S. M. George, *Thermal Atomic Layer Etching of Crystalline Aluminum Nitride Using Sequential, Self-Limiting Hydrogen Fluoride and $Sn(Acac)_2$ Reactions and Enhancement by H_2 and Ar Plasmas*, Journal of Vacuum Science & Technology A: Vacuum, Surfaces, and Films **34**, 050603 (2016).

[13] J. H. Dycus, K. J. Mirrielees, E. D. Grimley, R. Kirste, S. Mita, Z. Sitar, R. Collazo, D. L. Irving, and J. M. LeBeau, *Structure of Ultrathin Native Oxides on III–Nitride Surfaces*, ACS Applied Materials & Interfaces **10**, 10607 (2018).

[14] I. H. Hwang, H. Y. Cha, and K. S. Seo, *Low-damage and Self-limiting (Al)Gan Etching Process through Atomic Layer Etching Using O_2 and BCl_3 Plasma*, Coatings **11**, 1 (2021).

[15] R. J. Shul, L. Zhang, A. G. Baca, C. G. Willison, J. Han, S. J. Pearton, K. P. Lee, and F. Ren, *Inductively Coupled High-Density Plasma-Induced Etch Damage of GaN MESFETs*, Solid-State Electronics **45**, 13 (2001).

[16] Z. Mouffak, Plasma Reactive Ion Etching-Induced Damage in GaN, 2003.

[17] X. A. Cao, H. Cho, S. J. Pearton, G. T. Dang, A. P. Zhang, F. Ren, R. J. Shul, L. Zhang, R. Hickman, and J. M. Van Hove, *Depth and Thermal Stability of Dry Etch Damage in GaN Schottky Diodes*, Applied Physics Letters **75**, 232 (1999).

[18] S. J. Pearton, R. J. Shul, and F. Ren, *A Review of Dry Etching of GaN and Related Materials*, MRS Internet Journal of Nitride Semiconductor Research **5**, 1 (2000).

[19] C. Kauppinen, S. A. Khan, J. Sundqvist, D. B. Suyatin, S. Suihkonen, E. I. Kauppinen, and M. Sopanen, *Atomic Layer Etching of Gallium Nitride (0001)*, Journal of Vacuum Science & Technology A: Vacuum, Surfaces, and Films **35**, 060603 (2017).

APPENDIX A

COPYRIGHT PERMISSIONS

Copyright permission for the re-use/re-print of the following figures and tables were obtained or requested from the publishers. The detailed permission agreement for each figure or table with the copyright statement in the text can be provide upon request. Please contact me at kahatch2@asu.edu for any matters of copyright violation in this dissertation.

A. Permission Agreement Obtained for the Following Figures:

Figure 1.1: Reprinted/adapted by permission of John Wiley and Sons, Ultrawide-Bandgap Semiconductors: Research Opportunities and Challenges by J. Y. Tsao, S. Chowdhury, M. A. Hollis, *et al*. Copyright © 2017, John Wiley and Sons

Figure 2.4: Reprinted/adapted by permission of American Vacuum Society, Overview of Atomic Layer Etching in the Semiconductor Industry by K. J. Kanarik, T. Lill, E. A. Hudson, *et al*. Copyright © 2015, American Vacuum Society

Figure 6.1: Reprinted/adapted by permission of Springer Nature, Polarization Effects of GaN and AlGaN: Polarization Bound Charge, Band Bending, and Electronic Surface States by B. S. Eller, J. Yang, R. J. Nemanich. Copyright © 2014, Springer Nature

Figure 6.2: Reprinted/adapted by permission of Springer Nature, Polarization Effects of GaN and AlGaN: Polarization Bound Charge, Band Bending, and Electronic Surface States by B. S. Eller, J. Yang, R. J. Nemanich. Copyright © 2014, Springer Nature

Figure 7.1: Reprinted/adapted by permission of American Chemical Society, Structure of Ultrathin Native Oxides on III–Nitride Surfaces by J. H. Dycus, K. J. Mirrielees, E. D. Grimley, *et al*. Copyright © 2018, American Chemical Society

A. Permission Agreement Obtained for the Following Tables:

Table 1.1: Reprinted/adapted by permission of John Wiley and Sons, Ultrawide-Bandgap Semiconductors: Research Opportunities and Challenges by J. Y. Tsao, S. Chowdhury, M. A. Hollis, *et al*. Copyright © John Wiley and Sons

A. No Permission Agreement Required for the Following Figures:

Figure 2.2: Copyright © 2015, The Electrochemical Society

Figure 3.10: Copyright © 2020, Microscopy Society of America